



APPENDIX C

Geochemical Evaluation and Groundwater Transport Model for the Smith Ranch – Highland Uranium Project Mine Unit 1

FINAL REPORT

January 2018

Prepared for:



CAMECO RESOURCES
SMITH RANCH – HIGHLAND OPERATION
P.O. Box 1210
GLENROCK, WYOMING 82637

Prepared by:



Enchemica LLC
2335 Buckingham Circle
Loveland, Colorado 80538
(970) 203-0179

Summary of Comments on CamecoSRH_MineUnit1_AppendixC_ACL_Application_ML18186A337.pdf

Page: 1



Number: 1 Author: Vshea Subject: Sticky Note Date: 5/12/2021 9:59:19 AM
<https://www.nrc.gov/docs/ML1818/ML18186A337.pdf>

Table of Contents

Table of Contents	i
Mineral Formulas	ii
Tables.....	iii
Figures.....	v
Attachments	vii
Executive Summary.....	viii
1.0 Introduction	1
2.0 Site History.....	3
3.0 Characterization of Site Sediments and Groundwater	4
3.1 Mine Unit 1 Groundwater Flow	7
3.2 Upgradient Aquifer Sediments and Groundwater.....	9
3.3 Production Zone Aquifer Sediments and Groundwater	17
3.4 Downgradient Aquifer Sediments and Groundwater	29
3.5 Sequential Extractions	34
4.0 Transport Model.....	43
4.1 Modeled Constituents.....	43
4.2 Conceptual Model.....	43
4.3 Model Parameters	56
4.4 Sensitivity Evaluation.....	59
5.0 Transport Modeling Results	61
5.1 Major Elements and pH.....	61
5.2 Iron and Manganese.....	68
5.3 Uranium	72
5.4 Radium-226.....	79
5.5 Arsenic.....	81
5.6 Selenium	84
5.7 Effects of Groundwater Stability on Transport Modeling Results	87
6.0 Summary and Conclusions	91
7.0 References	92

Mineral Formulas

Albite	$\text{NaAlSi}_3\text{O}_8(\text{s})$
Barite	$\text{BaSO}_4(\text{s})$
Calcite	$\text{CaCO}_3(\text{s})$
Ca-montmorillonite	$\text{Ca}_{0.165}\text{Al}_{2.33}\text{Si}_{3.67}\text{O}_{10}(\text{OH})_2(\text{s})$
Chalcedony	$\text{SiO}_2(\text{s})$
Chlorite	$\text{Mg}_5\text{Al}_2\text{Si}_3\text{O}_{10}(\text{OH})_8(\text{s})$
Coffinite	$\text{USiO}_4 \cdot n\text{H}_2\text{O}(\text{s})$
Ferrihydrite	$\text{Fe}(\text{OH})_3(\text{s})$
Ferroselite	$\text{FeSe}_2(\text{s})$
Illite	$\text{K}_{0.6}\text{Mg}_{0.25}\text{Al}_{2.3}\text{Si}_{3.5}\text{O}_{10}(\text{OH})_2(\text{s})$
Kaolinite	$\text{Al}_2\text{Si}_2\text{O}_5(\text{OH})_4(\text{s})$
K-feldspar	$\text{KAlSi}_3\text{O}_8(\text{s})$
Muscovite	$\text{KAl}_3\text{Si}_3\text{O}_{10}(\text{OH})_2(\text{s})$
Native Se	$\text{Se}(\text{s})$
Quartz	$\text{SiO}_2(\text{s})$
Pyrite	$\text{FeS}_2(\text{s})$
Realgar	$\text{AsS}(\text{s})$
Uraninite	$\text{UO}_2(\text{s})$

Tables

Table C.3-1	Mine Unit 1 Restoration Target Values, maximum concentrations during baseline sampling, drinking water standards and maximum groundwater concentrations during stability monitoring
Table C.3-2	Upgradient and downgradient sediment mineralogy
Table C.3-3	Upgradient and downgradient sediment chemistry
Table C.3-4	Upgradient baseline groundwater quality
Table C.3-5	Upgradient and cross-gradient July 2015 groundwater quality
Table C.3-6	Production zone sediment mineralogy
Table C.3-7	Production zone sediment chemistry
Table C.3-8	Production zone groundwater quality
Table C.3-9	Downgradient groundwater quality
Table C.3-10	CEC data for production zone and downgradient sediment samples
Table C.3-11	Iron oxide and hydroxide sequential extraction results
Table C.4-1	Groundwater flow path distances from upgradient monitoring ring
Table C.4-2	Sequential extraction results for production zone and downgradient aquifer sediments
Table C.4-3	Mineral parameters used in PHREEQC reactive transport modeling calculations
Table C.4-4	Hydrogeologic parameters
Table C.5-1	Measured and modeled groundwater pH at POE locations
Table C.5-2	Effects of parameter variations on POE A modeled groundwater pH and constituent concentrations
Table C.5-3	Measured and modeled groundwater TDS concentrations at POE locations
Table C.5-4	Measured and modeled groundwater iron concentrations at POE locations
Table C.5-5	Measured and modeled groundwater manganese concentrations at POE locations
Table C.5-6	Initial uranium concentrations in production zone sediments based on model calibration
Table C.5-7	Measured and modeled groundwater uranium concentrations at POE locations
Table C.5-8	Maximum predicted groundwater uranium concentrations at Well B-4

Tables (contd)

Table C.5-9	Effects of initial Well B-4 pH on modeled initial uranium concentration adsorbed on $\text{Fe}(\text{OH})_3(\text{a})$
Table C.5-10	Adsorbed (Step III and Step IV sequential extractions) and total (EPA 3050) uranium concentrations in production zone sediments
Table C.5-11	Production zone uranium and downgradient pyrite mass balance calculation results for Flow Paths A through F
Table C.5-12	Measured and modeled groundwater radium-226 concentrations at POE locations
Table C.5-13	Measured and modeled groundwater arsenic concentrations at POE locations
Table C.5-14	Measured and modeled groundwater selenium concentrations at POE locations
Table C.5-15	Results of statistical evaluation for stability of arsenic, radium-226, selenium and uranium in Mine Unit 1 POC wells (Cameco 2017)
Table C.5-16	Radium-226 concentrations in Well B-1, B-5 and B-11 groundwater samples
Table C.5-17	Uranium concentrations in Well B-1, B-3, B-5 and B-19 samples

Figures

Figure C.1-1	Relative locations of Mine Unit 1 and other SRH site features (from Cameco 2014)
Figure C.3-1	Locations of Mine Unit 1 production-zone monitoring wells (B-wells), monitoring ring wells (M-wells) and particle track paths (from AquiferTek 2017)
Figure C.3-2	Mine Unit 1 aquifer sediment core locations
Figure C.3-3	Concentrations of: (a) chloride, (b) total alkalinity and (c) uranium in groundwater samples from upgradient and cross-gradient monitoring ring Wells M-20, M-21, M-22, M-23 and M-24
Figure C.3-4	Arsenic concentration contour map, March 2016
Figure C.3-5	Iron concentration contour map, March 2016
Figure C.3-6	Uranium concentration contour map, March 2016
Figure C.3-7	Radium-226+228 concentration contour map, March 2016
Figure C.3-8	Concentrations of (a) chloride, (b) total alkalinity and (c) uranium in groundwater samples from downgradient monitoring ring Wells M-2, M-3, M-4, M-5, M-7, M-8, M-9 and M-10
Figure C.3-9	Sequential extraction results for Step III (amorphous iron oxides and hydroxides) and Step IV (crystalline iron oxides)
Figure C.4-1	Selenium concentrations in production-zone monitoring well groundwater stability samples; concentrations in samples from Wells B-16 and B-17 were below analytical detection limit of 0.001 mg/L
Figure C.4-2	Native Se saturation index values for production-zone monitoring well samples during the stability monitoring period; concentrations in samples from Wells B-16 and B-17 were below analytical detection limit of 0.001 mg/L
Figure C.5-1	Flow Path A groundwater pH: (a) as a function of time and distance; (b) as a function of time at POE location A
Figure C.5-2	Flow Path A groundwater alkalinity as a function of time and distance
Figure C.5-3	Flow Path A groundwater calcium concentrations as a function of time and distance
Figure C.5-4	Flow Path A groundwater TDS (calculated) as a function of time and distance; (b) as a function of time at POE location A
Figure C.5-5	Flow Path A groundwater log P _{CO2} as a function of time and distance

Figures (contd)

Figure C.5-6	Flow Path A groundwater chloride concentrations as a function of time and distance
Figure C.5-7	Flow Path A groundwater sulfate concentrations as a function of time and distance
Figure C.5-8	Flow Path A groundwater iron concentrations: (a) as a function of time and distance; (b) as a function of time at POE location A
Figure C.5-9	Flow Path A groundwater manganese concentrations: (a) as a function of time and distance; (b) as a function of time at POE location A
Figure C.5-10	Flow Path A groundwater pe as a function of time and distance
Figure C.5-11	Flow Path A groundwater uranium concentrations: (a) as a function of time and distance; (b) as a function of time at POE location A
Figure C.5-12	Effect of initial Well B-4 pH values on predicted Well B-4 groundwater uranium concentrations
Figure C.5-13	Effects of initial pH at Well B-4 on predicted groundwater uranium concentrations along Flow Path B after 1,000 years
Figure C.5-14	Flow Path A groundwater radium-226 concentrations: (a) as a function of time and distance; (b) as a function of time at POE location A
Figure C.5-15	Flow Path A groundwater arsenic concentrations as a function of time and distance
Figure C.5-16	Predicted arsenic concentrations at Wells B-1, B-4 and B-18 as a function of time and initial arsenic concentrations
Figure C.5-17	Effect of initial Well B-4 pH values on predicted Well B-4 groundwater arsenic concentrations
Figure C.5-18	Flow Path A groundwater selenium concentrations: (a) as a function of time and distance; (b) as a function of time at POE location A
Figure C.5-19	Predicted selenium concentrations at Wells B-3, B-5 and B-13 as a function of time and initial selenium concentrations

Attachments

Attachment C-1	Groundwater quality data: laboratory reports and field data sheets
Attachment C-2	Swapp (2016) MU1 Core Description and Analysis Including MU1-DG, MU1-ST, & MU1-UG
Attachment C-3	Aquifer sediment data: core logs, core photographs, chemistry laboratory reports and physical property laboratory reports
Attachment C-4	Schott (2017) Scanning Electron Microscopy Analysis
Attachment C-5	Enchemica.R1.dat database and documentation
Attachment C-6	Aquifer solid to water mass ratios and input values of CEC and mineral quantities
Attachment C-7	PHREEQC input and output files
Attachment C-8	Groundwater concentration profiles along Flow Paths B through F and groundwater concentrations over time at POE locations B through F

Executive Summary




Groundwater restoration was completed in September 2014 at Cameco's Smith Ranch – Highland Project Mine Unit 1. Groundwater composition and stability within Mine Unit 1 have been monitored since September 2014. Site groundwater chemistry, aquifer sediment chemistry, aquifer sediment physical properties and site hydrology data were used to develop a one-dimensional PHREEQC groundwater transport model to predict the effects of groundwater transport from the Mine Unit 1 production zone on groundwater quality at the downgradient aquifer exemption boundary.

Mine Unit 1 injection, production and monitoring ring wells were completed in the Q-Sand within the Fort Union Formation. The Q-Sand is overlain by the R-Shale and underlain by the P-Shale, and these shale units act as hydrologic barriers that have limited the effects of Mine Unit 1 uranium in situ recovery (ISR) to the Q-Sand. Q-Sand samples were collected from cores obtained from two locations upgradient of Mine Unit 1, five locations within the Mine Unit 1 production zone and four downgradient locations. The visual appearance of the Q-Sand cores was recorded, and samples were submitted for physical property testing, mineralogy by X-ray diffraction (XRD), scanning electron microscopy (SEM) with energy-dispersive spectroscopy (EDS) and chemical analysis. The chemical analyses included EPA 3050 extractions, sulfur speciation and total, inorganic and organic carbon analysis.

The Q-Sand is an arkosic sandstone, principally composed of quartz, K-feldspar, albite and clay, with the clay consisting mostly of smectite with smaller amounts of kaolinite, illite and mica. Small amounts of barite and organic carbon are also present in the Q-Sand samples. Upgradient sediments contained accessory iron oxides and small amounts of calcite. Characterization of production zone sand samples showed the presence of iron oxides, native selenium, pyrite and calcite in some samples. Pyrite was observed in the downgradient sediment samples, both by SEM/EDS examination and by analysis for pyritic sulfur. Calcite was also observed in downgradient core samples.

Production zone groundwater has field pH values that are generally lower than baseline groundwater because of the CO₂(g) added during ISR. Post-restoration CO₂(g) partial pressures remain elevated over baseline in the production zone groundwater. Post-restoration uranium, arsenic, radium-226 and selenium concentrations exceeded restoration target values (RTVs) and primary drinking water standards in some groundwater stability monitoring samples. Iron, manganese and total dissolved solids (TDS) exceeded RTVs and secondary drinking water standards in some groundwater stability monitoring samples.

Production zone and downgradient sediment samples were analyzed using sequential extractions. The sequential extraction results provided cation exchange capacities and

	Number: 1	Author: Vshea	Subject: Highlight	Date: 8/22/2018 4:20:24 PM
Q-Sand samples were collected from cores obtained from two locations upgradient of Mine Unit 1, five locations within the Mine Unit 1 production zone and four downgradient locations.				
	Number: 2	Author: Vshea	Subject: Highlight	Date: 8/22/2018 4:24:25 PM
The visual appearance of the Q-Sand cores was recorded, and samples were submitted for physical property testing, mineralogy by X-ray diffraction (XRD), scanning electron microscopy (SEM) with energy-dispersive spectroscopy (EDS) and chemical analysis.				
	Number: 3	Author: Vshea	Subject: Highlight	Date: 8/22/2018 4:24:37 PM
The chemical analyses included EPA 3050 extractions, sulfur speciation and total, inorganic and organic carbon analysis.				

concentrations of iron oxides and hydroxides for the geochemical transport model calculations. Sequential extractions also provided information on the association of constituents with different solids in the production zone sediments. In the production zone sediments, 59% to 85% of uranium was associated with reduced organics and sulfides, with the remaining uranium associated with clays or iron oxides. From 30% to 71% of arsenic in production zone sediment samples was associated with reduced organics and sulfides, with the remaining arsenic mostly associated with iron oxides. Radium-226 in the production zone sediment samples was mostly associated with clays (19% to 64%) and iron oxides (17% to 46%), with smaller amounts (13% to 35%) associated with reduced organics and sulfide phases. Most of the selenium (55% to 97%) in the production zone sediment samples was associated with reduced organics and sulfide phases. Most uranium, arsenic and selenium in the downgradient sediment samples was found to be associated with reduced phases (organics and sulfides). Radium-226 concentrations in the downgradient samples were distributed between clays, iron oxides and reduced phases.

PHREEQC one-dimensional reactive transport modeling calculations were developed for six flow paths that extend from the upgradient monitoring ring wells to the downgradient aquifer exemption boundary. The flow paths were selected based on predicted long-term groundwater flow directions and because the flow paths pass through locations with elevated arsenic, iron, manganese, radium-226+228, selenium and uranium concentrations. The flow paths were geographically distributed across Mine Unit 1 and included 10 of the 19 production-zone monitoring well locations.

The reactive transport modeling results show that the dissolved uranium, radium-226, arsenic and selenium in Mine Unit 1 groundwater will be attenuated by the reducing sediments and clay minerals downgradient of the production zone and will not significantly affect groundwater concentrations at the aquifer exemption boundary. Modeled uranium concentrations in downgradient groundwater are extremely low because of uranium reduction by pyrite and precipitation as uraninite. Mass balance calculations based on uranium concentrations in the production zone sediments and pyrite concentrations in downgradient sediments demonstrate that a large excess of pyrite (188 to 2,726 times the amount required) is available in downgradient sediments to reduce and attenuate production-zone uranium before groundwater reaches the aquifer exemption boundary. Radium-226 will be attenuated by cation exchange on clays and by precipitation as a barite- $\text{RaSO}_4(\text{s})$ solid solution, with a smaller amount of attenuation by adsorption on iron oxides. Arsenic will be attenuated by adsorption on downgradient iron oxides, and selenium will be precipitated in the downgradient sediments as ferroselite.

Slight increases are predicted in TDS at the aquifer exemption boundary for some flow paths, although TDS concentrations are predicted to remain slightly below the secondary drinking water standard at most aquifer exemption boundary locations. Dissolved iron and

manganese concentrations are predicted to increase slightly in groundwater at the aquifer exemption boundary as a result of transport from the Mine Unit 1 production zone, and may slightly exceed secondary drinking water standards.

1.0 Introduction

The Smith Ranch – Highland Uranium Project (SRH) is located in the southern Powder River Basin in Converse County, Wyoming, approximately 35 kilometers (22 miles) northeast of the City of Douglas. Rio Algom Mining Corporation began in situ recovery (ISR) of uranium in Mine Unit 1 in 1997. Power Resources Inc., doing business as Cameco Resources, assumed operations at the site in 2002. Figure C.1-1 illustrates the relative locations of Mine Unit 1 and other features at the SRH site. Uranium ISR in Mine Unit 1 ended in 2006 and Cameco recently completed restoration of Mine Unit 1 groundwater.

The potential effects of restored Mine Unit 1 groundwater on downgradient groundwater chemistry have been investigated. The production and restoration history of Mine Unit 1 are summarized in Section 2.0 and the pre-ISR and current post-restoration aquifer sediment chemistry and groundwater quality conditions in Mine Unit 1 are described in Section 3.0. Site data were used to develop a one-dimensional PHREEQC groundwater transport model to predict the effects of groundwater transport from Mine Unit 1 point of compliance (POC) wells within the production zone to downgradient point of exposure (POE) wells at the aquifer exemption boundary. The transport modeling approach is summarized in Section 4.0 and the modeling results are provided in Section 5.0.

The transport modeling results show that groundwater pH and concentrations of uranium, radium-226, arsenic and selenium at the POE locations will not be significantly affected by transport from the Mine Unit 1 production zone because of attenuation by downgradient reducing sediments. Small increases in TDS, manganese and iron concentrations may occur at the POE locations within the modeled 1,000-year period.

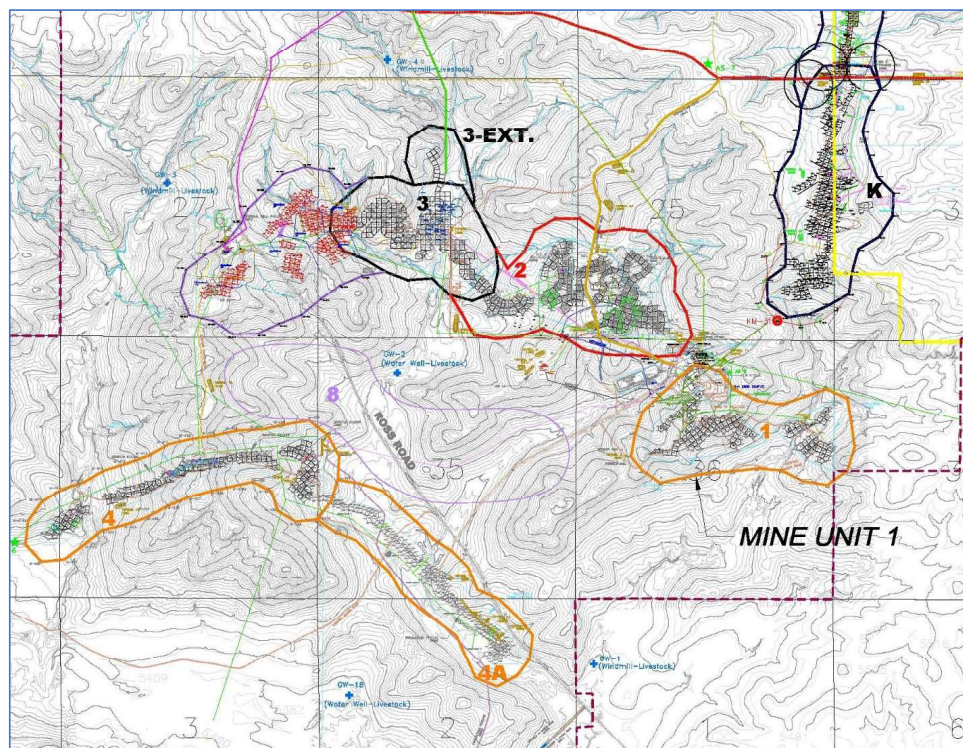


Figure C.1-1. Relative locations of Mine Unit 1 and other SRH site features (from Cameco 2014)

2.0 Site History

Uranium ISR began in Mine Unit 1 in 1997 and concluded in September 2006. The lixiviant consisted of site groundwater with added dissolved $\text{CO}_2(\text{g})$ and $\text{O}_2(\text{g})$. Lixiviant was injected into the subsurface, where it traveled through the mineralized sand, was pumped to the surface and passed through an ion-exchange (IX) process to recover uranium. The groundwater was then re-fortified with dissolved $\text{CO}_2(\text{g})$ and $\text{O}_2(\text{g})$ and recirculated into the subsurface to continue the ISR process. A small amount of groundwater (approximately 1%) was removed from the circuit to maintain a hydrologic cone of depression and ensure affected groundwater was contained within the wellfield. No excursions occurred at Mine Unit 1 during operations or subsequent restoration.

Groundwater restoration at Mine Unit 1 is described in detail by Cameco (2014). Mine Unit 1 groundwater restoration began in September 2006 with groundwater sweep and continued until September 2014. From September 2006 through May 2007, groundwater extraction was carried out without re-injection. Recirculation of treated groundwater began in May 2007. Groundwater was passed through IX columns to remove uranium, then treated by reverse osmosis (RO) to remove residual constituents from the groundwater. Approximately 20% of the treated groundwater was disposed of as brine, with the remaining 80% permeate re-injected into the Mine Unit 1 aquifer. Approximately 900 million gallons of groundwater, equivalent to 14.3 pore volumes, were produced and treated during restoration. An estimated 762 million gallons of treated permeate were re-injected into the aquifer. The volume of treated groundwater began to decline in May 2013 as areas within the Mine Unit 1 aquifer were determined to be restored and production was suspended from individual well patterns or pattern groups.

Sodium sulfide ($\text{Na}_2\text{S}\cdot 3\text{H}_2\text{O}$) was added to treated permeate before reinjection from July 2011 through April 2013. Sodium sulfide was added to re-injected groundwater to promote reducing conditions in the aquifer, which would decrease the solubility of redox-sensitive constituents such as uranium and selenium. Approximately 17,581 pounds of sodium sulfide were added to Mine Unit 1 over the course of restoration.

3.0 Characterization of Site Sediments and Groundwater

Uranium mineralization at Smith Ranch occurs in the Paleocene-aged Fort Union Formation (Cameco 2012, Cameco 2014). The Fort Union Formation consists of arkosic fluvial channel sands separated by semi-continuous confining layers composed of shale, siltstone or claystone. The fluvial sands are fine- to coarse-grained, sub-angular and fair to poorly sorted. Uranium roll-front deposits within the sandstones formed as relatively oxidizing groundwater flowed from south to north. Uranium was precipitated as uraninite and coffinite when uranium-bearing, relatively oxidizing groundwater encountered reducing sediments containing pyrite and organic carbon. Mineralization in Mine Unit 1 is distributed along an east-west trend.

Mine Unit 1 injection, production and monitoring ring wells were completed in the Q-Sand within the Fort Union Formation. The thickness of the Q-Sand ranges from 0 to 15.2 m (0 to 50 ft). The Q-Sand is overlain by the R-Shale and underlain by the P-Shale, and these shale units act as barriers to fluid movement from sand to sand in Mine Unit 1 (Rio Algom 1997). Nineteen production-zone monitoring wells (Wells B-1 through B-19) were completed in the Q-Sand, and 25 monitoring ring wells (Wells M-1 through M-25) were completed in the Q-Sand surrounding Mine Unit 1 (Figure C.3-1).

Baseline groundwater concentrations were established using four rounds of groundwater samples collected from the production-zone monitoring and monitoring ring wells in late 1996 and early 1997 (Attachment C-1). Restoration target values (RTVs) were determined from the arithmetic mean concentrations of each constituent or parameter in the samples from the production-zone monitoring wells (Table C.3-1). Additional groundwater samples and water-level elevations were obtained from monitoring ring wells M-2 through M-10 and wells M-20 through M-24 in July 2015. Groundwater samples and water-level elevations were obtained during December 2014 through March 2017 from production-zone monitoring Wells B-1 through B-19 to evaluate the stability of post-restoration groundwater quality.

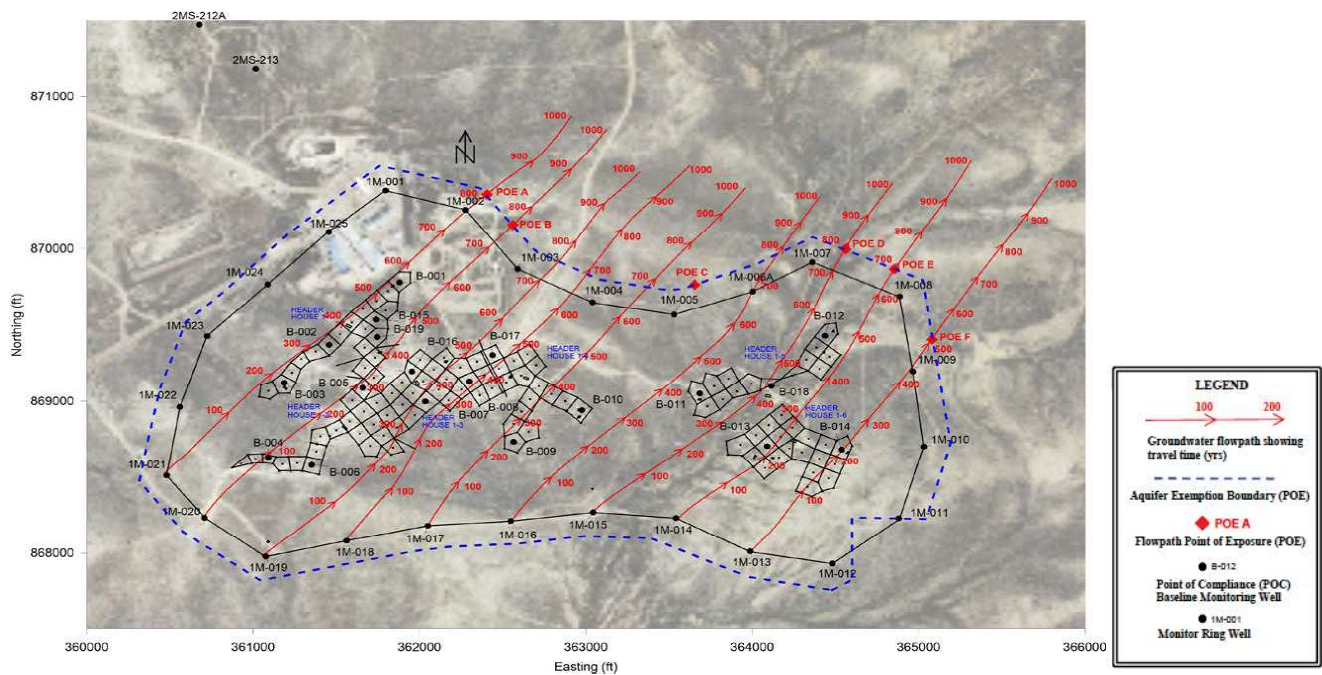


Figure C.3-1. Locations of Mine Unit 1 production-zone monitoring wells (B-wells), monitoring ring wells (M-wells) and particle track paths (from AquiferTek 2017)

Table C.3-1. Mine Unit 1 Restoration Target Values, maximum concentrations during baseline sampling, drinking water standards and maximum groundwater concentrations during stability monitoring

	Units	Restoration Target Value (Cameco 2014) ^a	Maximum During Baseline Sampling (Cameco 2014)	Drinking Water Standard	Maximum During Stability Monitoring
Laboratory pH	s.u.	7.1 - 7.8	7.8	6.5 - 8.5 (s)	7.3 - 8.2 ^b
Field pH	s.u.	n.r.	n.r.	6.5 - 8.5 (s)	6.1 - 7.3 ^b
Calcium	mg/L	73	78	n.a.	149
Magnesium	mg/L	17.4	18.6	n.a.	38
Potassium	mg/L	7.3	8.1	n.a.	13
Sodium	mg/L	22.5	24.5	n.a.	29
Silica as SiO ₂	mg/L	17	19	n.a.	15
Chloride	mg/L	4.2	6.3	250 (s)	32
Fluoride	mg/L	0.32	0.37	4.0	0.30
Sulfate	mg/L	113	120	250 (s)	235
Total Alkalinity (as CaCO ₃)	mg/L	186	201	n.a.	354
Bicarbonate as HCO ₃	mg/L	228	249	n.a.	432
Total Dissolved Solids	mg/L	330	433	500 (s)	760
Ammonia Nitrogen (As N)	mg/L	0.05	0.05	n.a.	1.3
Dissolved Aluminum	mg/L	n.d.	n.d.	0.05 (s)	< 0.1
Dissolved Arsenic	mg/L	0.001	0.003	0.01	0.048
Dissolved Barium	mg/L	n.d.	n.d.	2	< 0.1
Dissolved Iron	mg/L	0.05	0.05	0.3 (s)	7.0
Dissolved Manganese	mg/L	0.02	0.03	0.05 (s)	0.92
Dissolved Selenium	mg/L	0.001	0.002	0.05	0.099
Dissolved Uranium	mg/L	0.0645	0.159	0.03	5.5
Radium-226 (Dissolved)	pCi/L	726	1,500	5 (226+228)	1,250
Radium-228 (Dissolved)	pCi/L	n.r.	n.r.	5 (226+228)	21.3

a - results from Well B-6 were excluded from the uranium RTV calculation because they were identified as outliers

b - minimum to maximum values

(s) - secondary standard

n.a. - not applicable

n.d. - not detected

n.r. - not reported

Swapp (2016, Attachment C-2) describes mineralogical and chemical analyses of an initial set of aquifer sediment core samples (Figure C.3-2) obtained from Q-Sand locations that were upgradient (UG-1), within the production zone (ST-1) and downgradient of Mine Unit 1 (DG-1). Additional sediment cores were obtained from the Q-Sand for investigation from locations cross-gradient of Mine Unit 1 (DG-5), within Mine Unit 1 (ST-2 through ST-5) and from downgradient locations (DG-2 through DG-4, Figure C.3-2). Cores were obtained along the entire thickness of the Q-Sand at each location, photographed and described in field notes (Attachment C-3). Representative samples were selected for analysis of mineralogical, chemical and physical properties from transmissive zones for the upgradient, cross-gradient and downgradient samples, from depths consistent with production fluid contact within the Mine Unit 1 production zone.

The cores were visually examined, and representative segments were selected for analysis from each location. Each core segment was split lengthwise and the splits were submitted for mineralogical analysis using X-ray diffraction (XRD) and total chemical (EPA 3050) analysis (Attachment C-3). If visual inspection indicated the presence of significant amounts of clay, XRD determination of clay mineralogy was also carried out. Some of the core segments were examined using scanning electron microscopy (SEM) with energy-dispersive spectroscopy (EDS) to determine textural features and mineralogical relationships of constituents (Attachment C-4). Sequential extractions were performed on selected production zone and downgradient core samples to determine the phase associations of different constituents (Land et al. 2002). Additional samples were obtained from the core locations for physical testing, including dry bulk density, total porosity, effective porosity and particle size analysis.

The water-level elevations, aquifer sediment and groundwater quality data have been used to characterize groundwater flow, aquifer sediment chemistry and mineralogy and groundwater geochemistry upgradient of Mine Unit 1, within the Mine Unit 1 production zone and downgradient of Mine Unit 1.

3.1 Mine Unit 1 Groundwater Flow

AquiferTek (2017) developed a regional groundwater flow model to evaluate long-term groundwater flow directions in the Mine Unit 1 aquifer (Figure C.3-1). Over the long term, groundwater will travel from the south-southwest to the north-northeast across Mine Unit 1. The long-term flow direction is similar to the flow direction that prevailed during formation of the uranium roll-front deposits, so groundwater affected by ISR in the production zone will flow into reducing sediments. Examination of roll-front maps for Mine Unit 1 confirmed the presence of reducing sediments downgradient of the production zone.

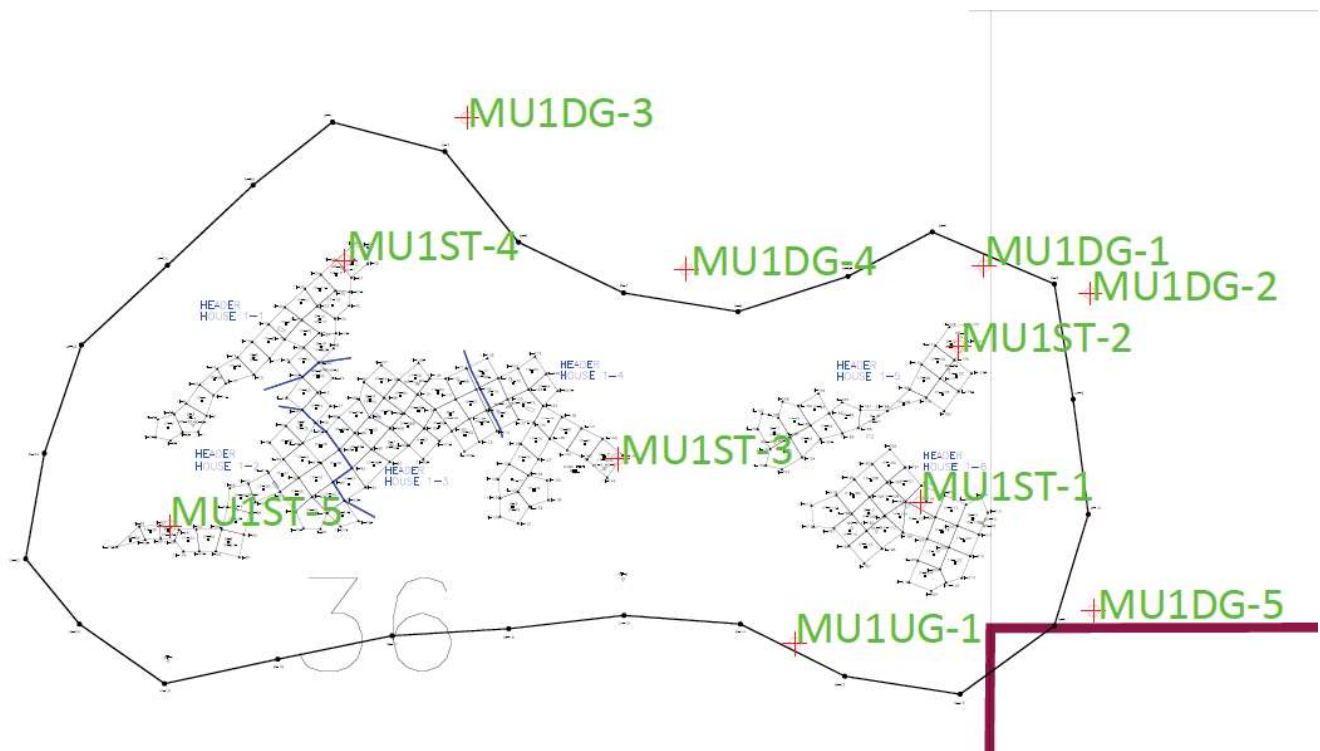


Figure C.3-2. Mine Unit 1 aquifer sediment core locations; the red line in the southeast corner of the figure represents the permit boundary

3.2 Upgradient Aquifer Sediments and Groundwater

The mineralogy of samples from upgradient core UG-1 (Swapp 2016, Attachment C-2) consisted mainly of quartz, K-feldspar, albite and clay, with accessory iron oxides, rare barite and minimal calcite. The clay minerals in the upgradient core samples were mainly smectite, with small amounts of kaolinite, illite and chlorite. Pyrite was absent in all but one sample from this location.

Core DG-5 also represents aquifer material upgradient of the uranium roll front based on its location (Figure C.3-2), visual appearance and mineralogy. The DG-5 core samples had a reddish-brown oxidized appearance with visible organic carbon material. XRD results indicated the sediments were composed primarily of quartz, K-feldspar, albite and clay (Table C.3-2). The principal clay in this core was smectite, with smaller amounts of muscovite, illite and kaolinite. Chemical analysis of a DG-5 core sample (Table C.3-3) shows it contained low uranium concentrations and no reduced sulfur (organic sulfur or pyritic sulfur), consistent with its oxidized appearance.

Baseline upgradient groundwater quality was determined with four rounds of groundwater samples collected in late 1996 and early 1997 (Table C.3-4). Additional upgradient and cross-gradient monitoring ring groundwater samples were collected in July 2015 (Table C.3-5). Upgradient and cross-gradient groundwater has moderate pH values, with a predominantly calcium-bicarbonate composition and low concentrations of sodium, magnesium and sulfate (Tables C.3-4 and C.3-5). Chloride, total alkalinity, uranium and other constituent concentrations have remained unchanged since the pre-operational period (Figure C.3-3), demonstrating that significant changes in the upgradient groundwater chemistry did not occur during ISR.

Concentrations of redox-sensitive elements in upgradient groundwater samples, including iron and manganese, are very low (Tables C.3-4 and C.3-5). These low iron and manganese concentrations are consistent with the relatively oxidizing groundwater conditions upgradient of the Mine Unit 1 uranium roll-front deposit. Although the field ORP measurements in July 2015 were consistently negative (Table C.3-5), these measurements would be poorly poised by the low concentrations of redox-sensitive elements in the groundwater and are of questionable utility. Concentrations of many constituents of potential concern at the Mine Unit 1 site are relatively low in the upgradient groundwater, including chloride, sulfate, arsenic and selenium (Tables C.3-4 and C.3-5). However, uranium concentrations in samples from all upgradient wells (Wells M-13 through M-21) exceed the drinking water standard of 0.03 mg/L (Tables C.3-4 and C.3-5). Radium-226+228 concentrations in most upgradient groundwater samples also exceed the 5 pCi/L drinking water standard.

Table C.3-2. Upgradient and downgradient sediment mineralogy

Location		Upgradient	Upgradient	Downgradient	Downgradient	Downgradient	Downgradient
Sample	Units	DG-5	DG-5	DG-2	DG-2	DG-3	DG-4
Depth	ft	528.5-529	541-542	477-478	487.5-488.5	543-544	516-517
Quartz	%	49	47	49	54	51	62
K-Feldspar	%	26	13	26	22	24	17
Plagioclase	%	19	10	21	17	21	15
Mica	%	2	n.d.	2	3	2	3
Pyrite	%	n.d.	n.d.	n.d.	n.d.	n.d.	n.d.
Unaccounted	%	<5	n.m.	<5	<5	<5	<5
Total Clay	%	n.m.	30	n.m.	n.m.	n.m.	n.m.
Smectite	%	n.m.	26	n.m.	n.m.	n.m.	n.m.
Illite/Mica	%	n.m.	2	n.m.	n.m.	n.m.	n.m.
Kaolinite	%	n.m.	2	n.m.	n.m.	n.m.	n.m.

n.d. - not detected
n.m. - not measured

Table C.3-3. Upgradient and downgradient sediment chemistry

Location		Upgradient	Downgradient	Downgradient	Downgradient
Sample Number	Units	DG-5	DG-2	DG-3	DG-4
Depth	ft	528.5-529	487.5-488.5	543-544	516-517
Aluminum	mg/Kg	4560	4370	8780	4610
Arsenic	mg/Kg	25.3	15.6	5.5	2.3
Barium	mg/Kg	7.8	8.8	10	6.1
Cadmium	mg/Kg	< 0.5	< 0.5	< 0.5	< 0.5
Calcium	mg/Kg	1910	2140	2210	2020
Chromium	mg/Kg	7	7	15	9
Copper	mg/Kg	1	4	4	2
Iron	mg/Kg	11300	8660	19700	5690
Magnesium	mg/Kg	1460	1740	3770	1870
Manganese	mg/Kg	66.1	26.3	68.2	22.5
Molybdenum	mg/Kg	< 2	< 2	< 2	< 2
Nickel	mg/Kg	3.7	8.6	12.1	6.4
Phosphorus	mg/Kg	110	160	130	110
Potassium	mg/Kg	350	450	510	330
Selenium	mg/Kg	0.36	0.64	0.33	0.17
Silica, recoverable	mg/Kg	1930	1780	2130	1970
Silver	mg/Kg	< 1	< 1	1	< 1
Sodium	mg/Kg	40	50	50	50
Strontium	mg/Kg	17.6	19.1	19.5	16.6
Sulfur	mg/Kg	< 30	4870	4660	1680
Uranium	mg/Kg	2.02	557	8.71	8.96
Vanadium	mg/Kg	23.9	7.5	14.8	7.4
Zinc	mg/Kg	19	38	15	10
Radium 226	pCi/g	8.2	88	18	9.8
Radium 228	pCi/g	97	51	35	41
Carbon, total (TC)	%	< 0.1	0.4 B	< 0.1	0.2 B
Carbon, total inorganic (TIC)	%	< 0.1	< 0.1	< 0.1	< 0.1
Carbon, total organic (TOC)	%	< 0.1	0.4 B	< 0.1	0.2 B
Sulfur Organic Residual	%	< 0.01	0.04	0.05	0.01
Sulfur Pyritic Sulfide	%	< 0.01	0.54	0.43	0.17
Sulfur Sulfate	%	< 0.01	0.1	0.02	0.02
Sulfur Total	%	< 0.01	0.68	0.5	0.2
Total Sulfur minus Sulfate	%	< 0.01	0.58	0.48	0.18

B – Analyte concentration detected at a value between the method detection limit and practical quantitation limit; the associated value is an estimated quantity

Table C.3-4. Upgradient baseline groundwater quality

Well Number		M-13	M-13	M-14	M-14	M-15
Sample Date		12/11/1996	12/27/1996	12/11/1996	12/27/1996	12/11/1996
Lab pH	s.u.	7.67	7.57	7.52	7.51	7.53
Conductivity	µmhos/cm	551	540	557	544	554
Calcium	mg/L	65.3	72.5	66.6	72.6	64.3
Magnesium	mg/L	16.2	16.6	16.1	16.5	15.8
Potassium	mg/L	8.0	6.7	7.3	6.4	6.97
Sodium	mg/L	23.1	22.4	22.8	22.1	20.8
Silica (as SiO ₂)	mg/L	15.6	15.6	16.3	16.3	15.7
Chloride	mg/L	3.5	2.8	3.7	3.2	3.6
Fluoride	mg/L	0.26	0.30	0.32	0.34	0.30
Sulfate	mg/L	114	118	112	117	114
Alkalinity (as CaCO ₃)	mg/L	165	165	193	167	171
Bicarbonate (as HCO ₃)	mg/L	201	201	235	204	209
Total Dissolved Solids	mg/L	393	341	401	335	398
Nitrite +Nitrate (as N)	mg/L	< 0.1	NM	< 0.1	< 0.1	< 0.1
Aluminum ^a	mg/L	0.0007	0.0006	0.0005	0.0005	0.0005
Arsenic	mg/L	< 0.001	< 0.001	< 0.001	< 0.001	< 0.001
Barium ^a	mg/L	0.024	0.023	0.024	0.024	0.024
Manganese	mg/L	0.02	0.03	0.02	0.03	0.02
Selenium	mg/L	< 0.001	< 0.001	< 0.001	< 0.001	< 0.001
Uranium	mg/L	0.041	0.038	0.044	0.038	0.049
Radium-226	pCi/L	4.2	4.1	7.9	7.4	6.3
log P _{CO2}	atm	-2.45	-2.35	-2.24	-2.29	-2.30
Calcite Saturation Index	--	0.12	0.06	0.04	0.00	-0.01
Chalcedony Saturation Index	--	0.11	0.11	0.13	0.13	0.11
Speciated Charge Balance	%	0.2	2.6	-4.3	2.0	-2.9

a – aluminum and barium concentrations were below analytical detection limits of 0.1 mg/L, values shown were calculated from solubilities of Ca-montmorillonite and barite, respectively

note – carbonate (as CO₃²⁻), ammonia-N, and dissolved boron, cadmium, chromium, iron, molybdenum, vanadium and zinc were below analytical detection limits in all samples

Table C.3-4. Upgradient baseline groundwater quality (contd)

Well Number		M-15	M-16	M-17	M-18
Sample Date		12/27/1996	12/23/1996	12/23/1996	12/23/1996
Lab pH	s.u.	7.51	7.46	7.44	7.37
Conductivity	µmhos/cm	541	558	560	607
Calcium	mg/L	68.7	72.7	73.2	81.0
Magnesium	mg/L	15.8	17.1	17.5	19.4
Potassium	mg/L	6.3	6.6	6.6	6.9
Sodium	mg/L	20.3	21.3	20.9	21.5
Silica (as SiO ₂)	mg/L	17.2	17.4	17.2	17.9
Chloride	mg/L	3.5	3.9	4.2	4.7
Fluoride	mg/L	0.35	0.34	0.34	0.32
Sulfate	mg/L	112	108	109	119
Alkalinity (as CaCO ₃)	mg/L	175	180	185	195
Bicarbonate (as HCO ₃)	mg/L	214	220	226	238
Total Dissolved Solids	mg/L	329	364	380	402
Nitrite +Nitrate (as N)	mg/L	< 0.1	< 0.1	< 0.1	< 0.1
Aluminum ^a	mg/L	0.0004	0.0004	0.0004	0.0003
Arsenic	mg/L	0.002	< 0.001	< 0.001	< 0.001
Barium ^a	mg/L	0.024	0.025	0.025	0.024
Manganese	mg/L	0.02	0.02	0.02	0.03
Selenium	mg/L	< 0.001	0.006	< 0.001	< 0.001
Uranium	mg/L	0.049	0.046	0.042	0.051
Radium-226	pCi/L	5.3	4.5	4.0	5.9
log P _{CO2}	atm	-2.27	-2.21	-2.17	-2.08
Calcite Saturation Index	--	0.00	-0.01	-0.02	-0.03
Chalcedony Saturation Index	--	0.15	0.16	0.15	0.17
Speciated Charge Balance	%	-1.6	1.4	0.6	1.9

a – aluminum and barium concentrations were below analytical detection limits of 0.1 mg/L, values shown were calculated from solubilities of Ca-montmorillonite and barite, respectively

note – carbonate (as CO₃²⁻), nitrate-N, and dissolved beryllium, boron, cadmium, chromium, copper, lead, mercury, molybdenum, nickel, vanadium and zinc were below analytical detection limits in all samples

Table C.3-4. Upgradient baseline groundwater quality (contd)

Well Number		M-19	M-19	M-20	M-21
Sample Date		12/13/1996	12/27/1996	12/23/1996	12/23/1996
Lab pH	s.u.	7.42	7.38	7.44	7.43
Conductivity	µmhos/cm	617	597	599	586
Calcium	mg/L	80.2	78.4	77.8	77.0
Magnesium	mg/L	19.4	19.8	19.2	17.8
Potassium	mg/L	7.2	7.0	6.7	6.9
Sodium	mg/L	22.7	20.3	21.5	21.8
Silica (as SiO ₂)	mg/L	18.2	17.2	18.1	17.4
Chloride	mg/L	4.5	4.5	4.8	4.2
Fluoride	mg/L	0.30	0.30	0.31	0.33
Sulfate	mg/L	119	112	115	110
Alkalinity (as CaCO ₃)	mg/L	200	193	206	194
Bicarbonate (as HCO ₃ ⁻)	mg/L	244	235	251	237
Total Dissolved Solids	mg/L	402	372	397	398
Nitrite +Nitrate (as N)	mg/L	< 0.1	0.11	< 0.1	< 0.1
Aluminum	mg/L	0.0003	0.0003	0.0003	0.0004
Arsenic	mg/L	< 0.001	0.002	< 0.001	< 0.001
Barium	mg/L	0.024	0.025	0.025	0.025
Manganese	mg/L	0.03	0.02	0.02	0.03
Selenium	mg/L	< 0.001	< 0.001	< 0.001	< 0.001
Uranium	mg/L	0.047	0.061	0.062	0.076
Radium-226	pCi/L	6.6	6.5	8.2	69.0
log P _{CO2}	atm	-2.12	-2.10	-2.13	-2.14
Calcite Saturation Index	--	0.03	-0.03	0.05	0.01
Chalcedony Saturation Index	--	0.18	0.15	0.18	0.16
Speciated Charge Balance	%	1.3	2.2	-0.7	1.1

a – aluminum and barium concentrations were below analytical detection limits of 0.1 mg/L, values shown were calculated from solubilities of Ca-montmorillonite and barite, respectively

note – carbonate (as CO₃²⁻), nitrate-N, and dissolved beryllium, boron, cadmium, chromium, copper, lead, mercury, molybdenum, nickel, vanadium and zinc were below analytical detection limits in all samples

Table C.3-5. Upgradient and cross-gradient July 2015 groundwater quality

Well Number		M-20	M-21	M-22	M-23	M-24
Sample Date		7/8/2015	7/8/2015	7/8/2015	7/8/2015	7/8/2015
Lab pH	s.u.	8.1	8.2	8.3	8.3	8.3
Field pH	s.u.	7.3	7.3	7.6	7.6	7.4
Field Temperature	°C	13.3	15.5	12.9	n.m.	13.3
Field ORP	mvolts	-112	-130	-105.5	n.m.	-215
Field conductivity	µmhos/cm	583	578	573	590	562
Calcium	mg/L	75	72	73	68	69
Magnesium	mg/L	19	17	18	16	17
Potassium	mg/L	8	8	8	9	9
Sodium	mg/L	21	21	22	24	23
Silica as SiO ₂	mg/L	18	18	17	14	15
Chloride	mg/L	4	4	4	2	3
Fluoride	mg/L	0.3	0.3	0.3	0.3	0.3
Sulfate	mg/L	104	100	104	104	106
Total Alkalinity (as CaCO ₃)	mg/L	217	204	202	195	191
Bicarbonate (as HCO ₃)	mg/L	265	248	247	237	234
Total Dissolved Solids	mg/L	400	390	400	380	380
Ammonia Nitrogen (As N)	mg/L	< 0.1	0.2	< 0.1	0.1	0.1
Dissolved Aluminum ^a	mg/L	0.000271	0.000363	0.000467	0.000697	0.000433
Dissolved Arsenic	mg/L	0.001	0.001	< 0.001	< 0.001	< 0.001
Dissolved Barium ^a	mg/L	0.027	0.034	0.026	0.026	0.026
Dissolved Iron	mg/L	< 0.05	< 0.05	0.15	< 0.05	0.21
Dissolved Manganese	mg/L	0.04	0.03	0.03	0.04	0.02
Dissolved Selenium	mg/L	0.001	0.003	< 0.001	0.007	0.006
Dissolved Uranium	mg/L	0.044	0.057	0.029	0.0014	0.0067
Radium-226 (Dissolved)	pCi/L	8.3 ± 0.3	65.2 ± 1.0	400 ± 2.4	1.5 ± 0.1	2.0 ± 0.2
Radium-228 (Dissolved)	pCi/L	1.2 ± 1.2	< 1	1.8 ± 2.0	2.0 ± 1.1	1.7 ± 1.2
Gross Alpha (Dissolved)	pCi/L	73.7 ± 4.1	115 ± 4.9	394 ± 9.9	3.0 ± 1.1	6.1 ± 1.4
Gross Beta (Dissolved)	pCi/L	22.7 ± 2.0	42.1 ± 2.4	129 ± 4.1	8.6 ± 1.7	11.3 ± 1.8
log P _{CO2}	atm	-1.9	-1.9	-2.3	-2.3	-2.1
Calcite Saturation Index	--	-0.10	-0.12	0.14	0.14	-0.08
Chalcedony Saturation Index	--	0.17	0.14	0.15	0.06	0.09
Speciated Charge Balance	%	-1.7	-1.4	-0.3	-1.2	-0.3

n.m. – not measured, wellhead on M-23 could not be removed

a – aluminum and barium concentrations were below analytical detection limits of 0.1 mg/L, values shown were calculated from solubilities of Ca-montmorillonite and barite, respectively

note – carbonate (as CO₃²⁻), nitrate-N, and dissolved beryllium, boron, cadmium, chromium, copper, lead, mercury, molybdenum, nickel, vanadium and zinc were below analytical detection limits in all samples

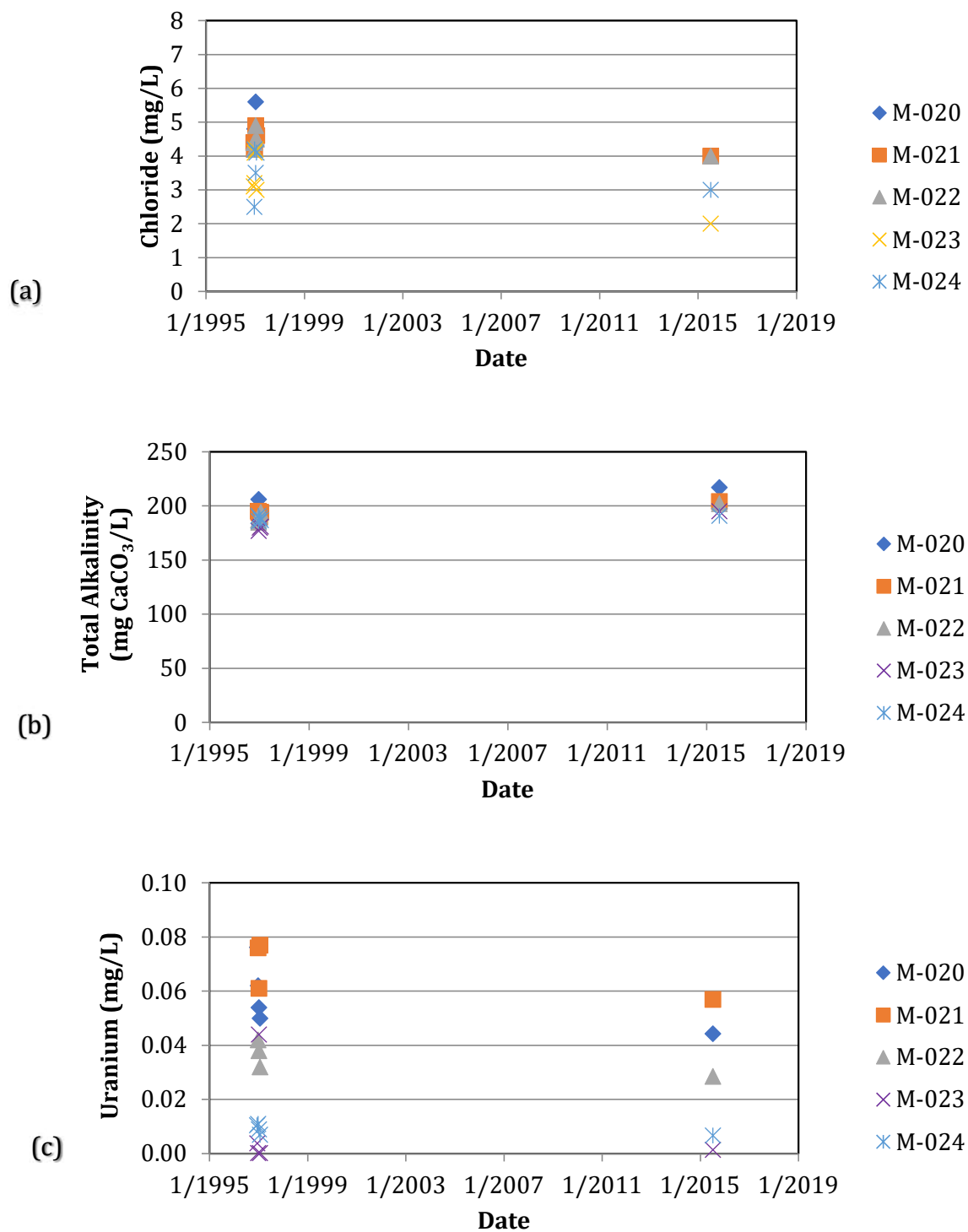


Figure C.3-3. Concentrations of: (a) chloride, (b) total alkalinity and (c) uranium in groundwater samples from upgradient and cross-gradient monitoring ring wells M-20, M-21, M-22, M-23 and M-24

The baseline upgradient water quality data were modeled using PHREEQC (Table C.3-4). Only laboratory pH values were available, which can be unreliable because of possible CO₂(g) loss from the samples during transport to the laboratory. However, the reported baseline pH values (Table C.3-4) are consistent with the field pH values measured in July 2015 and equilibrium modeling of the baseline samples using the laboratory pH values resulted in reasonable charge balances (-4.3% to 2.6%). Equilibrium geochemical modeling also was performed for the July 2015 upgradient groundwater samples. The baseline (Table C.3-4) and July 2015 (Table C.3-5) groundwater samples were saturated with respect to calcite and chalcidony, which is consistent with identification of calcite and quartz in the upgradient aquifer sediments. Because of the similar pH values, CO₂(g) partial pressures (P_{CO2}) and calcite saturation index values for the baseline and July 2015 samples (Tables C. 3-4 and C.3-5), the laboratory pH values for the baseline samples appear to reliably represent groundwater conditions.

Aqueous uranium in the upgradient groundwater is predominantly (99%) present as the Ca₂UO₂(CO₃)₃⁰ and CaUO₂(CO₃)₃²⁻ species. Barium and aluminum concentrations were below analytical detection limits in the upgradient groundwater samples (Tables C.3-4 and C.3-5), even though barite and clay minerals are present in the upgradient aquifer sediments. Assuming barium concentrations were controlled by the solubility of barite resulted in modeled barium concentrations of 0.026 to 0.043 mg/L, which are below the analytical detection limit (0.1 mg/L). Similarly, assuming aluminum concentrations are controlled by Ca-montmorillonite solubility results in below-detection-limit aluminum concentrations (< 0.1 mg/L).

3.3 Production Zone Aquifer Sediments and Groundwater

The principal minerals present in the arkosic sandstones hosting the SRH mineral deposits are quartz, K-feldspar, albite and clay. Other minerals present in the deposits include calcite, pyrite, native Se, ferroselite and goethite, and abundant organic carbon is typically present (Granger and Warren 1969, Davis and Curtis 2007). Within the uranium roll front, uranium is present as coffinite and uraninite (Ludwig and Grauch 1980, Stewart 2002).

The mineralogy and groundwater chemistry in the production zone has been altered by ISR processes. Before ISR, the sediments and groundwater were reducing, with low groundwater concentrations of constituents such as uranium. Immediately after ISR, elevated concentrations of redox-sensitive constituents such as uranium and constituents associated with the ISR process, such as sulfate, remain in solution. Exchange of chloride for uranium during IX increased groundwater chloride concentrations. Groundwater restoration reduced the concentrations of many constituents and the addition of sodium sulfide affected sediment mineralogy and groundwater chemistry.

Aquifer sediment cores were collected from five locations in the Mine Unit 1 production zone (Figure C.3-2). Core samples from location ST-1 were arkosic sandstones consisting of quartz, K-feldspar, albite and clay (Swapp 2016). The clay was mostly smectite, with lesser amounts of kaolinite, illite, and chlorite. SEM/EDS examination of the ST-1 samples showed the presence of pyrite framboids, but uranium mineralization was not identified in the ST-1 samples (Swapp 2016). XRD results for samples obtained at the ST-2, ST-3, ST-4 and ST-5 locations indicate that these sediments were also arkosic sandstones, composed mainly of quartz, K-feldspar, albite and clay (Table C.3-6). In the ST-2 and ST-4 samples with significant clay contents, the clay consisted mainly of smectite or kaolinite, with smaller amounts of illite. Mica in the Mine Unit 1 production zone samples appears to be muscovite (Swapp 2016).

Core location ST-2 is in the northeastern portion of Mine Unit 1. The presence of calcite was noted in ST-2 core hand specimens at 464.6 – 465 ft and at 473 – 473.3 ft. Organic carbon was observed in the cores at 460 – 461 ft and from 470 – 477.7 ft (Attachment C-3). Two representative ST-2 samples were selected for XRD and chemical analysis. XRD results obtained for these ST-2 core samples show significant clay fractions (Table C.3-6).

The ST-2 463 – 464 ft sample was dark gray with visible pyrite and organic carbon (Attachment C-3; Attachment C-4) and contained approximately 2% pyrite (Table C.3-6). SEM/EDS examination of this sample showed organic carbon material with included uranium solids. The uranium solids had peaks associated with silica, indicating a coffinite-like solid phase (Attachment C-4). Uranium solids were also identified associated with clays, quartz and feldspar and appeared rarely as fracture/pit fillings in silicates (Attachment C-4). Relatively high concentrations of uranium (4,950 mg/kg), sulfur and radium-226 were present in this sample compared to other production zone core samples (Table C.3-7). The visual appearance of the core segment, high pyrite concentration and presence of uranium minerals indicate that the ST-2 463 – 464 ft sample was not affected by production fluids during ISR. Although this sample was obtained at a depth expected to be in the production zone, low permeability or other aquifer heterogeneities resulted in this material not being in contact with ISR production fluids.

The 472 – 473 ft sample from location ST-2 appeared oxidized, with red streaks apparent in the core photograph and visible organic carbon was also noted in this sample (Attachment C-3). This sample did not have pyrite visible in hand specimen or detectable by XRD (Table C.3-6) and had low uranium and pyritic sulfur concentrations (Table C.3-7). Consequently, the ST-2 472 – 473 ft sample appears to have been contacted by production fluids and is likely representative of production zone sediments.



Number: 1 Author: Vshea Subject: Highlight Date: 8/22/2018 4:41:04 PM

Although this sample was obtained at a depth expected to be in the production zone, low permeability or other aquifer heterogeneities resulted in this material not being in contact with ISR production fluids.



Author: Vshea Subject: Sticky Note Date: 8/22/2018 4:41:24 PM

This statement indicates that the core samples were collected after ISR operations.

Table C.3-6. Production zone sediment mineralogy

Sample Number	Units	ST-2	ST-2	ST-3	ST-3	ST-4	ST-4	ST-4	ST-5	ST-5
Sample Depth	ft	463-464	472-473	463-464	474-475	479-480	488-489	497-498	494-495	499-500
Quartz	%	44	42	53	46	58	47	53	43	49
K-Feldspar	%	16	21	21	27	7	27	13	30	27
Plagioclase	%	14	23	22	23	6	20	13	22	19
Mica	%	n.d.	n.d.	2	2	n.d.	2	n.d.	2	2
Pyrite	%	2	n.d.	n.d.	n.d.	n.d.	n.d.	n.d.	n.d.	n.d.
Unaccounted	%	n.m.	n.m.	<5	<5	n.m.	<5	n.m.	<5	<5
Total Clay	%	24	14	n.m.	n.m.	29	n.m.	21	n.m.	n.m.
Smectite	%	18	10	n.m.	n.m.	16	n.m.	8	n.m.	n.m.
Illite/Mica	%	1	n.d.	n.m.	n.m.	2	n.m.	1	n.m.	n.m.
Kaolinite	%	5	4	n.m.	n.m.	12	n.m.	12	n.m.	n.m.

n.d. – not detected

n.m. – not measured

Table C.3-7. Production zone sediment chemistry

Sample Number	Units	ST-2	ST-2	ST-3	ST-3
Depth	ft	463-464	472-473	463-464	474-475
Aluminum	mg/Kg	6890	5090	3520	6280
Arsenic	mg/Kg	881	14.7	5.8	25.1
Barium	mg/Kg	11.8	8.7	6.9	10.9
Cadmium	mg/Kg	< 0.5	< 0.5	< 0.5	< 0.5
Calcium	mg/Kg	3510	2500	1840	3900
Chromium	mg/Kg	11	8	12	11
Copper	mg/Kg	< 2	4	3	7
Iron	mg/Kg	30400	9220	4730	8710
Magnesium	mg/Kg	2710	2040	1290	2290
Manganese	mg/Kg	26.4	28.9	27.1	42
Molybdenum	mg/Kg	< 2	< 2	< 2	< 2
Nickel	mg/Kg	10.4	10.7	2.9	13.7
Phosphorus	mg/Kg	170	130	480	130
Potassium	mg/Kg	480	350	280	480
Selenium	mg/Kg	< 4	29.2	0.91	50.5
Silica, recoverable	mg/Kg	3080	2380	1960	2490
Silver	mg/Kg	2	< 1	< 1	< 1
Sodium	mg/Kg	40 B	40 B	30 B	80 B
Strontium	mg/Kg	32.2	22.1	11.7	31.9
Sulfur	mg/Kg	28600	3390	580	230
Uranium	mg/Kg	4950	421	40.2	195
Vanadium	mg/Kg	6	19	9.8	94.9
Zinc	mg/Kg	9	14	18	22
Radium-226	pCi/g	1000	360	74	45
Radium-228	pCi/g	1.6	0.78	16	19
Carbon, total (TC)	%	0.5	0.5	< 0.1	1.4
Carbon, total inorganic (TIC)	%	0.1 B	< 0.1	< 0.1	0.3 B
Carbon, total organic (TOC)	%	0.4 B	0.5	< 0.1	1.1
Sulfur Organic Residual	%	0.22	0.04	< 0.01	0.03
Sulfur Pyritic Sulfide	%	2.54	0.22	0.06	< 0.01
Sulfur Sulfate	%	0.15	0.02	< 0.01	< 0.01
Sulfur Total	%	2.91	0.28	0.05	0.03
Total Sulfur minus Sulfate	%	2.76	0.26	0.05	0.03

B – Analyte concentration detected at a value between the method detection limit and practical quantitation limit; the associated value is an estimated quantity

Table C.3-7. Production zone sediment chemistry (contd)

Sample Number	Units	ST-4	ST-4	ST-5	ST-5
Depth	ft	479-480	488-489	494-495	499-500
Aluminum	mg/Kg	6560	4780	5150	6550
Arsenic	mg/Kg	15.2	3.1	258	720
Barium	mg/Kg	9	17.2	8.5	85.3
Cadmium	mg/Kg	< 0.5	< 0.5	< 0.5	< 0.5
Calcium	mg/Kg	2140	2100	2410	3220
Chromium	mg/Kg	16	10	5	7
Copper	mg/Kg	3	4	18	10
Iron	mg/Kg	11300	5650	17300	41900
Magnesium	mg/Kg	2000	1810	1710	2280
Manganese	mg/Kg	40.1	24.3	82	180
Molybdenum	mg/Kg	< 2	< 2	< 2	< 2
Nickel	mg/Kg	5.2	4.7	14.2	21.6
Phosphorus	mg/Kg	120	150	120	180
Potassium	mg/Kg	370	550	360	650
Selenium	mg/Kg	2.43	2.25	27.1	373
Silica, recoverable	mg/Kg	2290	2450	2780	2580
Silver	mg/Kg	< 1	< 1	20	1
Sodium	mg/Kg	40 B	60 B	50 B	50 B
Strontium	mg/Kg	18.7	18.1	21.4	29.9
Sulfur	mg/Kg	30	750	90	620
Uranium	mg/Kg	9.54	284	154	282
Vanadium	mg/Kg	33.3	6.1	204	477
Zinc	mg/Kg	17	14	22	36
Radium-226	pCi/g	9.1	210	26	63
Radium-228	pCi/g	10	7.7	8.3	8.3
Carbon, total (TC)	%	< 0.1	< 0.1	0.1 B	0.3 B
Carbon, total inorganic (TIC)	%	< 0.1	< 0.1	< 0.1	< 0.1
Carbon, total organic (TOC)	%	< 0.1	< 0.1	0.1 B	0.3 B
Sulfur Organic Residual	%	< 0.01	0.01	< 0.01	0.04
Sulfur Pyritic Sulfide	%	< 0.01	0.07	< 0.01	0.03
Sulfur Sulfate	%	< 0.01	< 0.01	< 0.01	< 0.01
Sulfur Total	%	< 0.01	0.07	< 0.01	0.05
Total Sulfur minus Sulfate	%	< 0.01	0.07	< 0.01	0.05

B – Analyte concentration detected at a value between the method detection limit and practical quantitation limit; the associated value is an estimated quantity

ST-3 core samples were tan to gray, with strings of organic carbon material, larger carbon fragments and trace amounts of pyrite (Attachment C-3; Attachment C-4). Concentrations of uranium and pyritic sulfur in the ST-3 samples were low (Table C.3-7). SEM/EDS examination of the 474 – 475 ft ST-3 core sample showed trace amounts of pyrite, with rims that were depleted in arsenic relative to the cores (Attachment C-4). Uranium was detected only in one small area of organic carbon mixed with clay and a single 2.5 µm grain of native Se was identified. Both ST-3 core samples appear to be representative of aquifer sediments contacted by production fluids. The arsenic depletion in the pyrite rims indicates that arsenic was preferentially leached during ISR, and the remaining arsenic in the pyrite appears to remain in the less-accessible cores of the pyrite grains. The presence of native Se indicates that restoration, including addition of sodium sulfide as a reductant, succeeded in creating moderately reducing aquifer conditions. The presence of residual pyrite in the production zone is likely to help maintain these reducing conditions.

Core samples from ST-4 were gray-brown, with organic carbon visible in hand specimen (Attachment C-3). The sample from 479 – 480 ft had a significant clay fraction (Table C.3-6), low uranium concentration and below-detection pyritic sulfur concentration (Table C.3-7). The core from 483 – 487 ft had visible carbon (Attachment C-3). The 488 – 489 ft sample had only minor amounts of clay, with low uranium and pyritic sulfur concentrations. These core materials appear to be representative of production zone aquifer material, based on their visual appearance, mineralogy, chemistry and depth within the production zone. Calcite cement was noted at 489.5 ft, with an organic carbon layer observed at 492 ft.

Lignite and calcite was noted in the ST-5 core at various depths (Attachment C-3). ST-5 core samples obtained at 494 – 495 ft and 499 – 500 ft had minor clay contents (Table C.3-6). The 499 – 500 ft sample had an oxidized appearance, with visible ferric solids and relict pyrite and marcasite (Attachment C-4). Both samples had relatively low uranium and pyritic sulfur concentrations (Table C.3-7). SEM/EDS examination of the 499 – 500 ft sample did not detect uranium minerals in the solid phases. Iron oxides and organic carbon in this sample contained small crystals of native Se and thin strings of native Se in fractures. Barite was also associated with the iron oxides (Attachment C-4).

The core samples representative of the production zone (ST-2 472 – 473 ft, ST-3, ST-4 and ST-5) are arkosic sandstones with variable clay content (< 5% to 29%, Table C.3-6). Trace amounts of pyrite were observed during SEM examination and low pyritic sulfur concentrations were detected (< 0.01% to 0.22%). Total uranium concentrations were low, ranging from 9.54 to 421 mg/kg (Table C.3-7). Arsenic concentrations varied in the samples, from 258 to 720 mg/kg in samples from ST-5 to 3.1 to 25.1 mg/kg in samples from ST-2, ST-3 and ST-4 (Table C.3-7). The higher arsenic concentrations in the ST-5 core



Number: 1 Author: Vshea Subject: Highlight Date: 8/22/2018 4:42:12 PM

Both ST-3 core samples appear to be representative of aquifer sediments contacted by production fluids.



Number: 2 Author: Vshea Subject: Highlight Date: 8/22/2018 4:42:46 PM

The presence of residual pyrite in the production zone is likely to help maintain these reducing conditions.

samples correspond to higher groundwater arsenic concentrations in samples from nearby production-zone monitoring Well B-4 (Table C.3-8). Groundwater samples from Well B-1 had similarly high groundwater arsenic concentrations (Table C.3-8), but core samples from nearby location ST-4 had relatively low arsenic concentrations (3.1 to 15.2 mg/kg). Considerable variation in selenium concentrations was observed in the production zone core samples, ranging from 0.91 to 373 mg/kg (Table C.3-7). Core sample ST-5 (499 – 500 ft) had the highest selenium concentration and was also the sample with native Se observed during SEM/EDS examination. Groundwater selenium concentrations in nearby Well B-4 were quite low (0.001 mg/L in March 2016), likely because of its precipitation as native Se.

Production zone groundwater quality data for samples collected in March 2016 are summarized in Table C.3-8. At the time of this investigation, March 2016 represented the most recent quarter for which complete groundwater analyses were available for samples from all production-zone monitoring wells. March 2016 Mine Unit 1 field pH values fall at the low end of the secondary drinking water standard range. Major elements and constituents in the Mine Unit 1 groundwater that have RTVs but do not have drinking water standards include calcium, magnesium, sodium, potassium, silica, total alkalinity and bicarbonate. These constituents are close to or below the RTVs in the March 2016 samples. Fluoride concentrations are below the RTV and drinking water standard in all samples. Chloride concentrations in the March 2016 samples mostly exceed the RTV, but are significantly less than the 250 mg/L secondary drinking water standard in all samples. Sulfate concentrations exceed the RTV in four samples, but all samples had sulfate concentrations below the 250 mg/L secondary drinking water standard. Only two March 2016 groundwater samples had TDS concentrations that exceed the 500 mg/L secondary drinking water standard, and many samples had TDS concentrations close to or below the RTV.

Low ammonia-N concentrations reported for some Mine Unit 1 groundwater samples are believed to be anomalous, because there is no known source of ammonia or other nitrogen compounds for Mine Unit 1 groundwater. Because a colorimetric method was used for ammonia analysis, it appears that an unidentified interference caused some reported low groundwater ammonia-N concentrations.

Groundwater arsenic concentrations generally exceed the RTV, but are below the drinking water standard of 0.01 mg/L in most of the March 2016 groundwater samples. The distribution of arsenic in the March 2016 Mine Unit 1 groundwater samples is illustrated in Figure C.3-4. Dissolved aluminum and barium concentrations are below analytical detection limits in all March 2016 samples.

Table C.3-8. Production zone groundwater quality

Well		B-1	B-2	B-3	B-4
Sample Date		3/8/2016	3/8/2016	3/8/2016	3/8/2016
Lab pH	s.u.	7.6	7.7	7.6	7.7
Field pH	s.u.	6.3	6.2	6.1	6.3
Field Temperature	°C	12.84	13.82	12.87	12.47
Field ORP	mvolts	-71.4	-81.5	-90.5	-198
pe from Fe ²⁺ /Fe ³⁺ , Fe(OH) ₃ (a)	--	3.93	4.78	4.14	4.16
Field Conductivity	µmhos/cm	378	468	485	507
Calcium	mg/L	44	63	68	65
Magnesium	mg/L	12	16	16	16
Potassium	mg/L	7	8	8	7
Sodium	mg/L	15	16	19	22
Silica as SiO ₂	mg/L	14	13	14	13
Chloride	mg/L	9	11	5	5
Fluoride	mg/L	< 0.1	< 0.2	< 0.2	0.1
Sulfate	mg/L	76	80	118	119
Total Alkalinity (as CaCO ₃)	mg/L	104	163	145	146
Bicarbonate as HCO ₃	mg/L	126	199	177	179
Total Dissolved Solids (180)	mg/L	240	300	340	340
Ammonia Nitrogen (As N)	mg/L	0.1	0.1	0.1	0.6
Dissolved Aluminum	mg/L	0.000793	0.00288	0.00532	0.000884
Dissolved Arsenic	mg/L	0.025	0.004	0.009	0.023
Dissolved Barium	mg/L	0.029	0.032	0.023	0.022
Dissolved Iron	mg/L	2.04	0.43	4.13	1.34
Dissolved Manganese	mg/L	0.06	0.07	0.16	0.09
Dissolved Selenium	mg/L	< 0.001	0.002	0.019	0.001
Dissolved Uranium	mg/L	0.044	0.794	0.511	3.22
Radium 226 (Dissolved)	pCi/L	296 ± 2.5	458 ± 3.1	1250 ± 5.1	898 ± 4.3
Radium 228 (Dissolved)	pCi/L	3.7 ± 1.5	4.8 ± 1.6	21.3 ± 2.3	15.8 ± 2.1
Gross Alpha (Dissolved)	pCi/L	509 ± 9.9	1420 ± 18.0	2130 ± 21.8	4050 ± 30.0
log P _{CO2}	atm	-1.3	-1.0	-1.0	-1.1
Calcite Saturation Index	--	-1.58	-1.30	-1.45	-1.33
Chalcedony Saturation Index	--	0.07	0.02	0.07	0.04
Speciated Charge Balance	%	2.26	1.43	3.53	2.66

a – aluminum and barium concentrations were below analytical detection limits of 0.1 mg/L, values shown were calculated from solubilities of Ca-montmorillonite and barite, respectively

note – carbonate (as CO₃²⁻), nitrate-N, and dissolved beryllium, boron, cadmium, chromium, copper, lead, mercury, molybdenum, nickel, vanadium and zinc were below analytical detection limits in all samples

Table C.3-8. Production zone groundwater quality (contd)

Well		B-5	B-6	B-7	B-8
Sample Date		3/8/2016	3/8/2016	3/8/2016	3/8/2016
Lab pH	s.u.	7.8	7.5	7.9	7.9
Field pH	s.u.	6.5	6.3	6.4	6.6
Field Temperature	°C	14.06	13.71	14.97	13.93
Field ORP	mvolts	-100	-192	-42.6	-165
pe from Fe ²⁺ /Fe ³⁺ , Fe(OH) ₃ (a)	--	3.97	3.77	3.82	3.58
Field Conductivity	µmhos/cm	378	478	444	440
Calcium	mg/L	48	59	64	60
Magnesium	mg/L	12	15	16	15
Potassium	mg/L	7	8	8	7
Sodium	mg/L	10	18	12	13
Silica as SiO ₂	mg/L	13	14	13	12
Chloride	mg/L	8	8	10	10
Fluoride	mg/L	0.2	0.1	0.2	0.2
Sulfate	mg/L	56	104	66	67
Total Alkalinity (as CaCO ₃)	mg/L	131	132	167	157
Bicarbonate as HCO ₃	mg/L	160	162	204	192
Total Dissolved Solids (180)	mg/L	230	310	290	280
Ammonia Nitrogen (As N)	mg/L	0.2	0.4	0.1	0.1
Dissolved Aluminum ^a	mg/L	0.000822	0.000765	0.000960	528
Dissolved Arsenic	mg/L	0.004	0.009	0.008	0.004
Dissolved Barium ^a	mg/L	0.041	0.026	0.040	0.037
Dissolved Iron	mg/L	0.61	3.24	1.13	0.7
Dissolved Manganese	mg/L	0.07	0.08	0.13	0.07
Dissolved Selenium	mg/L	0.023	0.005	0.005	0.007
Dissolved Uranium	mg/L	0.264	0.360	0.393	0.899
Radium-226 (Dissolved)	pCi/L	377 ± 2.9	601 ± 3.5	378 ± 2.7	544 ± 3.3
Radium-228 (Dissolved)	pCi/L	3.9 ± 1.6	5.0 ± 1.9	5.6 ± 1.6	7.4 ± 1.9
Gross Alpha (Dissolved)	pCi/L	825 ± 12.7	1370 ± 16.5	847 ± 13.4	1530 ± 17.2
log P _{CO2}	atm	-1.3	-1.2	-1.2	-1.4
Calcite Saturation Index	--	-1.27	-1.38	-1.09	-1.00
Chalcedony Saturation Index	--	0.02	0.06	0.01	-0.01
Speciated Charge Balance	%	0.23	2.94	2.97	2.06

a – aluminum and barium concentrations were below analytical detection limits of 0.1 mg/L, values shown were calculated from solubilities of Ca-montmorillonite and barite, respectively

note – carbonate (as CO₃²⁻), nitrate-N, and dissolved beryllium, boron, cadmium, chromium, copper, lead, mercury, molybdenum, nickel, vanadium and zinc were below analytical detection limits in all samples

Table C.3-8. Production zone groundwater quality (contd)

Well		B-9	B-10	B-11	B-12
Sample Date		3/8/2016	3/8/2016	3/8/2016	3/8/2016
Lab pH	s.u.	7.8	7.9	7.9	7.7
Field pH	s.u.	6.3	6.4	6.6	6.4
Field Temperature	°C	13.40	13.88	13.51	12.08
Field ORP	mvolts	-40.3	-87.4	-104	-53.7
pe from Fe ²⁺ /Fe ³⁺ , Fe(OH) ₃ (a)	--	3.82	4.17	4.16	3.35
Field Conductivity	µmhos/cm	544	763	660	541
Calcium	mg/L	80	117	97	69
Magnesium	mg/L	19	29	22	18
Potassium	mg/L	8	10	8	8
Sodium	mg/L	16	20	18	15
Silica as SiO ₂	mg/L	15	15	14	13
Chloride	mg/L	16	28	18	15
Fluoride	mg/L	0.2	0.1	0.2	0.1
Sulfate	mg/L	101	152	98	100
Total Alkalinity (as CaCO ₃)	mg/L	187	254	244	163
Bicarbonate as HCO ₃	mg/L	228	310	298	199
Total Dissolved Solids (180)	mg/L	370	540	440	350
Ammonia Nitrogen (As N)	mg/L	0.4	< 0.1	< 0.1	0.2
Dissolved Aluminum	mg/L	0.00141	0.000341	0.000370	0.000510
Dissolved Arsenic	mg/L	0.016	0.001	0.001	0.005
Dissolved Barium	mg/L	0.028	0.024	0.031	0.026
Dissolved Iron	mg/L	2.44	0.55	0.18	4.39
Dissolved Manganese	mg/L	0.17	0.12	0.08	0.10
Dissolved Selenium	mg/L	0.002	0.004	0.007	0.004
Dissolved Uranium	mg/L	0.866	2.08	1.23	0.199
Radium 226 (Dissolved)	pCi/L	280 ± 2.0	349 ± 2.3	280 ± 2.0	360 ± 2.3
Radium 228 (Dissolved)	pCi/L	< 1	< 1	< 1	9.5 ± 1.8
Gross Alpha (Dissolved)	pCi/L	1190 ± 16.1	2380 ± 25.1	1610 ± 19.9	1050 ± 15.6
log P _{CO2}	atm	-1.0	-1.0	-1.2	-1.2
Calcite Saturation Index	--	-1.09	-0.72	-0.63	-1.14
Chalcedony Saturation Index	--	0.09	0.08	0.06	0.04
Speciated Charge Balance	%	2.38	2.13	1.60	1.75

a – aluminum and barium concentrations were below analytical detection limits of 0.1 mg/L, values shown were calculated from solubilities of Ca-montmorillonite and barite, respectively

note – carbonate (as CO₃²⁻), nitrate-N, and dissolved beryllium, boron, cadmium, chromium, copper, lead, mercury, molybdenum, nickel, vanadium and zinc were below analytical detection limits in all samples

Table C.3-8. Production zone groundwater quality (contd)

Well		B-13	B-14	B-15	B-16
Sample Date		3/8/2016	3/8/2016	3/8/2016	3/8/2016
Lab pH	s.u.	8.0	7.9	7.7	7.8
Field pH	s.u.	6.6	6.3	6.2	6.2
Field Temperature	°C	14.64	13.60	14.50	14.74
Field ORP	mvolts	-115	-109	-78.9	-24.2
pe from Fe ²⁺ /Fe ³⁺ , Fe(OH) ₃ (a)	--	3.44	4.06	4.28	4.14
Field Conductivity	µmhos/cm	740	341	192	387
Calcium	mg/L	106	45	23	50
Magnesium	mg/L	27	11	5	13
Potassium	mg/L	10	7	4	7
Sodium	mg/L	25	12	8	12
Silica as SiO ₂	mg/L	12	12	15	14
Chloride	mg/L	12	6	2	9
Fluoride	mg/L	0.2	0.2	0.2	0.2
Sulfate	mg/L	153	53	24	67
Total Alkalinity (as CaCO ₃)	mg/L	256	127	76	128
Bicarbonate as HCO ₃	mg/L	313	155	92	156
Total Dissolved Solids (180)	mg/L	530	230	130	260
Ammonia Nitrogen (As N)	mg/L	0.1	< 0.1	0.1	0.3
Dissolved Aluminum	mg/L	0.000495	0.00193	0.00277	0.00360
Dissolved Arsenic	mg/L	0.005	0.003	0.020	0.004
Dissolved Barium	mg/L	0.024	0.041	0.073	0.037
Dissolved Iron	mg/L	1.01	1.16	1.26	2.61
Dissolved Manganese	mg/L	0.35	0.06	0.04	0.09
Dissolved Selenium	mg/L	0.010	0.001	< 0.001	< 0.001
Dissolved Uranium	mg/L	0.730	0.212	0.064	0.228
Radium-226 (Dissolved)	pCi/L	740 ± 3.3	460 ± 2.7	417 ± 2.5	276 ± 2.0
Radium-228 (Dissolved)	pCi/L	5.5 ± 2.2	7.8 ± 1.7	7.1 ± 1.8	4.4 ± 1.6
Gross Alpha (Dissolved)	pCi/L	1920 ± 23.2	1030 ± 14.1	942 ± 12.9	767 ± 12.7
log P _{CO2}	atm	-1.2	-1.2	-1.3	-1.1
Calcite Saturation Index	--	-0.59	-1.44	-1.99	-1.53
Chalcedony Saturation Index	--	-0.02	-0.01	0.08	0.04
Speciated Charge Balance	%	1.67	0.08	-0.50	2.09

a – aluminum and barium concentrations were below analytical detection limits of 0.1 mg/L, values shown were calculated from solubilities of Ca-montmorillonite and barite, respectively

note – carbonate (as CO₃²⁻), nitrate-N, and dissolved beryllium, boron, cadmium, chromium, copper, lead, mercury, molybdenum, nickel, vanadium and zinc were below analytical detection limits in all samples

Table C.3-8. Production zone groundwater quality (contd)

Well		B-17	B-18	B-19
Sample Date		3/8/2016	3/8/2016	3/8/2016
Lab pH	s.u.	7.9	8.0	7.9
Field pH	s.u.	6.6	6.8	6.4
Field Temperature	°C	13.48	14.20	14.30
Field ORP	mvolts	-120	-143	-111
pe from $\text{Fe}^{2+}/\text{Fe}^{3+}$, $\text{Fe}(\text{OH})_3(\text{a})$	--	3.07	2.63	3.98
Field Conductivity	$\mu\text{mhos/cm}$	463	294	311
Calcium	mg/L	59	39	41
Magnesium	mg/L	15	8	10
Potassium	mg/L	7	6	5
Sodium	mg/L	15	9	11
Silica as SiO_2	mg/L	13	14	12
Chloride	mg/L	17	5	5
Fluoride	mg/L	0.2	0.2	0.2
Sulfate	mg/L	85	31	46
Total Alkalinity (as CaCO_3)	mg/L	127	108	115
Bicarbonate as HCO_3	mg/L	155	132	141
Total Dissolved Solids (180)	mg/L	300	180	210
Ammonia Nitrogen (As N)	mg/L	0.2	0.2	0.2
Dissolved Aluminum ^a	mg/L	0.000402	0.000269	0.00105
Dissolved Arsenic	mg/L	0.025	0.005	0.010
Dissolved Barium ^a	mg/L	0.030	0.064	0.046
Dissolved Iron	mg/L	1.67	1.01	0.66
Dissolved Manganese	mg/L	0.06	0.12	0.07
Dissolved Selenium	mg/L	< 0.001	< 0.001	< 0.001
Dissolved Uranium	mg/L	0.325	0.062	0.688
Radium-226 (Dissolved)	pCi/L	196 ± 1.8	179 ± 1.7	431 ± 2.6
Radium-228 (Dissolved)	pCi/L	4.5 ± 1.4	3.4 ± 1.4	7.2 ± 1.9
Gross Alpha (Dissolved)	pCi/L	704 ± 12.3	327 ± 7.8	1190 ± 14.6
log P_{CO_2}	atm	-1.5	-1.8	-1.4
Calcite Saturation Index	--	-1.06	-1.04	-1.40
Chalcedony Saturation Index	--	0.03	0.05	-0.02
Speciated Charge Balance	%	3.15	4.21	1.74

a – aluminum and barium concentrations were below analytical detection limits of 0.1 mg/L, values shown were calculated from solubilities of Ca-montmorillonite and barite, respectively

note – carbonate (as CO_3^{2-}), nitrate-N, and dissolved beryllium, boron, cadmium, chromium, copper, lead, mercury, molybdenum, nickel, vanadium and zinc were below analytical detection limits in all samples

Iron and manganese concentrations are elevated in the March 2016 Mine Unit 1 groundwater samples relative to the RTVs. These concentrations likely result from the reducing conditions produced by sodium sulfide addition during groundwater restoration and consequent reductive dissolution of iron and manganese oxides and hydroxides. All iron and manganese groundwater concentrations exceed their respective RTVs and most concentrations exceed the secondary drinking water standards of 0.3 mg/L for iron and 0.05 mg/L for manganese. The distribution of iron concentrations in the March 2016 Mine Unit 1 groundwater samples is illustrated in Figure C.3-5.

Selenium concentrations in the Mine Unit 1 groundwater samples are low, and are below the 0.05 mg/L drinking water standard in all March 2016 samples. Uranium concentrations exceed the RTV in most of the March 2016 groundwater samples, and all concentrations exceed the drinking water standard. Radium-226 concentrations were below the RTV in the March 2016 groundwater samples from all but two of the production-zone monitoring wells (Wells B-3 and B-4). The distributions of uranium and radium-226+228 in the March 2016 Mine Unit 1 groundwater samples are illustrated in Figures C.3-6 and C.3-7, respectively.

Other trace metals, such as molybdenum and zinc, were below analytical detection limits in the production zone groundwater before ISR and after groundwater restoration (Attachment C-1). Consequently, these constituents were not included in the groundwater transport model.

3.4 Downgradient Aquifer Sediments and Groundwater

Aquifer sediment cores were collected from four locations downgradient of the Mine Unit 1 production zone (Figure C.3-2). Swapp (2016) characterized five sediment samples from core DG-1 as arkosic sandstone containing quartz, albite, K-feldspar and clay. Clays in these samples were identified as smectite, with smaller amounts of kaolinite, illite and chlorite. Calcite and organic carbon were visible in hand specimen and detected by SEM/EDS examination in one sample (451– 452 ft). Pyrite was not observed during visual examination of the samples. SEM/EDS examination indicated the presence of pyrite in all samples, although only rare pyrite was observed in the sample from 456 – 457 ft and most pyrite in that sample appeared to be replaced by iron oxides and hydroxides.

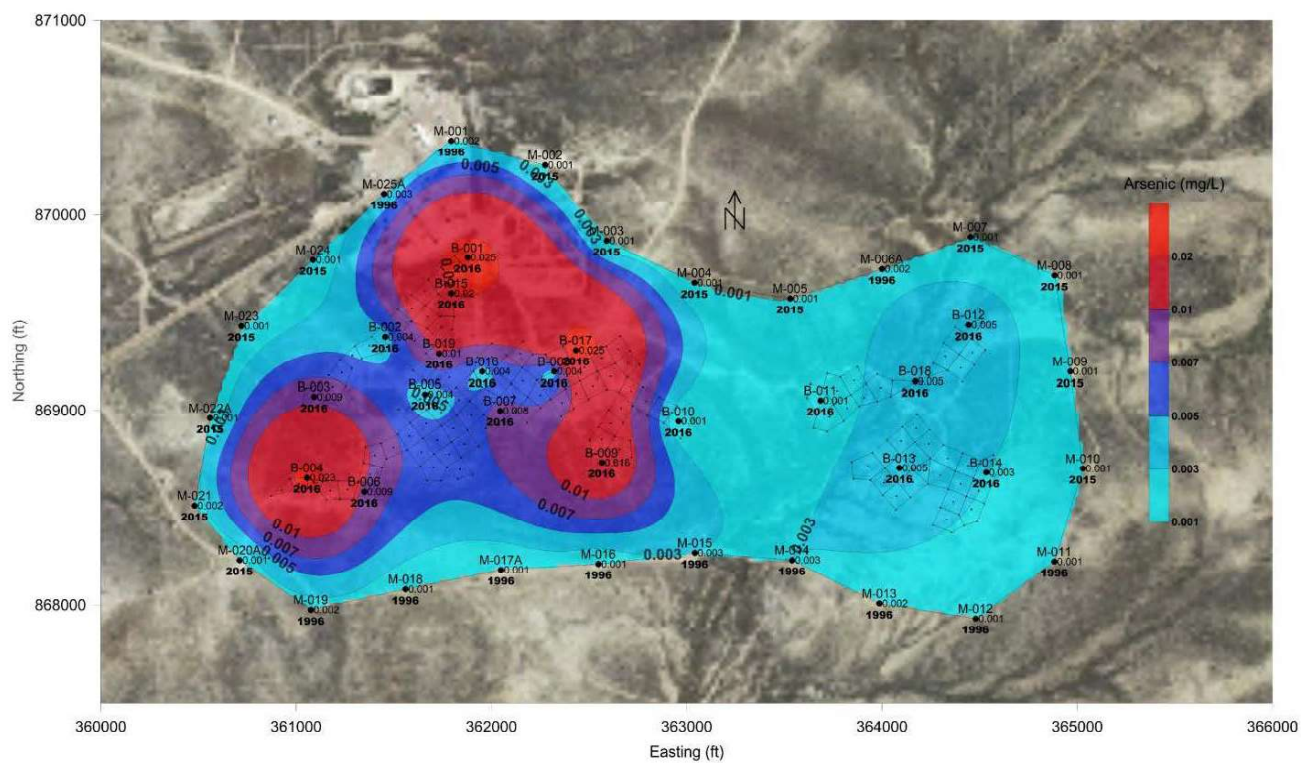


Figure C.3-4. Arsenic concentration contour map, March 2016

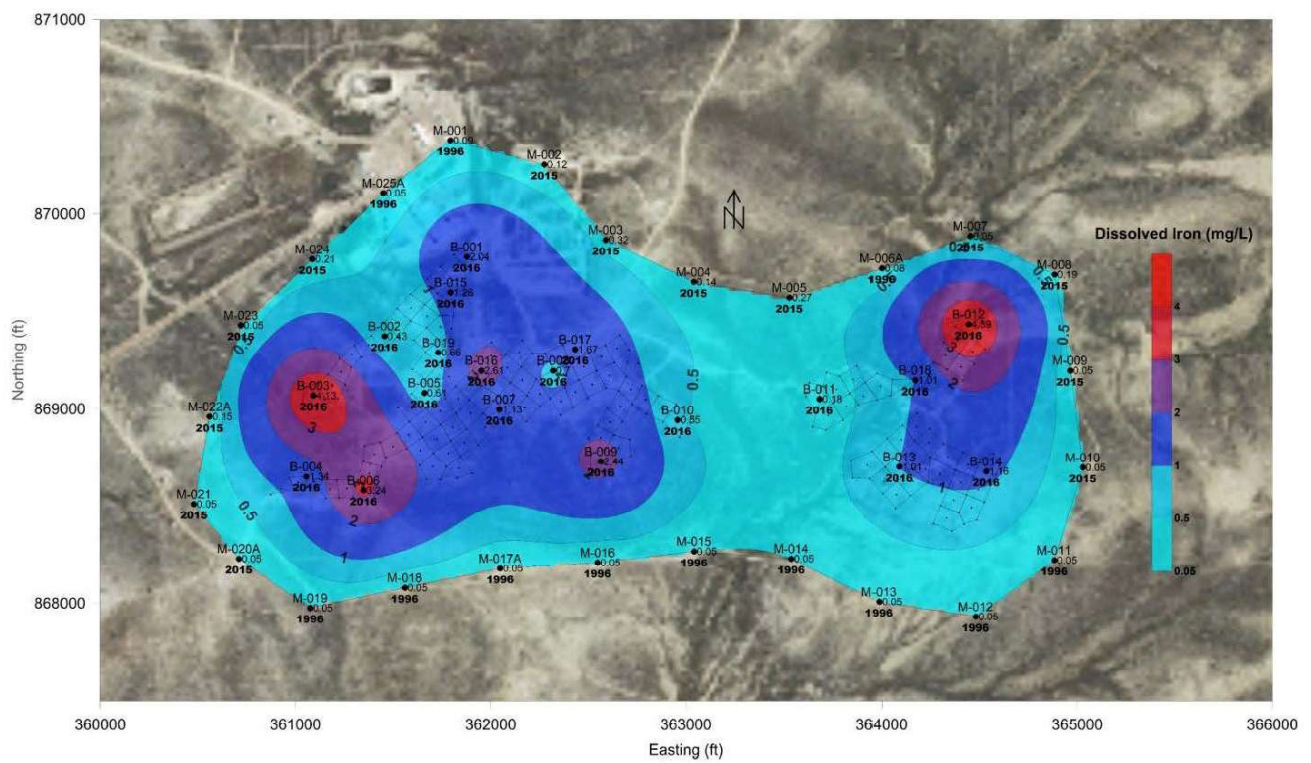


Figure C.3-5. Iron concentration contour map, March 2016

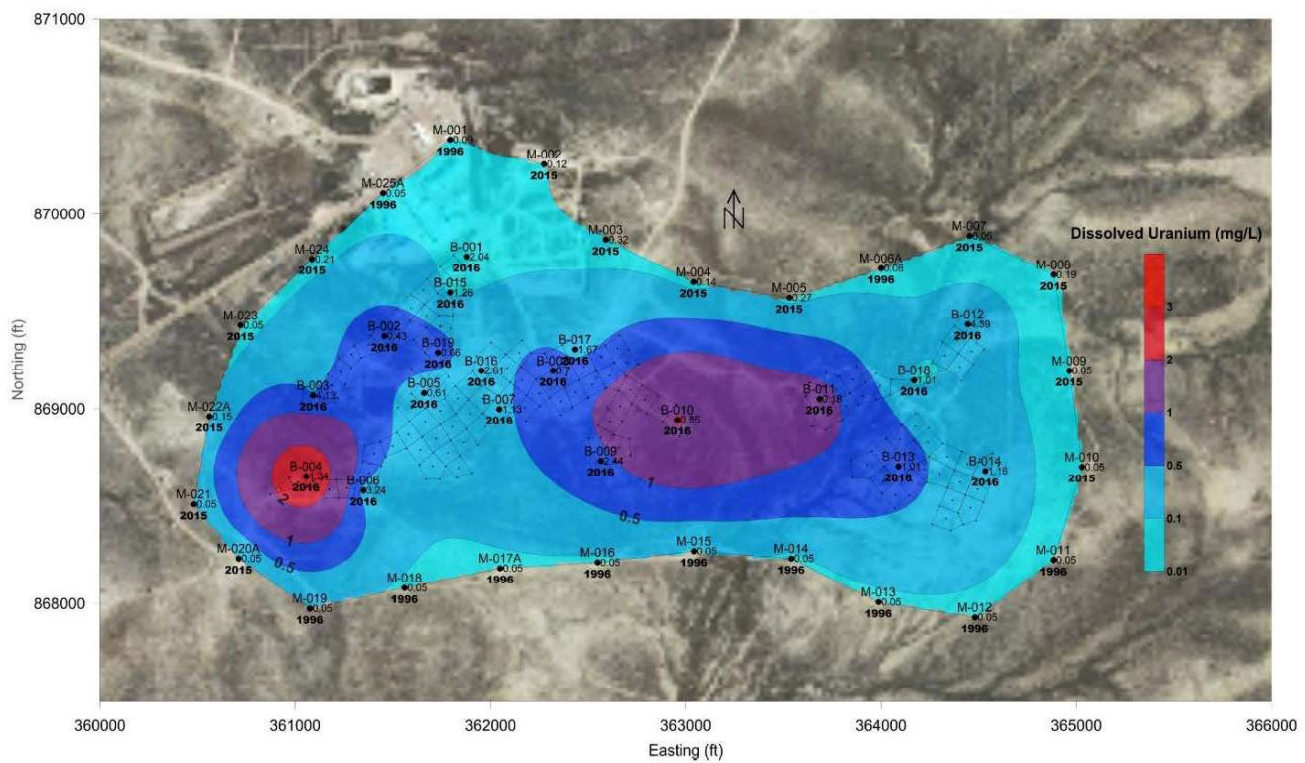


Figure C.3-6. Uranium concentration contour map, March 2016

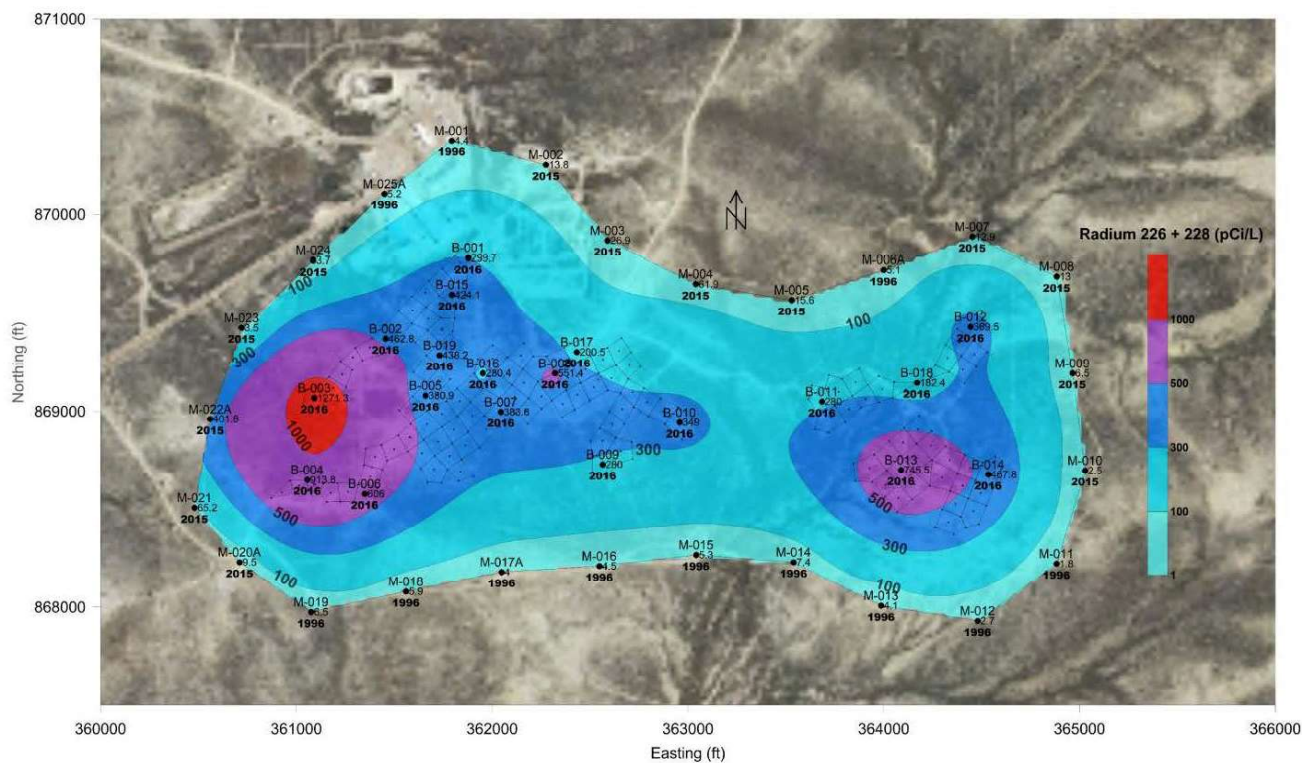


Figure C.3-7. Radium-226+228 concentration contour map, March 2016

Downgradient samples from core locations DG-2, DG-3 and DG-4 were also arkosic sandstones, consisting primarily of quartz, K-feldspar, albite and mica (Table C.3-2). All samples were poorly sorted and gray in appearance, with some visible organic carbon (Attachment C-3). Calcite cement was noted in the DG-3 and DG-4 core (Attachment C-3). Although pyrite was not noted during visual inspection of hand specimens, pyritic sulfur concentrations in the downgradient core samples ranged from 0.17% to 0.54%, with detectable organic sulfur concentrations (Table C.3-3).

Downgradient water quality samples had moderate field pH values, and major element compositions were dominated by calcium and bicarbonate, with low concentrations of sodium, magnesium and sulfate (Table C.3-9). Comparison of chloride, total alkalinity and uranium concentrations (Figure C.3-8) and other constituents from the pre-operational period to post-restoration demonstrates that there have been no significant changes in the downgradient groundwater chemistry during or since ISR, consistent with the lack of excursions during Mine Unit 1 operations.

Measurable iron and manganese concentrations are present in most of the downgradient groundwater samples, consistent with reducing conditions downgradient of the uranium roll-front deposit (Table C.3-9). The dissolved iron concentration in the sample from Well M-3 slightly exceeds the 0.3 mg/L secondary drinking water standard for iron. Concentrations of many constituents downgradient of Mine Unit 1 are below drinking water standards, including chloride, sulfate, arsenic, selenium and uranium (Table C.3-9). However, radium-226+228 concentrations in all samples except from Well M-10 exceed the 5 pCi/L drinking water standard.

3.5 Sequential Extractions

Sequential extractions were performed on sediment samples from the production zone, unaltered mineralized sediments and downgradient aquifer sediment samples to investigate the association of various constituents with mineral phases. These results provide important information on the initial mineralogical or adsorption conditions for constituents in the aquifer sediments for the transport calculations.

Table C.3-9. Downgradient groundwater quality

Well Number		M-2	M-3	M-4	M-5
Date		7/8/2015	7/8/2015	7/8/2015	7/8/2015
Field pH	s.u.	7.3	7.3	7.3	7.3
Field Temperature	°C	12.74	13.48	13.83	13.16
Field ORP	mvolts	-107.8	-98.6	-102.6	-107
Field conductivity	µmhos/cm	534	547	555	543
Calcium	mg/L	68	69	73	71
Magnesium	mg/L	17	17	18	17
Potassium	mg/L	8	8	8	8
Sodium	mg/L	21	22	21	21
Silica as SiO ₂	mg/L	17	17	18	17
Chloride	mg/L	3	3	4	3
Fluoride	mg/L	0.3	0.3	0.3	0.3
Sulfate	mg/L	94	96	99	100
Total Alkalinity (as CaCO ₃)	mg/L	199	200	204	200
Bicarbonate as HCO ₃	mg/L	242	244	249	244
Total Dissolved Solids	mg/L	370	380	380	380
Nitrate-Nitrite Nitrogen	mg N/L	< 0.1	< 0.1	< 0.1	< 0.1
Ammonia Nitrogen	mg N/L	0.1	0.1	< 0.1	< 0.1
Dissolved Aluminum ^a	mg/L	0.00030	0.00033	0.00033	0.00031
Dissolved Arsenic	mg/L	< 0.001	< 0.001	< 0.001	< 0.001
Dissolved Barium ^a	mg/L	0.028	0.028	0.029	0.027
Dissolved Iron	mg/L	0.12	0.32	0.14	0.27
Dissolved Manganese	mg/L	0.02	0.02	0.02	0.03
Dissolved Selenium	mg/L	0.001	0.002	0.001	< 0.001
Dissolved Uranium	mg/L	0.0153	0.0146	0.0122	0.019
Radium-226 (Dissolved)	pCi/L	12.7 ± 0.4	24.5 ± 0.6	60.7 ± 0.9	14.2 ± 0.4
Radium-228 (Dissolved)	pCi/L	1.1 ± 1.1	2.4 ± 1.2	1.2 ± 1.2	1.4 ± 1.1
Gross Alpha (Dissolved)	pCi/L	30.0 ± 2.7	38.1 ± 3.2	61.2 ± 4.0	32.0 ± 2.9
Gross Beta (Dissolved)	pCi/L	18.4 ± 2.0	19.9 ± 2.0	30.4 ± 2.3	18.4 ± 2.0
log P _{CO2}	atm	-2.0	-2.0	-2.0	-2.0
Calcite Saturation Index	--	-0.12	-0.12	-0.06	-0.11
Chalcedony Saturation Index	--	0.15	0.14	0.16	0.15

a – aluminum and barium concentrations were below analytical detection limits of 0.1 mg/L, values shown were calculated from solubilities of Ca-montmorillonite and barite, respectively

note – carbonate (as CO₃²⁻), nitrate-N, and dissolved beryllium, boron, cadmium, chromium, copper, lead, mercury, molybdenum, nickel, vanadium and zinc were below analytical detection limits in all samples

Table C.3-9. Downgradient groundwater quality (contd)

Well Number		M-7	M-8	M-9	M-10
Date		7/8/2015	7/8/2015	7/8/2015	7/8/2015
Field pH	s.u.	7.6	7.4	7.3	7.3
Field Temperature	°C	n.m.	12.98	12.98	12.8
Field ORP	mvolts	n.m.	-116.4	44.2	131.5
Field conductivity	µmhos/cm	560	527	524	542
Calcium	mg/L	64	64	62	62
Magnesium	mg/L	15	15	14	14
Potassium	mg/L	8	8	8	8
Sodium	mg/L	23	24	21	21
Silica as SiO ₂	mg/L	17	16	15	15
Chloride	mg/L	3	4	3	3
Fluoride	mg/L	0.3	0.3	0.3	0.3
Sulfate	mg/L	107	103	93	90
Total Alkalinity (as CaCO ₃)	mg/L	188	175	177	182
Bicarbonate as HCO ₃	mg/L	229	214	213	220
Total Dissolved Solids	mg/L	360	350	330	340
Nitrate-Nitrite Nitrogen	mg N/L	< 0.1	< 0.1	0.3	0.6
Ammonia Nitrogen	mg N/L	0.2	< 0.1	< 0.1	< 0.1
Dissolved Aluminum ^a	mg/L	0.00051	0.00036	0.00036	0.00037
Dissolved Arsenic	mg/L	< 0.001	< 0.001	< 0.001	< 0.001
Dissolved Barium ^a	mg/L	0.025	0.025	0.027	0.028
Dissolved Iron	mg/L	0.05	0.19	< 0.05	< 0.05
Dissolved Manganese	mg/L	0.02	0.02	0.02	0.04
Dissolved Selenium	mg/L	0.004	0.001	0.003	0.007
Dissolved Uranium	mg/L	0.015	0.012	0.025	0.027
Radium-226 (Dissolved)	pCi/L	12.9 ± 0.4	13.0 ± 0.4	5.4 ± 0.3	2.5 ± 0.2
Radium-228 (Dissolved)	pCi/L	< 1	< 1	1.1 ± 1.1	< 1
Gross Alpha (Dissolved)	pCi/L	20.2 ± 2.3	17.8 ± 2.0	33.5 ± 2.7	26.4 ± 2.4
Gross Beta (Dissolved)	pCi/L	17.0 ± 2.0	13.4 ± 1.6	16.1 ± 1.7	15.2 ± 1.8
log P _{CO2}	atm	-2.3	-2.1	-2.0	-2.1
Calcite saturation index	--	0.10	-0.17	-0.23	-0.18
Chalcedony saturation index	--	0.15	0.12	0.09	0.10

a – aluminum and barium concentrations were below analytical detection limits of 0.1 mg/L, values shown were calculated from solubilities of Ca-montmorillonite and barite, respectively

n.m. – not measured, well head could not be removed from Well M-7

note – carbonate (as CO₃²⁻), nitrate-N, and dissolved beryllium, boron, cadmium, chromium, copper, lead, mercury, molybdenum, nickel, vanadium and zinc were below analytical detection limits in all samples

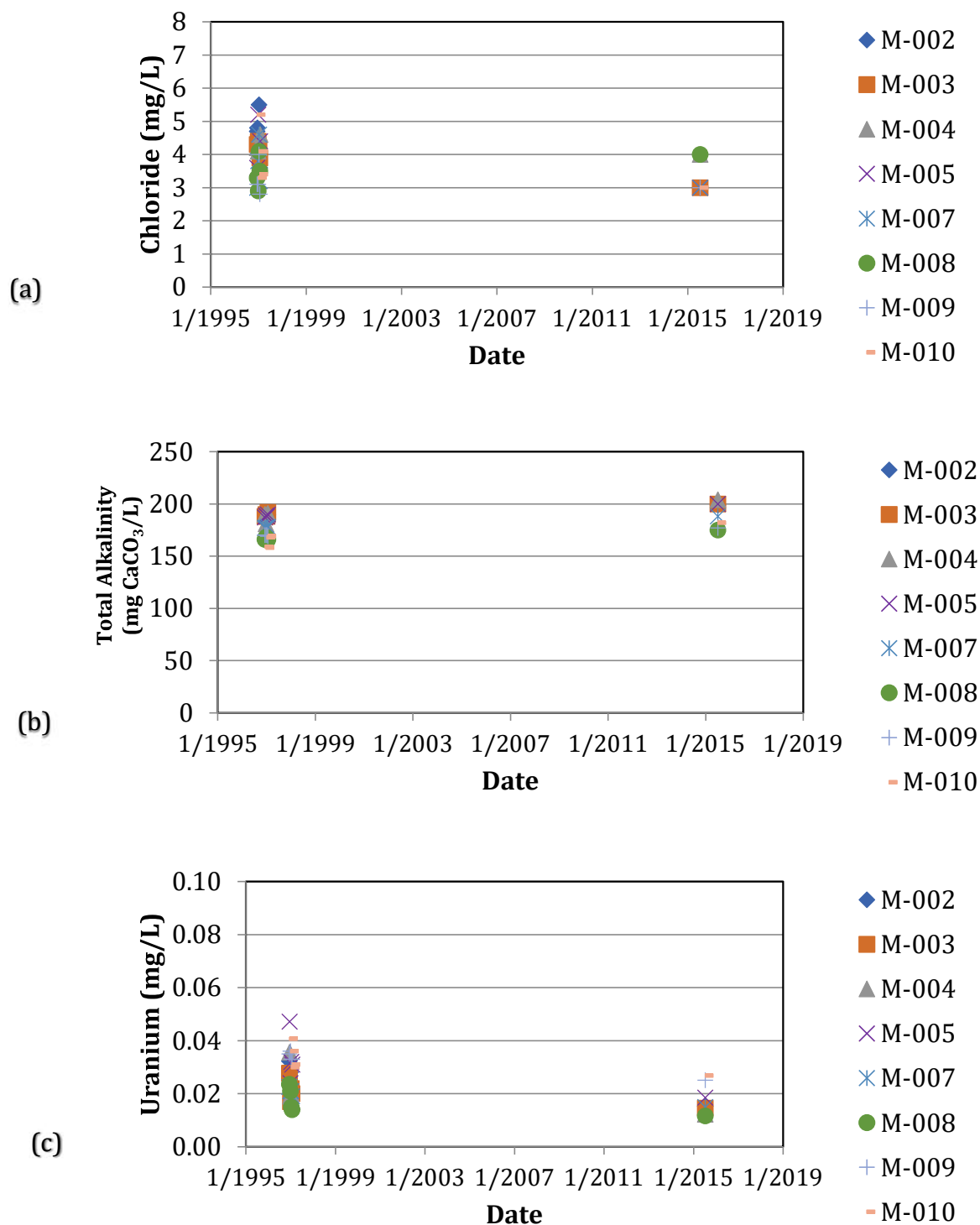


Figure C.3-8. Concentrations of (a) chloride, (b) total alkalinity and (c) uranium in groundwater samples from downgradient monitoring ring wells M-2, M-3, M-4, M-5, M-7, M-8, M-9 and M-10

The sequential extraction method described by Land et al. (2002) was used to identify the likely mineralogical associations of the constituents in the aquifer sediments. This extraction method is designed to distinguish between five fractions:

- I. Acetate-extractable [CH_3COONa] – exchangeable, adsorbed and carbonate
- II. Tetrasodium-pyrophosphate extractable [$\text{Na}_4\text{P}_2\text{O}_7$] – humics
- III. Lower concentration hydroxylamine hydrochloride extractable [0.25 M $\text{NH}_2\text{OH}\cdot\text{HCl}$] – amorphous iron oxides/hydroxides and manganese oxides
- IV. Higher concentration hydroxylamine hydrochloride extractable [1 M $\text{NH}_2\text{OH}\cdot\text{HCl}$] – crystalline iron oxides
- V. Potassium chlorate-extractable – organics and sulfides

The carbonate (total inorganic carbon) concentrations in the analyzed core sediment samples are very low to below-detection (Tables C.3-3 and C.3-7), so the results of Step I extractions mainly represent aquifer sediment exchangeable and adsorbed constituents. The results of the Step I extractions are summarized in Table C.3-10. The most important exchangeable cations are calcium and magnesium, with smaller amounts of potassium and iron. Uranium may also be present as an exchangeable cation or may be sorbed on mineral surfaces. The median cation exchange capacity calculated from the Step I extractions using the seven production zone samples is 10.25 meq/100 g. This cation exchange capacity falls within the range of 4.3 to 20 meq/100 g reported for Mine Unit A at the SRH site (Intera 2013). The median cation exchange capacity for the two downgradient samples is 7.65 meq/100g, which is also consistent with the range cited by Intera (2013) for Mine Unit A.

Steps II and V are selective for constituents associated with organics, sulfides and other reduced phases in the sediments. Steps III and IV are selective for ferric and manganese oxides and hydroxides and are designed to distinguish between amorphous oxides and hydroxides and crystalline oxides (Land et al. 2002), with the expectation that amorphous solids are more reactive and more likely to release adsorbed and coprecipitated constituents. It was anticipated that production-zone aquifer sediments could have relatively high proportions of amorphous iron oxides and hydroxides because of the rapid oxidation of pyrite during ISR. On the other hand, in aquifer sediments unaffected by ISR, such as sample ST-2 463-464 ft and the downgradient aquifer sediment samples (DG-2 487.5-488.5 and DG-4 516-517 ft), iron might be expected to be present as a more crystalline oxide. However, the sequential extraction results did not follow the expected pattern (Table C.3-11). Instead, relatively similar Step III iron concentrations were reported for all samples, with wide variations in the Step IV iron concentrations (Figure C.3-9). The Step IV results for sample ST-5 499-500 ft indicated that it contained an XRD-detectable amount of crystalline iron oxide (3.4 wt%), but the presence of crystalline iron oxide was not detected by XRD in this sample (Table C.3-6). Consequently, it appears that



This extraction method is designed to distinguish between five fractions:

Steps III and IV were not adequately selective for amorphous versus crystalline iron and manganese phases. It was therefore assumed that all iron and manganese solids extracted in Steps III and IV were available for reductive dissolution. Using the combined results of Steps III and IV to estimate available iron oxide and hydroxide solid phases should have a conservative effect on the transport calculations because it maximizes the amount of iron and manganese solids available in the production zone sediments for release of adsorbed constituents to the groundwater through desorption or by reductive dissolution of the iron and manganese solids. The possible effect of assuming higher iron oxide concentrations in the downgradient sediments was tested in sensitivity calculations of the transport model.

Table C.3-10. CEC data for production zone and downgradient sediment samples

	ST-2 472-473	ST-3 463-464	ST-3 474-475	ST-4 479-480	ST-4 488-489	ST-5 494-495	ST-5 499-500	DG-2 487.5-488.5	DG-4 516-517
Cation	production zone							downgradient	
Calcium (eq/kg)	0.0719	0.0299	0.1183	0.0569	0.0554	0.0614	0.0823	0.0554	0.0524
Iron (eq/kg)	0.0006	0.0058	0.0000	0.0011	0.0000	0.0017	0.0005	0.0000	0.0002
Magnesium (eq/kg)	0.0247	0.0197	0.0370	0.0197	0.0222	0.0247	0.0296	0.0197	0.0148
Potassium (eq/kg)	0.0123	0.0061	0.0169	0.0138	0.0092	0.0146	0.0084	0.0054	0.0046
Uranium (eq/kg)	0.0003	0.0000	0.0001	0.0000	0.0002	0.0001	0.0001	0.0005	0.0000
Radium-226 (eq/kg)	1.06E-09	1.81E-10	6.64E-11	3.45E-11	7.43E-10	7.96E-11	1.75E-10	1.38E-10	1.54E-11
Cation Exchange Capacity (eq/kg)	0.1098	0.0617	0.1723	0.0915	0.0870	0.1025	0.1211	0.0810	0.0720
Cation Exchange Capacity (meq/100 g)	10.98	6.17	17.23	9.15	8.70	10.25	12.11	8.10	7.20
Median Cation Exchange Capacity (eq/kg)	0.1025							0.0765	

Table C.3-11. Iron oxide and hydroxide sequential extraction results

Sample	Step III Iron (mg Fe/kg sediment)	Step IV Iron (mg Fe/kg sediment)	Step III Fe(OH) ₃ (s) (wt%)	Step IV Fe(OH) ₃ (s) (wt%)	Step III plus Step IV Iron (moles/kg sediment)
ST-2 472-473 ft	3,360	928	0.6%	0.2%	0.0768
ST-3 463-464 ft	1,971	472	0.4%	0.1%	0.0437
ST-3 474-475 ft	1,287	3,056	0.2%	0.6%	0.0778
ST-4 479-480 ft	1,995	3,364	0.4%	0.6%	0.0960
ST-4 488-489 ft	2,532	884	0.5%	0.2%	0.0612
ST-5 494-495 ft	1,791	6,880	0.3%	1.3%	0.1553
ST-5 499-500 ft	2,943	17,960	0.6%	3.4%	0.3743
Production Zone Median	2,268	4,792	0.4%	0.9%	0.0778
ST-2 463-464 ft (mineralized)	2,832	808	0.5%	0.2%	0.0652
DG-2 487.5-488.5 ft (downgradient)	2,649	612	0.5%	0.1%	0.0584
DG-4 516-517 ft (downgradient)	2,271	600	0.4%	0.1%	0.0514
Downgradient Arithmetic Mean	2,460	606	0.5%	0.1%	0.0549

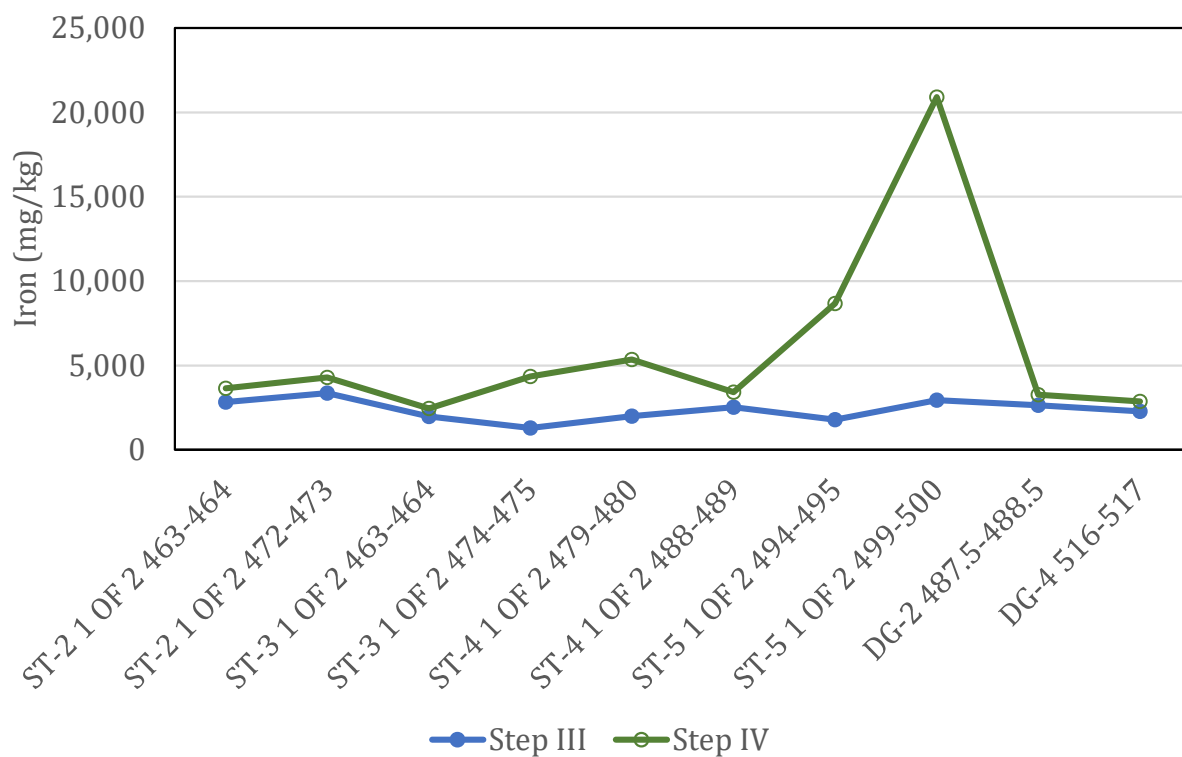


Figure C.3-9. Sequential extraction results for Step III (amorphous iron oxides and hydroxides) and Step IV (crystalline iron oxides)

4.0 Transport Model

All geochemical modeling calculations were performed using PHREEQC (version 3, Parkhurst and Appelo 2013) and the Enchemica.R1.dat database. This database includes major-element data from the wateq4f.dat database, with updated uranium aqueous speciation data and solids solubility data, including the ternary complexes of uranyl [UO_2^{2+}] and carbonate [CO_3^{2-}] with alkaline earth metals (Dong and Brooks 2006, 2008). The Enchemica.R1.dat database also includes updated data for other constituents. The database and documentation of the aqueous speciation, solubility, surface complexation and ion exchange data in the database are provided in Attachment C-5.

4.1 Modeled Constituents

The transport model includes pH and major groundwater constituents. Arsenic, iron, manganese and uranium transport to the POE locations are included in the transport model because production zone groundwater concentrations have exceeded RTVs or drinking water standards for these constituents during stability monitoring. Radium-226+228 concentrations were below the RTV in all but three wells during the stability monitoring period, indicating that groundwater treatment adequately restored groundwater concentrations. Recent selenium concentrations in the production zone groundwater samples are below drinking water standards. However, radium-226+228 and selenium transport were included in the transport model to address their potential remobilization as geochemical conditions evolve over time in the restored production zone.

4.2 Conceptual Model

The conceptual model consists of the hydrologic and geochemical processes and the initial conditions included in transport modeling.

4.2.1 Flow Paths




Flow paths representative of transport from the Mine Unit 1 production zone were selected based on predicted long-term groundwater flow directions (Figure C.3-1, AquiferTek 2017). The six modeled flow paths extend from the upgradient monitoring ring through production-zone point of compliance (POC) wells to POE locations at the downgradient edge of the aquifer exemption boundary:

Flow Path A: M-21 → B-3 → B-2 → B-1 → M-2 → POE A

Flow Path B: M-20 → B-4 → B-5 → M-2/M-3 → POE B

Flow Path C: M-16/M-17 → B-10 → M-5 → POE C

Flow Path D: M-15 → B-18 → B-12 → M-7/M-8 → POE D

	Number: 1	Author: Vshea	Subject: Highlight	Date: 8/22/2018 5:00:08 PM
4.0 Transport Model				
	Number: 2	Author: Vshea	Subject: Highlight	Date: 8/22/2018 5:01:35 PM
However, radium-226+228 and selenium transport were included in the transport model to address their potential remobilization as geochemical conditions evolve over time in the restored production zone.				
	Number: 3	Author: Vshea	Subject: Highlight	Date: 8/22/2018 5:02:24 PM
4.2 Conceptual Model				

Flow Path E: M-14 → B-13 → B-12 → M-8 → POE E

Flow Path F: M-13 → B-14 → M-9 → POE F

These flow paths pass through locations with elevated arsenic, iron, manganese, radium-226+228, selenium and uranium concentrations; are geographically distributed across Mine Unit 1; and include 10 of the 19 production-zone monitoring well locations.

The distances along each flow path (Table C.4-1) were used to assign initial groundwater chemistry and sediment mineralogy in each cell in the transport model calculations. For calculation of these distances, it was assumed that wellfield flare could have resulted in alteration of the sediments and groundwater within 15.2 m (50 ft) upgradient and downgradient of production patterns and these locations were assigned to the production zone. Because additional downgradient transport could have occurred during ISR or after restoration was completed, an additional 20 m (66 ft) of the downgradient flow paths were assigned the same aquifer sediment and groundwater characteristics as the production zone. This assumption is conservative, because it is unlikely that the sediments in this part of the aquifer would be completely oxidized, and because this assumption increased the total masses of dissolved constituents in initial groundwater and shortened the downgradient portions of the flow paths. Examination of roll front maps confirmed that the production patterns in Mine Unit 1 extended to the downgradient limits of the roll fronts and little to no uranium mineralization would be present downgradient of the production zone.

Table C.4-1. Groundwater flow path distances from upgradient monitoring ring

Flow Path	A	B	C	D	E	F
Upgradient Edge of Production Zone (m)	213	130	268	373	160	137
POC Wells (m)	B-3: 279 B-2: 396 B-1: 570	B-4: 170 B-5: 391	B-10: 305	B-18: 407 B-12: 541	B-13: 221 B-12: 479	B-14: 265
Downgradient Edge of Production Zone (m)	610	513	335	585	522	309
POE Location (m)	808	816	681	715	651	539

4.2.2 Initial Groundwater Compositions

There are no identified operations or processes occurring upgradient of Mine Unit 1 that are likely to affect groundwater, so it is assumed that inflowing groundwater compositions will remain constant at the concentrations measured in the baseline (December 1996 to January 1997) and July 2015 samples from the upgradient monitoring ring wells. The composition of inflowing groundwater for Flow Path C was obtained by mixing equal proportions of the groundwater samples from Wells M-16 and M-17.

The production zone cells were assumed to have initial groundwater compositions equal to the closest production-zone monitoring well along the flow path. The initial groundwater compositions in cells downgradient of the production zone were assumed equal to the composition of samples from the downgradient monitoring ring well on the flow path. The initial composition of groundwater downgradient of the production zone for Flow Path D was obtained by mixing equal proportions of the groundwater samples from Wells M-7 and M-8.

4.2.3 Major Constituents

Dissolved silica concentrations in the upgradient, production zone and downgradient groundwater samples are in equilibrium with chalcedony, which is typical of low-temperature groundwater. The concentrations of major cations including magnesium, potassium and sodium will depend on the composition of inflowing groundwater, dissolution of feldspars and other silicate minerals such as mica, precipitation of clays and ion-exchange on aquifer sediments. Groundwater aluminum concentrations are assumed to be controlled at low concentrations by the solubility of Ca-montmorillonite, a smectite clay, and groundwater barite concentrations are assumed to be controlled by the solubility of barite based on identification of these minerals in the aquifer sediments.

Geochemical modeling results for upgradient monitoring ring well groundwater compositions indicate that these samples are saturated with respect to calcite (saturation index of approximately zero, Tables C.3-4 and C.3-5), which is consistent with identification of calcite in aquifer sediment samples upgradient of Mine Unit 1 (Section 3.2). The $\text{CO}_2(\text{g})$ partial pressures in equilibrium with the upgradient samples range from $10^{-2.4}$ to $10^{-1.9}$ atm, with moderate field pH values of 7.3 to 7.6 (Tables C.3-4 and C.3-5). Saturation of the upgradient groundwater with respect to calcite indicates that pH and calcium, bicarbonate and total alkalinity concentrations are controlled by calcite solubility.

Relatively high $\text{CO}_2(\text{g})$ partial pressures, ranging from $10^{-1.8}$ to $10^{-1.0}$ atm, are calculated for the production zone groundwater samples and field pH values range from 6.1 to 6.8 (Table C.3-8). The groundwater samples are undersaturated with respect to calcite, with saturation indices ranging from -1.99 to -0.59, which is consistent with the lower groundwater pH and calcite dissolution during ISR. Calcite was observed in some of the

production zone sediment samples, but does not appear to be accessible to the groundwater. Consequently, calcite is modeled to be initially absent in the production zone aquifer, although it could precipitate because of changing groundwater conditions, such as increased pH or decreased CO₂(g) partial pressure.

Downgradient groundwater samples are in equilibrium with calcite, with CO₂(g) partial pressures that range from 10^{-2.3} to 10^{-2.0} atm and moderate pH values ranging from 7.3 to 7.6 (Table C.3-9). Under these conditions, calcite solubility likely controls the pH and calcium, bicarbonate and total alkalinity concentrations.

Barite is the only sulfate solid identified in the aquifer sediments and could have small effects on sulfate concentrations. Because of the presence of pyrite in downgradient aquifer sediments, sulfide mineral precipitation and dissolution and sulfide mineral oxidation could affect sulfate concentrations downgradient of the Mine Unit 1 production zone. Chloride will behave as a conservative constituent in the groundwater.

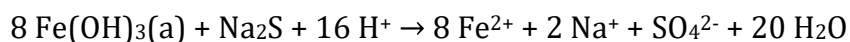
Measurements of total carbon, total inorganic carbon and organic carbon concentrations in the aquifer sediments were performed, but the results seem unreliable. For example, extremely low to non-detectable organic carbon concentrations were reported for core from locations DG-2, DG-3 and DG-4 (Table C.3-3), even though organic carbon was visible in hand specimen. It is uncertain whether this inconsistency was caused by analytical problems or heterogeneous distribution of the organic carbon.

4.2.4 Redox Conditions, Iron and Manganese

Upgradient groundwater samples from monitoring ring wells M-15 through M-21 had below-detection concentrations of iron and low manganese concentrations (Tables C.3-4 and C.3-5). These low groundwater iron and manganese concentrations are consistent with the low solubility of iron and manganese oxides and hydroxides under the relatively oxidizing conditions upgradient of Mine Unit 1. Because ORP measurements are typically unreliable in low-temperature groundwater and would be poorly poised by the upgradient groundwater composition, relatively oxidizing conditions (pe = 7) were assumed for inflowing upgradient groundwater.

Iron and manganese concentrations are elevated in the production-zone monitoring well samples (Table C.3-8), because of reductive dissolution of iron and manganese oxides and hydroxides in the aquifer sediments. XRD analysis of production zone sediments did not identify a crystalline iron hydroxide phase, although iron hydroxide was present in the production zone cores based on visual and SEM/EDS examination. The production zone iron hydroxide was formed by pyrite oxidation during ISR and appears to be amorphous, based on XRD results. The pe values used to establish initial redox conditions in the production zone groundwater (Table C.3-8) were calculated from the Fe²⁺/Fe³⁺ redox

couple, by assuming Fe^{3+} concentrations were controlled by the solubility of $\text{Fe}(\text{OH})_3(\text{a})$ (Macalady et al. 1990). The relatively high pe values (~ 4) despite sodium sulfide addition during restoration are a consequence of the reductive dissolution reaction:



Because of $\text{Fe}(\text{OH})_3(\text{a})$ reductive dissolution, groundwater conditions will remain mildly oxidizing as long as iron hydroxide solid remains in the aquifer sediments. Slightly oxidizing conditions are consistent with the low pyritic sulfur and organic sulfur concentrations in the production zone aquifer sediments (Table C.3-7).

The sequential extraction results for the production zone samples are summarized in Table C.4-2. Minimal to non-detectable amounts of iron and manganese were extracted in Step I, which is designed to extract exchangeable or adsorbed constituents. In the production zone, iron was extracted mostly as oxides and hydroxides in Steps III and IV and smaller amounts were extracted as humic- or sulfide-associated iron, consistent with widespread oxidation of pyrite during ISR. Manganese in all production zone samples was principally associated with iron oxides and hydroxides (Steps III and IV). In the mineralized sample that appeared unaffected by ISR (ST-2 463-464 ft), most of the iron was associated with either humics or sulfides (Steps II and V) and manganese was principally associated with iron oxides and hydroxides (Steps III and IV).

Dissolved iron concentrations are detectable in the downgradient groundwater samples (Table C.3-9). The presence of dissolved iron in the groundwater coupled with the presence of pyritic and organic sulfur in the sediments indicate that downgradient conditions are reducing. Initial redox conditions were established in the downgradient portion of the aquifer by assuming the groundwater redox was established by interaction of pyrite, goethite and coffinite. Sequential extractions of the downgradient sediment samples showed that most of the iron was associated with organics or sulfides (Table C.4-2, Steps II and V).

The moles of $\text{Fe}(\text{OH})_3(\text{a})$ in the aquifer sediments were calculated from the amounts of iron reported for Steps III and IV of the sequential extractions (Table C.3-11). The median amount of iron oxides and hydroxides for the seven production zone samples is 0.0778 moles/kg sediment, which was used to establish the initial concentration for the production zone aquifer sediments. The moles of iron oxides and hydroxides used to represent the downgradient sediments was based on the median amount in the two downgradient samples (0.0549 moles/kg sediment).

Table C.4-2. Sequential extraction results for production zone and downgradient aquifer sediments

Iron	Step I - adsorbed and clays (mg/kg)		Steps III & IV - iron oxides (mg/kg)		Steps II & V - organics and sulfides (mg/kg)	
ST-2 472-473 ft (production zone)	18	0.3%	4,288	61%	2,705	39%
ST-3 463-464 ft (production zone)	162	4.7%	2,443	71%	848	25%
ST-3 474-475 ft (production zone)	n.d.	n.d.	4,343	81%	1,007	19%
ST-4 479-480 ft (production zone)	30	0.5%	5,359	85%	898	14%
ST-4 488-489 ft (production zone)	n.d.	n.d.	3,416	78%	975	22%
ST-5 494-495 ft (production zone)	48	0.4%	8,671	77%	2,489	22%
ST-5 499-500 ft (production zone)	15	0.07%	20,903	94%	1,402	6.3%
ST-2 463-464 ft (mineralized)	21	0.08%	3,640	13%	23,914	87%
DG-2 487.5-488.5 ft (downgradient)	n.d.	n.d.	3,261	22%	11,393	78%
DG-4 516-517 ft (downgradient)	6	0.09%	2,871	41%	4,054	58%
Manganese	Step I - adsorbed and clays (mg/kg)		Steps III & IV - iron oxides (mg/kg)		Steps II & V - organics and sulfides (mg/kg)	
ST-2 472-473 ft (production zone)	n.d.	0%	17	87%	2.5	13%
ST-3 463-464 ft (production zone)	n.d.	0%	9	100%	n.d.	0%
ST-3 474-475 ft (production zone)	n.d.	0%	21	93%	1.5	7%
ST-4 479-480 ft (production zone)	n.d.	0%	22	92%	2	8%
ST-4 488-489 ft (production zone)	n.d.	0%	16	89%	2	11%
ST-5 494-495 ft (production zone)	n.d.	0%	39	88%	5.5	12%
ST-5 499-500 ft (production zone)	n.d.	0%	93	96%	4	4%
ST-2 463-464 ft (mineralized)	1.8	9%	16	81%	2	10%
DG-2 487.5-488.5 ft (downgradient)	n.d.	0%	16	29%	40	71%
DG-4 516-517 ft (downgradient)	n.d.	0%	12	100%	n.d.	0%

Table C.4-2. Sequential extraction results for production zone and downgradient aquifer sediments (contd)

Uranium	Step I - adsorbed and clays (mg/kg)		Steps III & IV - iron oxides (mg/kg)		Steps II & V - organics and sulfides (mg/kg)	
ST-2 472-473 ft (production zone)	37	13%	27	10%	218	77%
ST-3 463-464 ft (production zone)	3.1	13%	7	28%	14	59%
ST-3 474-475 ft (production zone)	17	11%	7	4.3%	138	85%
ST-4 479-480 ft (production zone)	0.60	8.9%	2	25%	4	66%
ST-4 488-489 ft (production zone)	23	11%	36	18%	146	71%
ST-5 494-495 ft (production zone)	11	9.4%	10	8.3%	95	82%
ST-5 499-500 ft (production zone)	15	6.8%	40	18%	168	75%
ST-2 463-464 ft (mineralized)	345	7.5%	1,979	43%	2,300	50%
DG-2 487.5-488.5 ft (downgradient)	62	11%	102	19%	375	70%
DG-4 516-517 ft (downgradient)	0.87	7.8%	3	27%	7	65%
Arsenic	Step I - adsorbed and clays (mg/kg)		Steps III & IV - iron oxides (mg/kg)		Steps II & V - organics and sulfides (mg/kg)	
ST-2 472-473 ft (production zone)	0.27	2.1%	4	27%	9	71%
ST-3 463-464 ft (production zone)	0.042	2.0%	0.78	37%	1	61%
ST-3 474-475 ft (production zone)	0.84	3.2%	16	61%	10	36%
ST-4 479-480 ft (production zone)	0.36	2.4%	9	62%	5	35%
ST-4 488-489 ft (production zone)	0.14	4.0%	1.3	37%	2	59%
ST-5 494-495 ft (production zone)	2.3	1.1%	141	69%	60	30%
ST-5 499-500 ft (production zone)	2.0	0.5%	270	68%	124	31%
ST-2 463-464 ft (mineralized)	1.1	0.1%	22	2%	893	97%
DG-2 487.5-488.5 ft (downgradient)	0.21	0.1%	2.5	0.6%	389	99%
DG-4 516-517 ft (downgradient)	0.090	0.8%	0.42	4%	10	95%

Table C.4-2. Sequential extraction results for production zone and downgradient aquifer sediments (contd)

Radium-226	Step I – adsorbed and clays (pCi/kg)		Steps III & IV – iron oxides (pCi/kg)		Steps II & V – organics and sulfides (pCi/kg)	
ST-2 472-473 ft (production zone)	120,000	38%	128,000	40%	71,250	22%
ST-3 463-464 ft (production zone)	20,400	42%	21,600	45%	6,310	13%
ST-3 474-475 ft (production zone)	7,500	19%	17,680	46%	13,435	35%
ST-4 479-480 ft (production zone)	3,900	64%	1,058	17%	1,132	19%
ST-4 488-489 ft (production zone)	84,000	55%	36,400	24%	32,750	21%
ST-5 494-495 ft (production zone)	9,000	39%	8,140	35%	5,875	26%
ST-5 499-500 ft (production zone)	19,800	42%	17,600	37%	9,835	21%
ST-2 463-464 ft (mineralized)	213,000	27%	434,000	54%	154,500	19%
DG-2 487.5-488.5 ft (downgradient)	15,600	31%	18,160	36%	16,850	33%
DG-4 516-517 ft (downgradient)	1,740	46%	1,158	31%	869	23%
Selenium	Step I – adsorbed and clays (mg/kg)		Steps III & IV – iron oxides (mg/kg)		Steps II & V – organics and sulfides (mg/kg)	
ST-2 472-473 ft (production zone)	4.1	17%	0.82	3%	19	79%
ST-3 463-464 ft (production zone)	0.20	17%	0.07	6%	0.93	77%
ST-3 474-475 ft (production zone)	1.1	2%	0.49	0.8%	58	97%
ST-4 479-480 ft (production zone)	0.18	6%	n.d.	0%	3.0	94%
ST-4 488-489 ft (production zone)	0.84	36%	0.21	9%	1.3	55%
ST-5 494-495 ft (production zone)	0.94	24%	0.26	7%	2.7	70%
ST-5 499-500 ft (production zone)	1.1	3%	0.82	3%	31	94%
ST-2 463-464 ft (mineralized)	0.19	8%	0.22	10%	1.9	82%
DG-2 487.5-488.5 ft (downgradient)	0.12	0.03%	0.12	0.03%	401	100%
DG-4 516-517 ft (downgradient)	0.06	13%	n.d.	0%	0.40	87%

4.2.5 Uranium

Uranium concentrations in groundwater samples from upgradient monitoring ring wells M-13 through M-21 range from 0.038 to 0.057 mg/L, which exceed the 0.03 mg/L drinking water standard (Tables C.3-4 and C.3-5). In groundwater samples obtained from the production-zone monitoring wells in March 2016, uranium concentrations range from 0.044 to 2.08 mg/L (Table C.3-8). The highest groundwater uranium concentration observed during the stability monitoring period was 5.5 mg/L in a December 2014 sample from Well B-4.

SEM/EDS evaluation of aquifer sediment samples representative of the production zone (ST-3 474 – 475 ft and ST-5 499 – 500 ft) did not indicate the location of uranium in the post-ISR production zone sediments. Although these core samples had the highest uranium concentrations among the production zone aquifer sediment samples, uranium concentrations in these core samples were fairly low (195 and 282 mg/kg, respectively, Table C.3-7).

Other investigations have examined the solid-phase associations of uranium in aquifer sediments at the SRH site after ISR and restoration. Although these investigations used aquifer sediment samples from Mine Unit 4, located west of Mine Unit 1 at the site (Figure C.1-1), the aquifer mineralogy and ISR and restoration processes are likely to be similar. Gallegos et al. (2015) examined post-restoration sediment core samples that had uranium concentrations up to 1,920 mg/kg and used X-ray absorption near edge spectroscopy to determine uranium was present as both U(IV) and U(VI). Using fission-track analysis, Gallegos et al. (2015) identified residual uranium minerals associated with low-permeability organic carbon that is unlikely to be readily available to post-restoration groundwater. Additional uranium was associated with secondary minerals such as iron hydroxides and iron-rich coatings associated with euhedral pyrite. Gallegos et al. (2015) noted that this secondary uranium is likely to be accessible to post-restoration groundwater.

WoldeGabriel et al. (2014) examined 7.32 m of continuous core from SRH Mine Unit 4. This core was obtained from an area currently undergoing post-ISR restoration using groundwater sweep and reverse osmosis. Sediment samples were analyzed for mineralogy using XRD and for chemical composition by X-ray fluorescence spectroscopy and organic carbon analysis. WoldeGabriel et al. (2014) also characterized an organic-rich subsample using optical and scanning-electron microscopy. The results showed that higher residual uranium concentrations, mostly U(IV), were present in samples with higher clay and organic carbon contents. WoldeGabriel et al. (2014) observed that the higher clay and organic carbon may have limited the contact of these sediments with lixiviant. Elevated concentrations of uranium, iron and other metals associated with carbonaceous materials in the sediments indicates that the organic materials have a high affinity for metal complexation and immobilization. Uranium was present as a coating on pyrite surfaces, consistent with the ability of pyrite to immobilize uranium. WoldeGabriel et al. (2014) did not observe uranium in the sediment samples with low organic carbon contents, likely because these aquifer materials were adequately contacted by lixiviant during ISR.

Sequential extraction results for uranium from production zone samples (Table C.4-2) indicate that relatively small amounts of uranium may be adsorbed or exchangeable (Step I) and a slightly higher range of uranium concentrations is associated with iron oxides and

hydroxides (Steps III and IV). However, most of the residual uranium in the production zone samples is associated with humics, organics and sulfides (Steps II and V). The uranium sequential extraction results are consistent with the fission-track analysis results obtained by Gallegos et al. (2015) and the association of uranium with high clay and organic carbon materials reported by WoldeGabriel et al. (2014). Because significant percentages of residual uranium in the production zone sediments are associated with organic carbon or sulfides, much of the residual uranium is unlikely to be readily released from the production zone sediments. The ST-2 463 – 464 ft sample that was unaffected by ISR has significant fractions of total uranium associated with iron oxides and hydroxides (Steps III and IV) and with organics and sulfides (Steps II and V).

Downgradient groundwater uranium concentrations range from 0.012 to 0.027 mg/L (Table C.3-9). Total uranium concentrations in the downgradient aquifer sediments (Table C.3-3) vary from approximately 9 mg/kg (samples DG-3 and DG-4) to 557 mg/kg (sample DG-2). Sequential extraction results from the DG-2 and DG-4 downgradient aquifer sediment samples (Table C.4-2) indicate that most uranium in downgradient sediments is associated with humics, organics and sulfides (Steps II and V), with smaller fractions associated with iron oxides and hydroxides (Steps III and IV) and adsorbed or associated with clays (Step I).

As uranium in the production zone groundwater migrates downgradient, the groundwater will encounter reducing sediments that contain significant pyrite. Iron sulfides such as pyrite have been shown to reduce and immobilize uranium (Hua and Deng 2008, Gallegos et al. 2013). Reimus et al. (2015) tested the ability of reduced sediments at the SRH site to attenuate uranium. In these field tests, groundwater from unrestored and partially restored portions of Mine Unit 4A was injected into the aquifer in Mine Unit 7, which had not been subjected to ISR. After periods of between 2 weeks and 3 months, the injected water was pumped back and analyzed. The results of these push-pull tests in previously undisturbed reducing sediments showed that uranium concentrations were significantly decreased relative to the injected concentrations.

4.2.6 Arsenic

Arsenic concentrations above the drinking water standard were observed in only a few of the March 2016 production zone groundwater samples. These wells (Wells B-1, B-4, B-9, B-15 and B-17) are located on the west side of Mine Unit 1 (Figure C.3-4). The groundwater samples with higher arsenic concentrations (0.016 to 0.025 mg/L) also have higher dissolved iron concentrations, ranging from 1.26 to 2.44 mg/L (Table C.3-8, Figure C.3-5). Geochemical modeling calculations indicate that arsenic in the production-zone monitoring well samples is present predominantly as arsenate [As(V)]. Downgradient monitoring ring

well groundwater samples have arsenic concentrations below the analytical detection limit of 0.001 mg/L.

Arsenic concentrations are relatively low in most of the production zone sediment samples (3.1 to 25.1 mg/kg, Table C.3-7), except for the two ST-5 samples (258 – 720 mg/kg); location ST-5 is near one of the higher-arsenic production-zone monitoring wells (Well B-4). SEM/EDS examination of the ST-5 499-500 ft sediment sample did not show the mineral association of the arsenic. However, SEM/EDS examination of the ST-3 474 – 475 ft core sample indicated that arsenic was present in unaltered pyrite cores, which are unlikely to be readily accessible to groundwater.

Sequential extraction results (Table C.4-2) indicate that arsenic is mainly associated with iron oxides and hydroxides (Steps III and IV) and organics and sulfides (Steps II and V). Production zone samples had significant percentages of arsenic associated with iron oxides and hydroxides, ranging from 27 to 69% of the arsenic in the samples. In contrast, virtually all arsenic in the unaltered mineralized sample (ST-2 463-464 ft) and in the downgradient samples was associated with sulfides or organics. The sequential extraction results and SEM observation of arsenic in pyrite cores in the ST-3 474 – 475 ft are consistent with the pre-ISR presence of arsenic in pyrite in the mineralized zone and downgradient sediments. During ISR, pyrite oxidation released arsenic and created iron oxides and hydroxides, which adsorbed or coprecipitated arsenic.

Arsenic available to the groundwater in the production zone will be associated with iron oxides and hydroxides, and may be desorbed or released during reductive dissolution of these materials (Smedley and Kinniburgh 2002). Arsenic transported downgradient from the production zone into reducing sediments would be expected to be attenuated through precipitation of arsenic sulfides, such as realgar, coprecipitation with pyrite or by adsorption on ferric oxides and hydroxides.

4.2.7 Radium-226

Relatively low groundwater radium-226 concentrations (4.0 to 8.3 pCi/L, Tables C.3-4 and C.3-5) were observed for all upgradient monitoring ring wells except Well M-21, which had radium-226 concentrations of 65.2 to 69.0 pCi/L. Radium-226 concentrations in the baseline production-zone monitoring well groundwater samples had an arithmetic mean of 764 pCi/L, which significantly exceeds the 5 pCi/L drinking water standard. The radium-226 concentrations in the March 2016 groundwater samples ranged from 179 to 1,250 pCi/L, with an arithmetic mean of 462 pCi/L. Only production-zone monitoring Wells B-3, B-4 and B-13 had radium-226 concentrations greater than the RTV during the stability monitoring period. The maximum radium-226 concentration observed in the post-restoration production-zone monitoring well samples is less than the maximum

concentration of 1,650 pCi/L observed in the baseline monitoring samples from the production-zone monitoring wells.

Sequential extraction results indicate that radium-226 in the Mine Unit 1 sediments is associated mainly with clays (Step I) or with iron oxides and hydroxides (Steps III and IV). Smaller but still significant percentages (13% – 35%) appear to be associated with organics and sulfides (Steps II and V). The extraction results are consistent with attenuation mechanisms identified in the literature for radium-226, which include exchange on clays and organic matter (Ames et al. 1983, Greeman et al. 1999), adsorption on iron oxides and hydroxides (e.g., Sajih et al. 2014) and coprecipitation with barium in a barite- BaSO_4 (s) solid solution (e.g., Curti et al. 2010).

4.2.8 *Selenium*

Selenium concentrations were below the drinking water standard in all March 2016 production-zone monitoring well groundwater samples (Table C.3-8). During stability monitoring, selenium concentrations exceeded the 0.05 mg/L drinking water standard in a few production zone groundwater samples (Figure C.4-1). Subsequent groundwater samples showed a general downward trend in selenium concentrations, with all selenium concentrations in samples from December 2015 and March 2016 below the drinking water standard. Geochemical modeling of the production-zone monitoring well groundwater samples showed that selenite [Se(IV)] was the dominant aqueous selenium oxidation state and the groundwater samples had progressively lower native Se saturation indices over time (Figure C.4-2). These modeling results demonstrate that native Se provides a reasonable upper bound for dissolved selenium concentrations in the production zone groundwater.

Selenium concentrations in the production zone sediments were relatively low in most core samples (Table C.3-7). The two core samples with the highest selenium concentrations were ST-5 499-500 ft and ST-3 474 – 475 ft. SEM/EDS examination of these higher-selenium samples revealed the presence of native Se, indicating that redox conditions were sufficiently reducing to cause its precipitation.

Sequential extractions of the aquifer sediment samples indicated that for most samples the largest percentages of selenium were extracted by the strong oxidant (Step V), as would be expected by the presence of native Se (Table C.4-2), with the next larger percentage associated with humics (Step II). Smaller percentages appear to be adsorbed or associated with clays (Step I) or associated with iron oxides and hydroxides (Steps III and IV). Sorption of selenite by clays and by iron oxides and hydroxides has been reported at the pH values measured in the production zone groundwater (e.g., Missana et al. 2009 and Balistrieri and Chao 1990).

Selenium present as native Se could be mobilized from the production zone if conditions become more oxidizing or if pH increases. As dissolved selenium is transported downgradient, it will be reduced by interaction with the reducing downgradient sediments, precipitating either as native Se or as ferroselite.

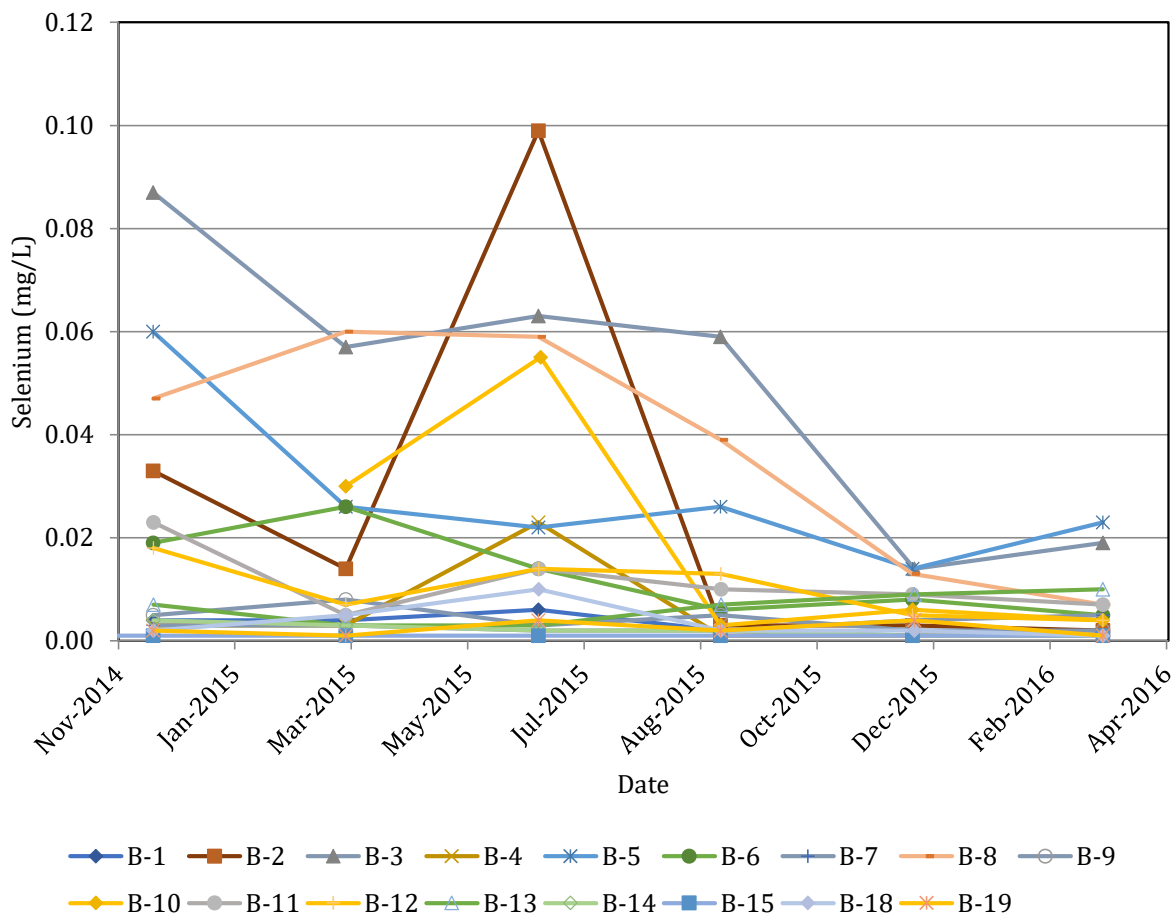


Figure C.4-1. Selenium concentrations in production-zone monitoring well groundwater stability samples; concentrations in samples from Wells B-16 and B-17 were below analytical detection limit of 0.001 mg/L

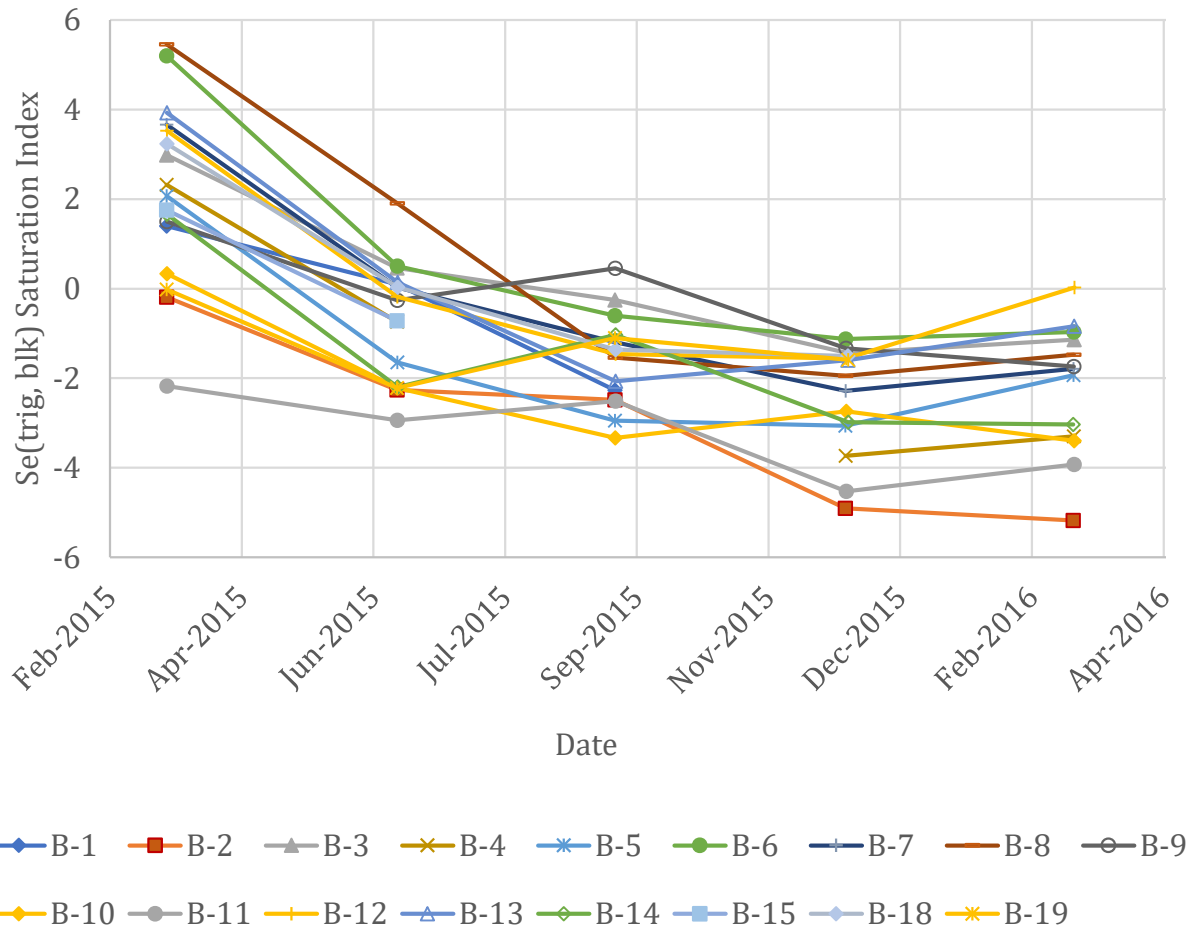


Figure C.4-2. Native Se saturation index values for production-zone monitoring well samples during the stability monitoring period; concentrations in samples from Wells B-16 and B-17 were below analytical detection limit of 0.001 mg/L

4.3 Model Parameters

PHREEQC calculations are carried out on the basis of 1 kg water for each cell in the transport model. The ratios of the mass of aquifer sediments to 1 kg groundwater were calculated from bulk density and porosity measurements for the production zone sediments (6.592 kg/kg H₂O) and downgradient sediments (6.085 kg/kg H₂O) (Attachment C-6). The concentrations of Fe(OH)₃(a) in the production zone sediments, goethite in the downgradient sediments, and CEC in the production zone and downgradient sediments used in the initial conditions of the transport model were calculated using these ratios (Table C.4-3, Attachment C-6) from the concentrations previously determined per kg of sediment.

Table C.4-3. Mineral parameters used in PHREEQC reactive transport modeling calculations

Parameter	Production Zone Aquifer Sediments	Downgradient Aquifer Sediments
Solids/water mass ratio (kg/kg H ₂ O)	6.592	6.085
Median CEC (eq/kg H ₂ O)	0.675	0.466
Minimum CEC (eq/ kg H ₂ O)	0.407	0.438
Median Step III extracted iron (mole/kg H ₂ O)	0.236	0.268
Median Step III + IV extracted iron (mole/kg H ₂ O)	0.513	0.334
Pyrite (moles/kg H ₂ O)	0.0617	0.408
Calcite (moles/kg H ₂ O)	0.0	0.608
Iron oxide/hydroxide specific surface area (m ² /mole)	64,110	53,310

4.3.1 Hydrogeologic Parameters

The hydrogeologic parameters used in the transport calculations are summarized in Table C.4-4. These parameters are based on the results of the long-term hydrologic model developed by AquiferTek (2017). The cell dimensions used for each flow path are provided in Table C.4-4. Shorter cell lengths were necessary for Flow Path A when modeling the increased groundwater flow rate and for Flow Paths D and E, possibly because of the effects of relatively high dissolved iron concentrations in the production zone along these flow paths.

Table C.4-4. Hydrogeologic parameters

Flow Path	Flow Path Length (m)	Travel Duration (y)	Average Groundwater Velocity (m/y)	Dispersivity (m)	Cell Length (m)	Number of Cells
A	807.7	795	1.02	10.9	2.5	323
A	807.7	397.5	2.03	10.9	1	808
B	815.3	755	1.08	10.9	2.5	326
C	680.9	740	0.92	10.2	2.5	272
D	715.7	790	0.91	10.5	1.0	716
E	649.8	690	0.94	10.1	1.5	433
F	539.5	510	1.06	9.39	2.5	216

4.3.2 Geochemical Reactions

Upgradient groundwater was assumed to be in equilibrium with chalcedony, barite, Ca-montmorillonite, goethite and calcite. An excess of these minerals was included in cells representing the upgradient aquifer.

The production zone sediments were assumed to be in initial equilibrium with chalcedony, $\text{Fe}(\text{OH})_3(\text{a})$, Ca-montmorillonite, and native Se. The moles of $\text{Fe}(\text{OH})_3(\text{a})$ included in the model was based on the median calculated from the total iron (Step III + Step IV) extractions from the production zone sediments (0.513 mole/kg H_2O , Attachment C-6). The moles of native Se included in the production zone sediments was the median calculated from the strong oxidant extractions of production zone sediments (2.21×10^{-4} mole/kg H_2O , Attachment C-6). Siderite, rhodochrosite, gypsum, calcite and uranophane were not initially present in the production zone sediments, but could precipitate if saturation was achieved. Initial barium concentrations were set equal to the concentration in equilibrium with barite, but barite was not included as an initial solid in the production zone sediments. A solid solution of barite with $\text{RaSO}_4(\text{s})$ could precipitate in response to changing groundwater composition. Ion exchange between the production zone groundwater and aquifer sediments was included as an exchange reaction, using the median production zone CEC of 0.675 eq/kg H_2O (Attachment C-6). Radium-226 exchange was assumed equal to barium exchange. Adsorption by $\text{Fe}(\text{OH})_3(\text{a})$ was included in the model, using the surface complexation data included in the Enchemica.R1.dat database (Attachment C-5). The default specific surface area of $6.411 \times 10^4 \text{ m}^2/\text{mole}$ was used for the $\text{Fe}(\text{OH})_3(\text{a})$ surface.

The downgradient sediments were assumed to be in equilibrium with goethite, chalcedony, Ca-montmorillonite and calcite. Pyrite was included in the aquifer sediments, but was only allowed to dissolve to reach a saturation index of -4.0. This lower saturation index limited the amount of pyrite dissolution and maintained initial dissolved iron concentrations in the downgradient groundwater consistent with current concentrations. The amount of pyrite included in the downgradient aquifer sediments was the median value calculated from pyritic sulfur concentrations in downgradient core samples (0.408 mole/kg H_2O , Attachment C-6). The amount of calcite included in the downgradient cells was assumed equal to 1% by weight, which is half the XRD detection limit. The amount of goethite included in the downgradient sediments was based on the median calculated from the total iron (Step III + Step IV) extractions from the downgradient aquifer sediments (0.334 mole/kg H_2O , Attachment C-6). Coffinite, uraninite, ferroselite, siderite, rhodochrosite, native Se, realgar and gypsum were not initially included in the downgradient aquifer sediments, but could precipitate if saturation was achieved. Initial barium concentrations were set equal to the concentration in equilibrium with barite, but solid barite was not initially included in the production zone sediments. A solid solution of barite with $\text{RaSO}_4(\text{s})$ could precipitate in response to changing groundwater compositions. Ion exchange

between the production zone groundwater and aquifer sediments was included as an exchange reaction, using the median production zone CEC of 0.466 eq/kg H₂O (Attachment C-6). Radium-226 exchange was assumed equal to barium exchange. Adsorption by goethite was included in the modeling calculations, using the surface complexation data included in the Enchemica.R1.dat database (Attachment C-5). The default specific surface area of 5.331×10^4 m²/mole was used for the goethite surface.

Initial concentrations of cations present on exchange sites in the production zone and downgradient sediments and the surface species adsorbed on Fe(OH)₃(a) in the production zone sediments and goethite in the downgradient sediments were established based on the concentrations in equilibrium with the initial groundwater.

4.4 Sensitivity Evaluation

The effects of higher initial arsenic, selenium, radium-226 and uranium concentrations on the transport modeling results were assessed by repeating the modeling calculations for all six flow paths using increased initial production zone groundwater concentrations of arsenic (0.10 mg/L), selenium (0.20 mg/L), radium-226 (2,000 pCi/L) and uranium (10 mg/L). These concentrations were selected because they significantly exceed all concentrations measured in the Mine Unit 1 production zone during stability monitoring.

The effects of variations in several other parameters were evaluated by performing additional calculations for Flow Path A, including increased groundwater flow rate, lower CEC available for ion exchange, lower goethite available for adsorption in the downgradient sediments and elimination of barite-RaSO₄(s) solid solution precipitation. Flow Path A was selected for assessing the sensitivity of the results to variations in these parameters because of the relatively high radium-226 concentration in a well along this flow path (1,250 pCi/L, Well B-3) and the reasonably short (198 m) distance from the downgradient edge of the production zone to POE location A. Because only limited amounts of pyrite and calcite were consumed by reaction, and this consumption took place almost exclusively within the first downgradient cell along each flow path, the effects of varying the amounts of these minerals in the downgradient sediments were not included in the sensitivity calculations.

Measured field pH values varied somewhat during stability monitoring, and the initial groundwater pH affects the calibrated initial amount of modeled uranium adsorbed on the Fe(OH)₃(a) surface in the production zone. The potential effects of uncertainty in the field pH measurements on Flow Path B transport modeling results for uranium were evaluated by increasing the initial modeled groundwater pH in Well B-4 on this flow path from the value of 6.3 measured in March 2016 to the maximum value of 7.0 measured in December 2016. Flow Path B was selected for this sensitivity evaluation because Well B-4

groundwater on this flow path resulted in the highest modeled initial adsorbed uranium concentrations in the production zone sediments.

5.0 Transport Modeling Results

The transport modeling results from Flow Path A are used to illustrate the geochemical changes along the flow paths, because similar results were obtained using the other five modeled flow paths. Additional graphs showing constituent concentrations as a function of time at POE locations B through F and constituent concentration profiles along Flow Paths B through F are provided in Attachment C-8.

5.1 Major Elements and pH

Initially, pH, alkalinity, calcium concentrations and TDS within the production zone are lower and carbon dioxide partial pressures and chloride concentrations are higher than the upgradient and downgradient groundwater (Figures C.5-1 through C.5-6). The production zone pH, alkalinity, calcium concentrations, TDS, carbon dioxide partial pressures and chloride concentrations evolve toward the concentrations in the upgradient groundwater over time. At the interface between the altered sediments in the production zone and downgradient reducing sediments, groundwater pH, alkalinity, calcium and TDS concentrations increase because of small amounts of pyrite and calcite dissolution. The amounts of pyrite and calcite consumed over the modeled 1,000-year period are small, and significant quantities of these minerals are dissolved only within the first downgradient cell on the flow path. Sulfate concentrations in the production zone groundwater initially increase slightly because of sulfate desorption from $\text{Fe}(\text{OH})_3(\text{a})$ as pH increases on the upgradient edge of the production zone (Figure C.5-7).

The current measured downgradient groundwater pH values are compared to the modeled pH values at the POE locations in Table C.5-1 and the pH variation over time is illustrated in Figure C.5-1(b). The modeled POE pH range is slightly lower than the current downgradient groundwater pH values (Table C.5-1), but all modeled pH values at POE location A are within the secondary drinking water standard range of 6.5 to 8.5. The modeled groundwater pH at POE location A is minimally affected by the tested parameter variations (Table C.5-2).

The modeled TDS concentrations at the POE locations are similar to current downgradient groundwater TDS concentrations and slightly exceed the 500 mg/L secondary drinking water standard only at POE location E (Table C.5-3). TDS concentrations are only gradually increasing at the end of the 1,000-year modeling period (Figure C.5-4(b)). Changes in the modeling parameters for Flow Path A had only small effects on the TDS calculated at POE location A (Table C.5-2).

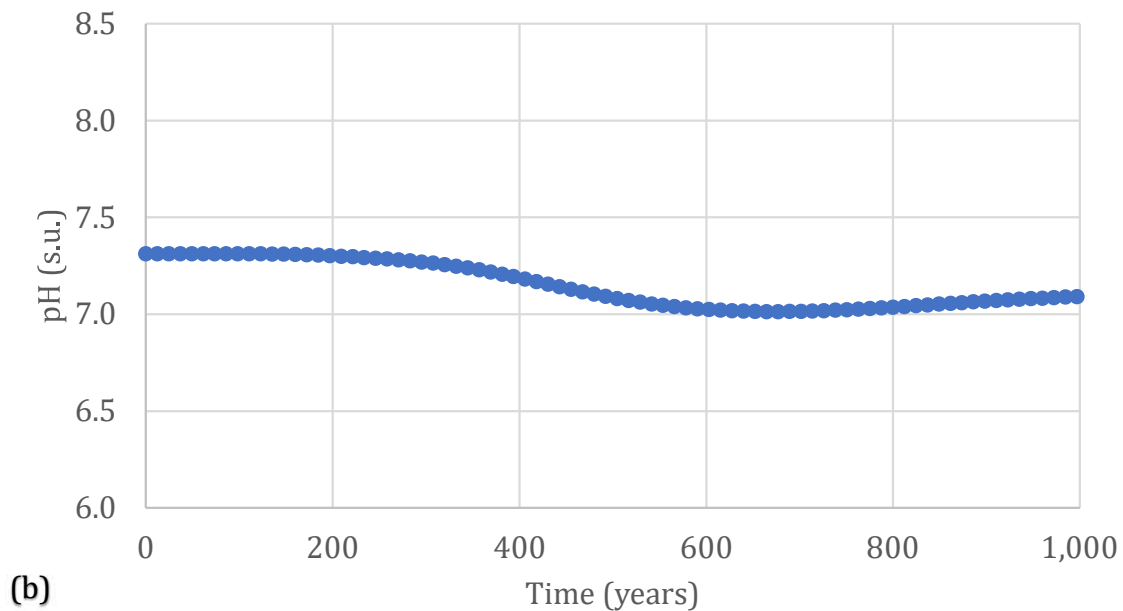
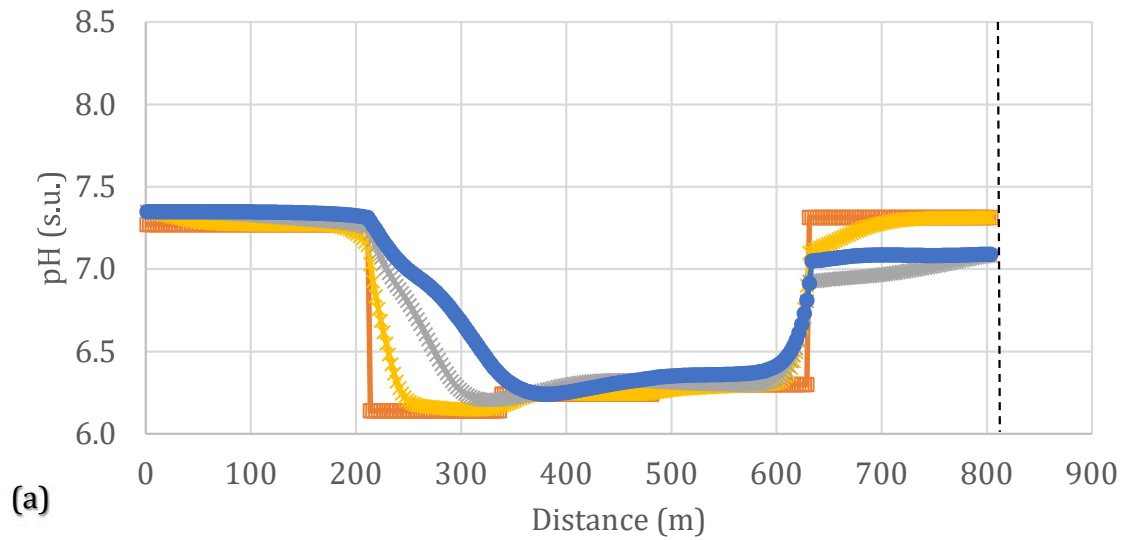


Figure C.5-1. Flow Path A groundwater pH: (a) as a function of time and distance; (b) as a function of time at POE location A. Well locations on Flow Path A are: upgradient monitoring ring Well M-21 at 0 m, Well B-3 at 279 m, Well B-2 at 396 m, Well B-1 at 570 m and POE location A (dashed vertical line) at 808 m

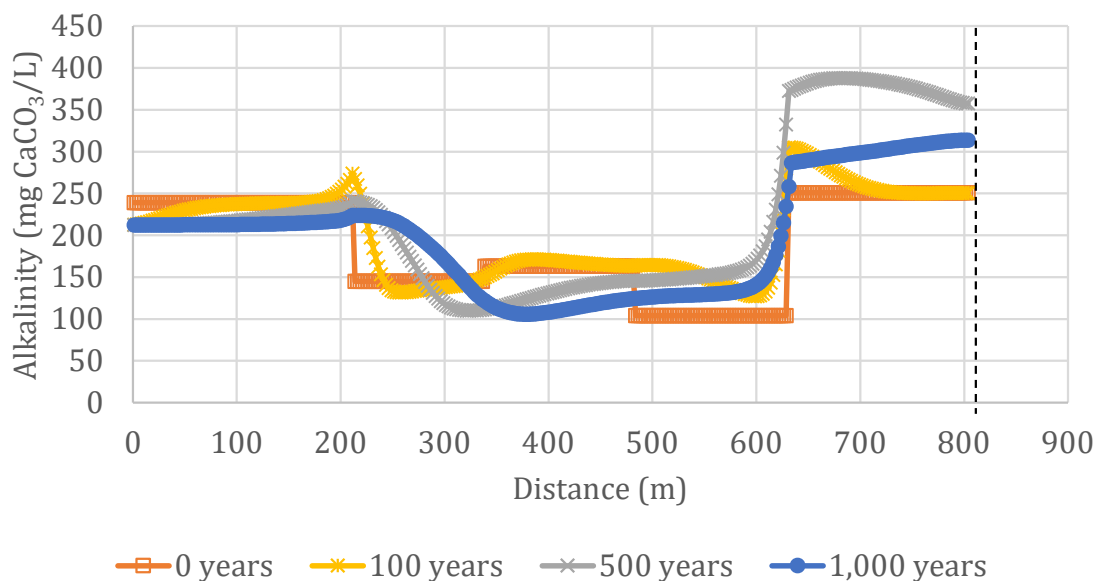


Figure C.5-2. Flow Path A groundwater alkalinity as a function of time and distance. Well locations on Flow Path A are: upgradient monitoring ring Well M-21 at 0 m, Well B-3 at 279 m, Well B-2 at 396 m, Well B-1 at 570 m and POE location A (dashed vertical line) at 808 m

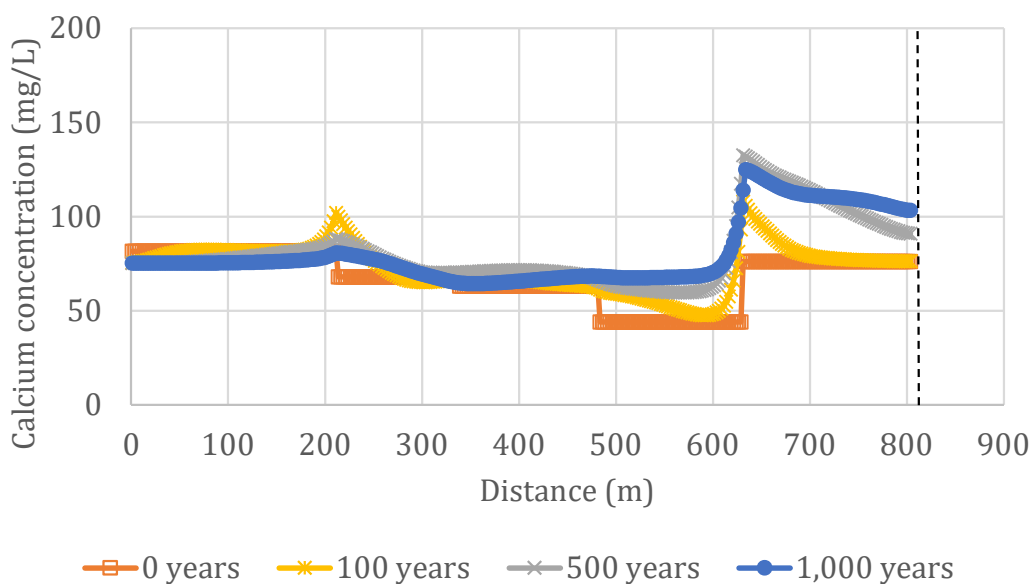
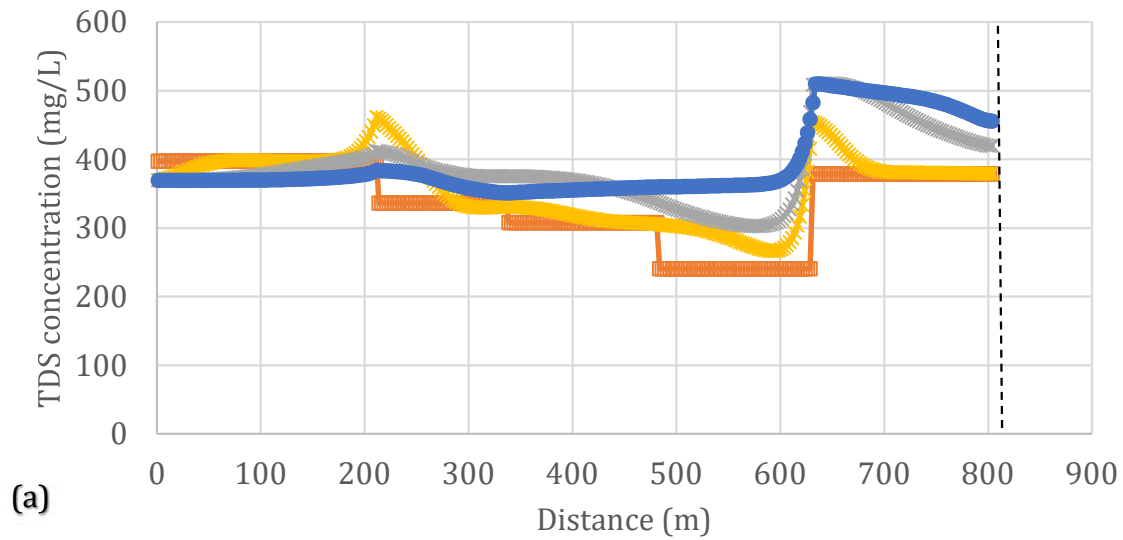


Figure C.5-3. Flow Path A groundwater calcium concentrations as a function of time and distance. Well locations on Flow Path A are: upgradient monitoring ring Well M-21 at 0 m, Well B-3 at 279 m, Well B-2 at 396 m, Well B-1 at 570 m and POE location A (dashed vertical line) at 808 m



—□— 0 years —*— 100 years —x— 500 years —●— 1,000 years

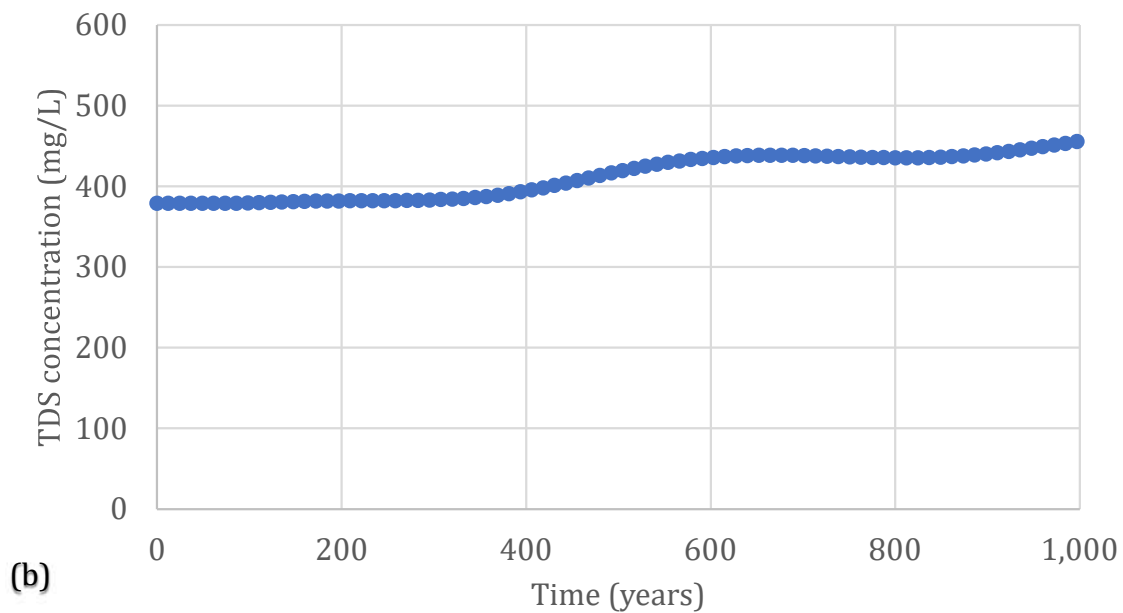


Figure C.5-4. Flow Path A groundwater TDS (calculated): (a) as a function of time and distance; (b) as a function of time at POE location A. Well locations on Flow Path A are: upgradient monitoring ring Well M-21 at 0 m, Well B-3 at 279 m, Well B-2 at 396 m, Well B-1 at 570 m and POE location A (dashed vertical line) at 808 m

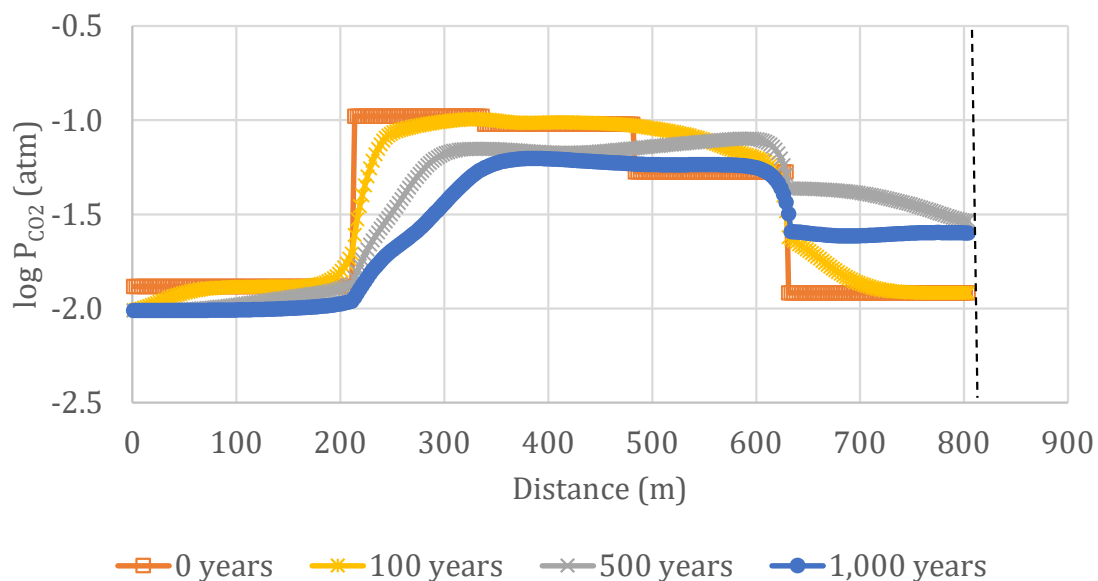


Figure C.5-5. Flow Path A groundwater log P_{CO_2} as a function of time and distance. Well locations on Flow Path A are: upgradient monitoring ring Well M-21 at 0 m, Well B-3 at 279 m, Well B-2 at 396 m, Well B-1 at 570 m and POE location A (dashed vertical line) at 808 m

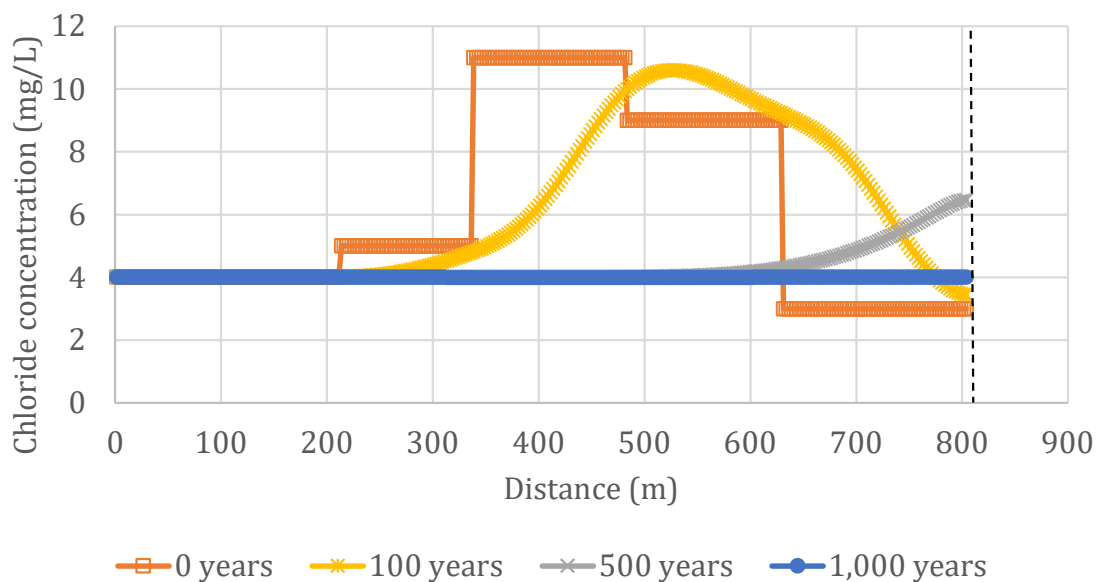


Figure C.5-6. Flow Path A groundwater chloride concentrations as a function of time and distance. Well locations on Flow Path A are: upgradient monitoring ring Well M-21 at 0 m, Well B-3 at 279 m, Well B-2 at 396 m, Well B-1 at 570 m and POE location A (dashed vertical line) at 808 m

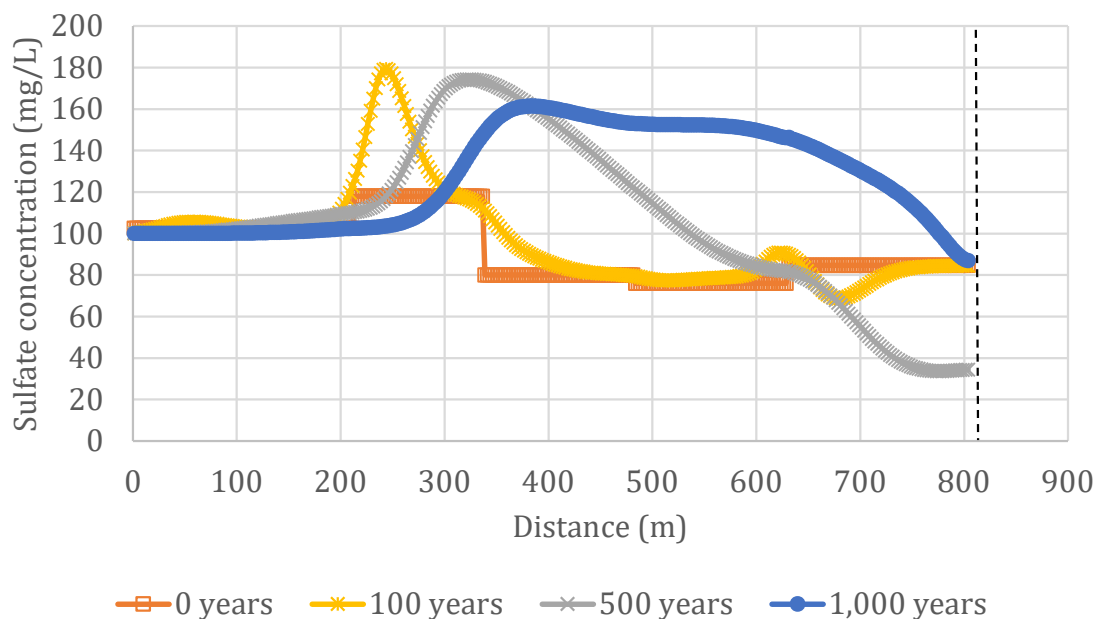


Figure C.5-7. Flow Path A groundwater sulfate concentrations as a function of time and distance. Well locations on Flow Path A are: upgradient monitoring ring Well M-21 at 0 m, Well B-3 at 279 m, Well B-2 at 396 m, Well B-1 at 570 m and POE location A (dashed vertical line) at 808 m

Table C.5-1. Measured and modeled groundwater pH at POE locations

POE	Downgradient Well	Measured Downgradient pH Range	Modeled POE pH Range
A	M-2	7.24 - 7.47	7.0 - 7.3
B	M-2/M-3	7.23 - 7.60	7.1 - 7.3
C	M-5	7.32 - 7.70	7.2 - 7.3
D	M-7/M-8	7.36 - 7.68	7.2 - 7.4
E	M-8	7.36 - 7.68	7.0 - 7.3
F	M-9	7.30 - 7.58	7.2 - 7.3

Table C.5-2. Effects of parameter variations on POE A modeled groundwater pH and constituent concentrations

Flow Path A	Measured Concentration Well M-2	Baseline Modeled POE Concentration	Modeled POE Concentrations with Increased Initial POC Well Concentrations ^a	Modeled POE Concentrations without Barite-RaSO ₄ (s) Solid Solution	Modeled POE Concentrations with Lower Downgradient Goethite Concentration	Modeled POE Concentrations with Lower Exchange Site Concentrations	Modeled POE Concentrations with Increased Groundwater Flow Rate
pH	7.24 – 7.47	7.0 – 7.3	7.1 – 7.3	7.0 – 7.3	7.1 – 7.3	7.0 – 7.3	7.0 – 7.3
TDS (mg/L)	250 – 370	379 – 458	379 – 415	379 – 458	378 – 414	379 – 460	379 – 506
Iron (mg/L)	0.06 – 0.20	0.20 – 0.65	0.19 – 0.54	0.20 – 0.65	0.19 – 0.56	0.20 – 0.65	0.20 – 0.65
Manganese (mg/L)	0.02	0.024 – 0.052	0.024 – 0.045	0.024 – 0.052	0.023 – 0.044	0.024 – 0.053	0.024 – 0.053
Uranium (mg/L)	0.0153 – 0.0323	< 0.0003	< 0.0003	< 0.0003	< 0.0003	< 0.0003	< 0.0003
Radium-226 (pCi/L)	12.7 – 15.7	14.4 – 19.5	14.2 – 17.7	14.4 – 19.9	14.1 – 17.3	14.4 – 19.5	14.1 – 19.7
Selenium (mg/L)	< 0.001 – 0.001	< 0.001	< 0.001	< 0.001	< 0.001	< 0.001	< 0.001
Arsenic (mg/L)	< 0.001	< 0.001	< 0.001	< 0.001	< 0.001	< 0.001	< 0.001

a – 0.1 mg/L arsenic, 2,000 pCi/L radium-226, 0.2 mg/L selenium and 10 mg/L uranium

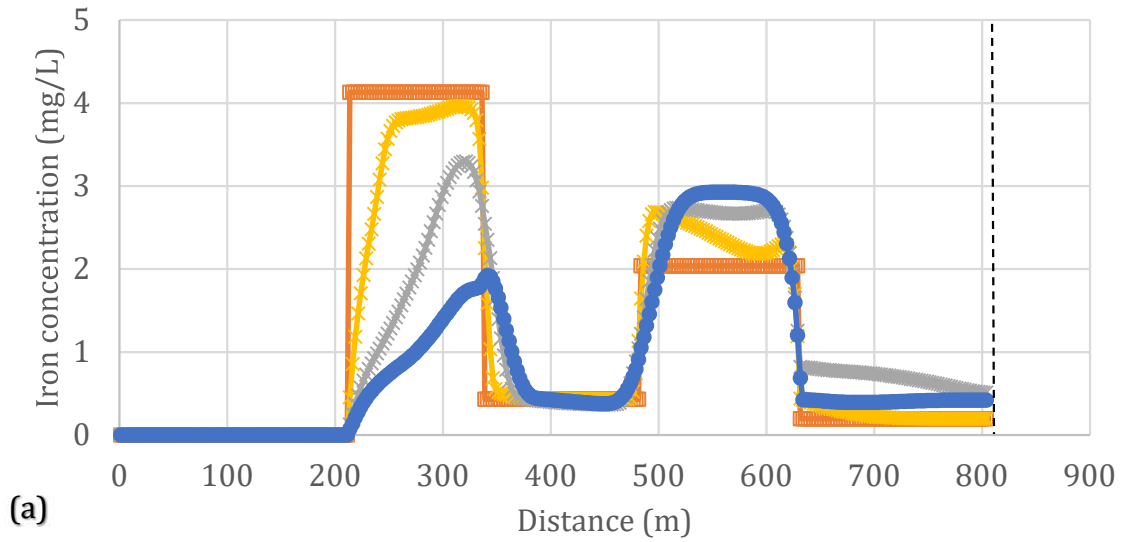
Table C.5-3. Measured and modeled groundwater TDS concentrations at POE locations

POE	Downgradient Well	Measured Downgradient TDS Concentrations (mg/L)	Modeled POE TDS Concentrations (mg/L)
A	M-2	250 - 370	379 - 458
B	M-2/M-3	250 - 417	379 - 393
C	M-5	227 - 407	396 - 423
D	M-7/M-8	275 - 401	352 - 412
E	M-8	293 - 387	396 - 550
F	M-9	273 - 374	385 - 435

5.2 Iron and Manganese

Iron and manganese concentrations are initially elevated in the production zone groundwater relative to upgradient and downgradient groundwater concentrations (Figures C.5-8(a) and C.5-9(a)). Aqueous iron concentrations decrease over time in the upgradient portion of the production zone, but exhibit a slight increase in the downgradient portion of the production zone over time. The amounts of $\text{Fe}(\text{OH})_3(\text{a})$ in the production zone do not change significantly during the 1,000-year modeling period, because inflowing upgradient groundwater is relatively oxidizing. Increased pH causes a small amount of precipitation near the interface between the production zone and the upgradient aquifer, which is later countered by a small amount of dissolution in these cells as pe slightly decreases (Figure C.5-10). A small amount of goethite is precipitated in downgradient sediments adjacent to the production zone, with small amounts of pyrite dissolution and ferroselite precipitation occurring in the downgradient sediments. Along the flow paths with higher initial production zone groundwater iron concentrations (Flow Paths A, D and E), small amounts of siderite also precipitate near the interface between the production zone sediments and downgradient sediments.

The ranges of modeled groundwater iron concentrations at the POE locations are slightly higher than the current concentrations at the downgradient monitoring ring wells (Table C.5-4). The upper limits of the modeled iron concentrations slightly exceed the secondary iron drinking water standard of 0.3 mg/L at four of the six POE locations. At the end of the 1,000-year modeling period, iron concentrations at POE location A exhibit a downward trend (Figure C.5-8(b)). The modeled groundwater iron concentrations at POE A are minimally affected by variation of the tested parameters (Table C.5-2).



—□— 0 years —*— 100 years —x— 500 years —●— 1,000 years

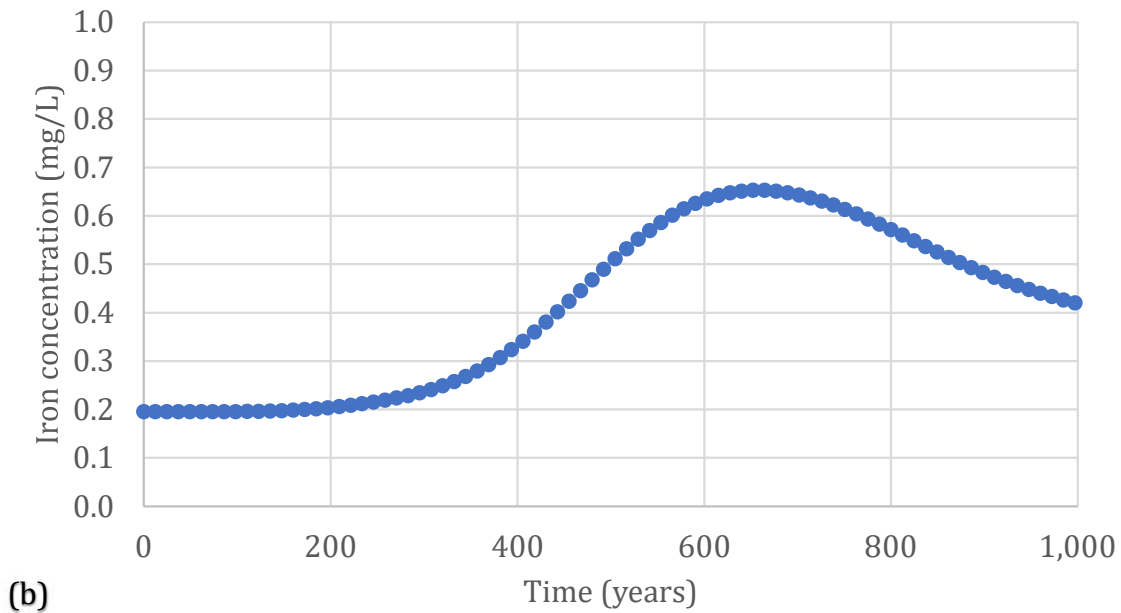
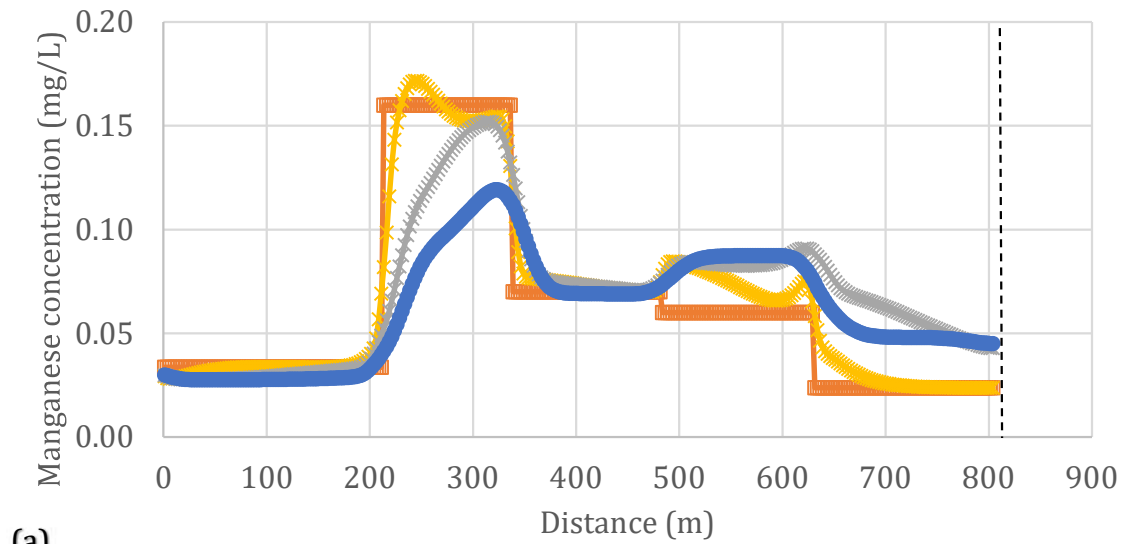
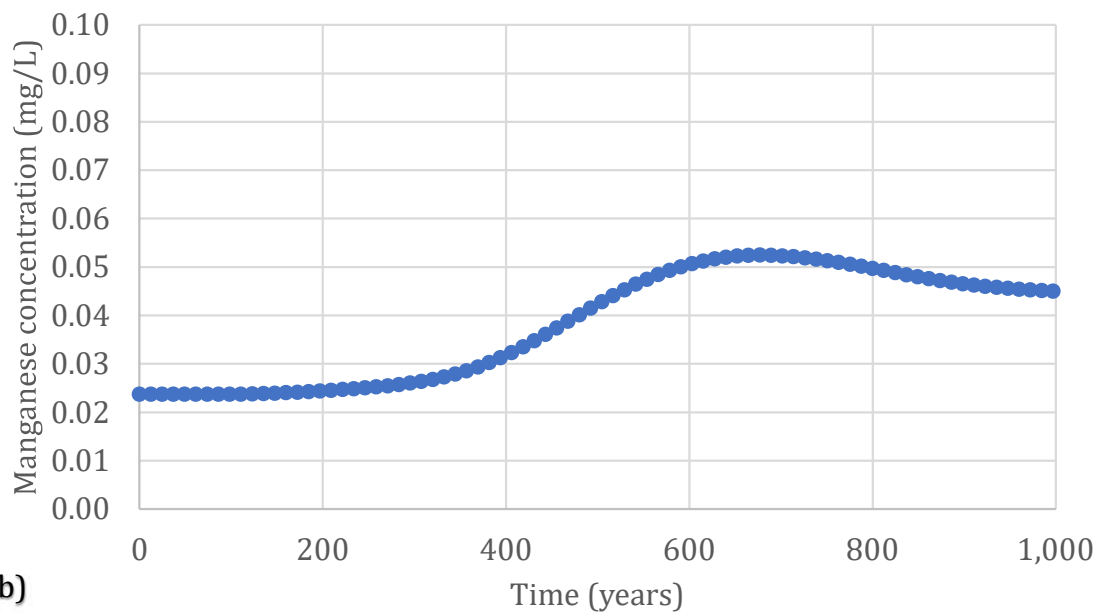


Figure C.5-8. Flow Path A groundwater iron concentrations: (a) as a function of time and distance; (b) as a function of time at POE location A. Well locations on Flow Path A are: upgradient monitoring ring Well M-21 at 0 m, Well B-3 at 279 m, Well B-2 at 396 m, Well B-1 at 570 m and POE location A (dashed vertical line) at 808 m



(a)

—□— 0 years —*— 100 years —x— 500 years —●— 1,000 years



(b)

Figure C.5-9. Flow Path A groundwater manganese concentrations: (a) as a function of time and distance; (b) as a function of time at POE location A. Well locations on Flow Path A are: upgradient monitoring ring Well M-21 at 0 m, Well B-3 at 279 m, Well B-2 at 396 m, Well B-1 at 570 m and POE location A (dashed vertical line) at 808 m

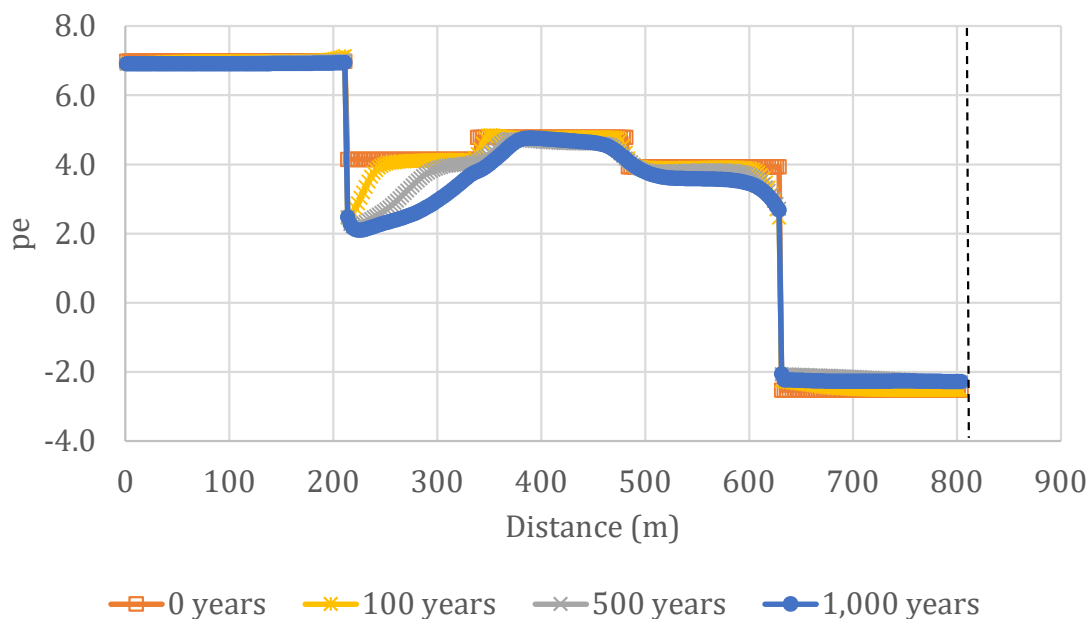


Figure C.5-10. Flow Path A groundwater pe as a function of time and distance. Well locations on Flow Path A are: upgradient monitoring ring Well M-21 at 0 m, Well B-3 at 279 m, Well B-2 at 396 m, Well B-1 at 570 m and POE location A (dashed vertical line) at 808 m

Table C.5-4. Measured and modeled groundwater iron concentrations at POE locations

POE	Downgradient Well	Measured Downgradient Iron Concentrations (mg/L)	Modeled POE Iron Concentrations (mg/L)
A	M-2	0.06 – 0.20	0.20 – 0.65
B	M-2/M-3	< 0.05 – 0.32	0.20 – 0.38
C	M-5	< 0.05 – 0.27	0.20 – 0.28
D	M-7/M-8	< 0.05 – 0.19	0.11 – 0.26
E	M-8	< 0.05 – 0.19	0.17 – 0.57
F	M-9	< 0.05	0.19 – 0.35

Manganese aqueous concentrations decrease over time in the upgradient portion of the production zone and increase slightly over time in the downgradient portion of the production zone (Figure C.5-9(a)). No manganese solid phases, such as rhodochrosite, are precipitated in the production zone or downgradient sediments. Manganese is attenuated in the production zone and downgradient sediments by exchange and by adsorption on

Fe(OH)₃(a) and goethite surfaces. The ranges of modeled groundwater manganese concentrations at the POE locations are higher than the measured concentrations in the downgradient monitoring ring wells, and the upper limit of the modeled manganese groundwater concentration ranges slightly exceed the secondary manganese drinking water standard of 0.05 mg/L at two of the six POE locations (Table C.5-5). Manganese concentrations at POE location A are below the secondary drinking water standard and exhibit a downward trend at the end of the 1,000-year modeling period, (Figure C.5-9(b)). Variation in modeling parameters for Flow Path A have little effect on manganese concentrations at POE A (Table C.5-2).

Table C.5-5. Measured and modeled groundwater manganese concentrations at POE locations

POE	Downgradient Well	Measured Downgradient Concentrations (mg/L)	Modeled POE Concentrations (mg/L)
A	M-2	0.02	0.024 - 0.052
B	M-2/M-3	0.02	0.023 - 0.034
C	M-5	0.02 - 0.03	0.034 - 0.041
D	M-7/M-8	0.02	0.021 - 0.039
E	M-8	0.02	0.024 - 0.057
F	M-9	0.02	0.028 - 0.039

5.3 Uranium

Uranium concentrations in the production zone groundwater are initially elevated relative to upgradient and downgradient groundwater (Figure C.5-11(a)). Over time, production-zone groundwater uranium concentrations are predicted to increase near the upgradient boundary of the production zone as pH, calcium concentrations and alkalinity increase and cause uranium desorption from the Fe(OH)₃(a) surface. It is reasonable that adsorbed uranium will be released from sediments at the upgradient edge of the production zone and re-adsorbed downgradient in response to changing groundwater compositions over time. However, the modeled uranium groundwater concentrations are likely overestimated in the upgradient portion of the production zone. The initial adsorbed uranium in the production zone sediments is based on equilibration with the initial groundwater composition, and the initial modeled adsorbed uranium concentrations range from 125 –

881 mg/kg (Table C.5-6). This modeled range exceeds both the range of production zone sediment uranium concentrations associated with iron oxides based on sequential extractions (2 – 40 mg/kg, Table C.4-2) and the range of total uranium concentrations in the production zone sediment samples (9.5 – 421 mg/kg, Table C.3-7).

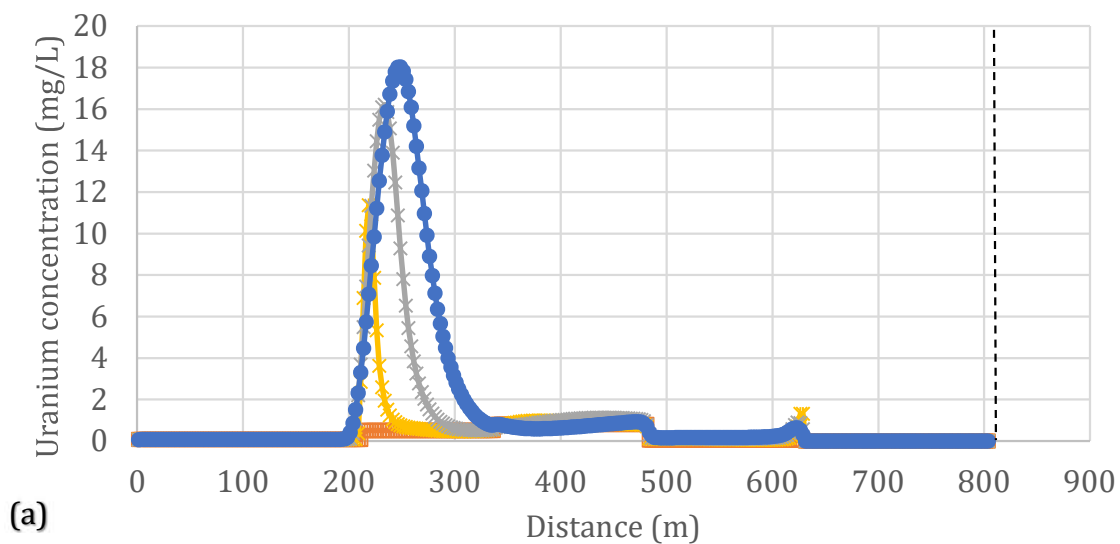
The sequential extraction results also indicate that uranium is associated with clays and therefore likely to be attenuated by exchange. This exchange reaction is not included in the transport model because of the lack of exchange constants for the uranyl ion. Remnant pyrite and organic carbon have also been identified in the production zone core samples. This pyrite and organic carbon may react with aqueous uranyl ion and result in its attenuation within the production zone through precipitation as reduced uranium such as uraninite or coffinite, limiting the increase in uranium concentrations caused by desorption from iron oxides and hydroxides.

Modeled uranium concentrations in downgradient groundwater are extremely low because of uranium reduction and precipitation as uraninite within the first downgradient cell that contains pyrite (Table C.5-7). Increasing the initial production zone concentration of uranium has insignificant effects on POE location A groundwater uranium concentrations because of uraninite precipitation (Table C.5-7). The effects of varying other parameters on POE A uranium concentrations are also negligible (Table C.5-2).

5.3.1 Effects of Initial Groundwater pH on Uranium Concentrations

The highest modeled uranium concentrations at a POC well location were at Well B-4 on Flow Path B. During stability monitoring, measured field pH values in Well B-4 groundwater samples varied from 6.2 (December 2015) to 7.0 (December 2016). The effects of initial Well B-4 groundwater pH on modeled groundwater uranium concentrations were evaluated by substituting increased Well B-4 pH values into the initial conditions for the PHREEQC Flow Path B groundwater transport model calculations. Increasing the initial groundwater pH from 6.3 to 7.0 decreased the maximum modeled groundwater uranium concentrations at Well B-4 (Figure C.5-12) and increased the time at which maximum groundwater uranium concentrations were achieved (Table C.5-8).

The maximum modeled groundwater uranium concentration along Flow Path B occurs near Well B-4 (Figure C.5-13). Modeled groundwater uranium concentrations increase over time at Well B-4 as the influx of upgradient groundwater causes increased pH and desorption of uranium from the surface of $\text{Fe}(\text{OH})_3(\text{a})$ in the production zone sediments. Initial concentrations of uranium adsorbed on $\text{Fe}(\text{OH})_3(\text{a})$ (Table C.5-9) are calculated by the PHREEQC transport model based on the initial groundwater composition. The initial adsorbed concentrations were found to decrease with increasing initial groundwater pH.



— 0 years * 100 years x 500 years ● 1,000 years

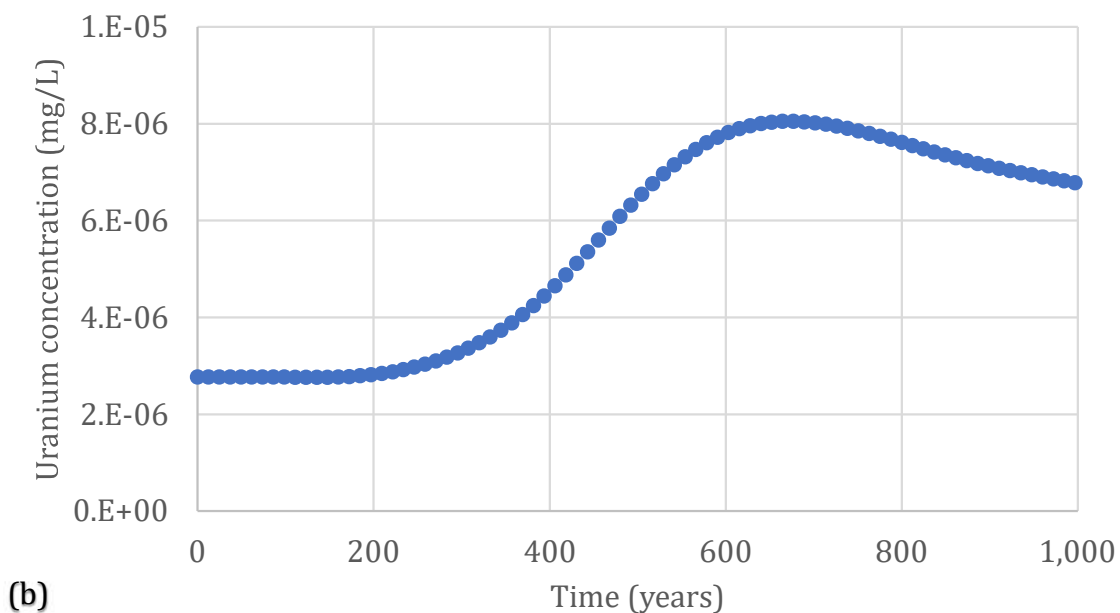


Figure C.5-11 Flow Path A groundwater uranium concentrations: (a) as a function of time and distance; (b) as a function of time at POE location A. Well locations on Flow Path A are: upgradient monitoring ring Well M-21 at 0 m, Well B-3 at 279 m, Well B-2 at 396 m, Well B-1 at 570 m and POE location A (dashed vertical line) at 808 m

Table C.5-6. Initial uranium concentrations in production zone sediments based on model calibration

Well	Modeled Adsorbed Uranium Concentration (mg/kg)
B-1	151
B-2	682
B-3	602
B-4	881
B-5	494
B-10	540
B-12	335
B-13	249
B-14	580
B-18	125
median	517
minimum	125
maximum	881

Table C.5-7. Measured and modeled groundwater uranium concentrations at POE locations

POE	Downgradient Well	Measured Downgradient Concentrations (mg/L)	Baseline Modeled POE Uranium Concentrations (mg/L)	Modeled POE Uranium Concentrations with Initial 10 mg/L POC Concentration
A	M-2	0.0153 - 0.0323	< 0.0003	< 0.0003
B	M-2/M-3	0.0146 - 0.0277	< 0.0003	< 0.0003
C	M-5	0.0185 - 0.0472	< 0.0003	< 0.0003
D	M-7/M-8	0.0116 - 0.0236	< 0.0003	< 0.0003
E	M-8	0.0116 - 0.0236	< 0.0003	< 0.0003
F	M-9	0.0251 - 0.036	< 0.0003	< 0.0003

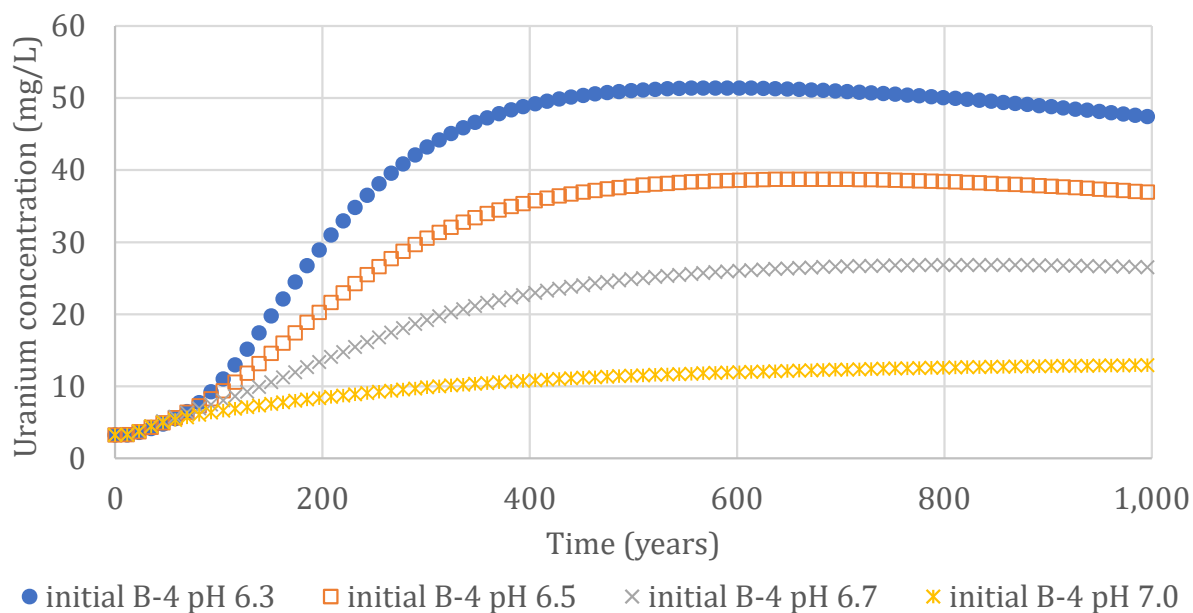


Figure C.5-12. Effect of initial Well B-4 pH values on predicted Well B-4 groundwater uranium concentrations

Table C.5-8. Maximum predicted groundwater uranium concentrations at Well B-4

Initial Well B-4 pH	Maximum Well B-4 Groundwater Uranium Concentration (mg/L)	Time Range for Maximum Well B-4 Groundwater Uranium Concentration (years)
6.3	51	463 - 762
6.5	39	579 - 776
6.7	27	671 - 995
7.0	13	776 - 1,000

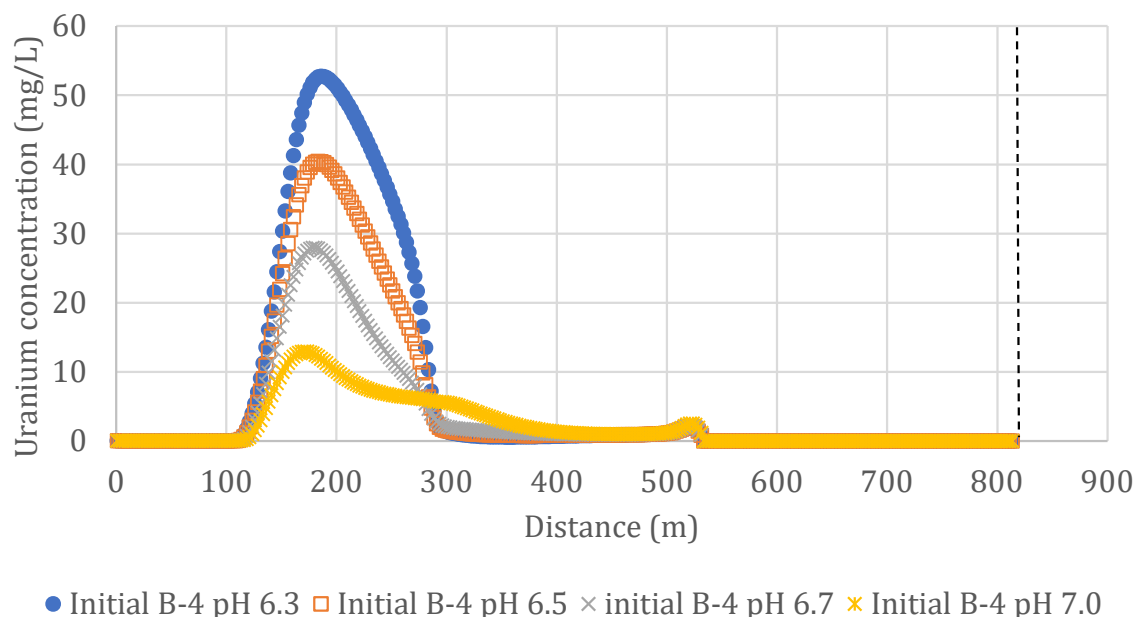


Figure C.5-13. Effects of initial pH at Well B-4 on predicted groundwater uranium concentrations along Flow Path B after 1,000 years. Well locations on Flow Path B are: upgradient monitoring ring Well M-20 at 0 m, Well B-4 at 170 m, Well B-5 at 391 m and POE location B (dashed vertical line) at 815 m

Table C.5-9. Effects of initial Well B-4 pH on modeled initial uranium concentration adsorbed on $\text{Fe}(\text{OH})_3(\text{a})$

Initial Well B-4 pH	Initial Modeled Adsorbed Uranium on Iron Oxides at Well B-4 (mg/kg)
6.3	881
6.5	741
6.7	586
7.0	360

The modeled initial adsorbed uranium concentrations at Well B-4 (Table C.5-9) significantly exceed measured uranium concentrations in Mine Unit 1 production zone sediments (Table C.5-10). The modeled initial concentrations exceed the maximum uranium concentrations adsorbed by iron oxides and hydroxides measured by sequential

extraction and range much higher than even total uranium sediment concentrations. Regardless of the maximum modeled groundwater uranium concentration at Well B-4, uranium concentrations at the POE B location remain extremely low (Figure C.5-13).

Table C.5-10. Adsorbed (Step III and Step IV sequential extractions) and total (EPA 3050) uranium concentrations in production zone sediments

Sample Number	Adsorbed Uranium on Fe(OH) ₃ (a) (mg/kg)	Total Uranium (mg/kg)
ST-2, 472 - 473 ft	27.0	421
ST-3, 463 - 464 ft	6.5	40.2
ST-3, 474 - 475 ft	7.0	195
ST-4, 479 - 480 ft	1.7	9.54
ST-4, 488 - 489 ft	35.9	284
ST-5, 494 - 495 ft	9.5	154
ST-5, 499 - 500 ft	40.4	282
Mean	18.3	198
Median	9.5	195
Range	1.7 - 40.4	9.54 - 421

5.3.2 Mass Balance for Production Zone Uranium and Downgradient Pyrite

Uranium transport in the downgradient aquifer is limited because of the reduction of U(VI) by pyrite. Mass balance calculations were performed to evaluate whether sufficient pyrite is present in the downgradient sediments for reduction of all U(VI) present in the production zone sediments. The reaction stoichiometry shows that one mole of pyrite can reduce seven moles of U(VI):



For the mass balance calculations, it was assumed that the uranium available for release from the production zone sediments equals the median EPA 3050 uranium concentration of 195 mg/kg sediment (Table C.3-7, excluding ST-2 463-464 ft). Converting this concentration to moles and multiplying by the production zone solids/solution mass ratio of 6.592 kg sediment/kg H₂O yields a production zone uranium concentration of 8.19×10^{-4} moles U/kg H₂O. The quantity of pyrite available in the downgradient sediments was assumed equal to the median concentration used in the transport model calculations (0.408 moles/kg H₂O, Table C.4-3).

The total amounts of production zone uranium and downgradient pyrite were calculated for each flow path assuming 1 m cell sizes (Table C.5-11). The results of these calculations show that the amounts of pyrite present in each downgradient flow path exceed the amounts required to reduce all uranium in the production zone, with an excess pyrite factor ranging from 188 for Flow Path E to a factor of 2,726 for Flow Path C (Table C.5-11).

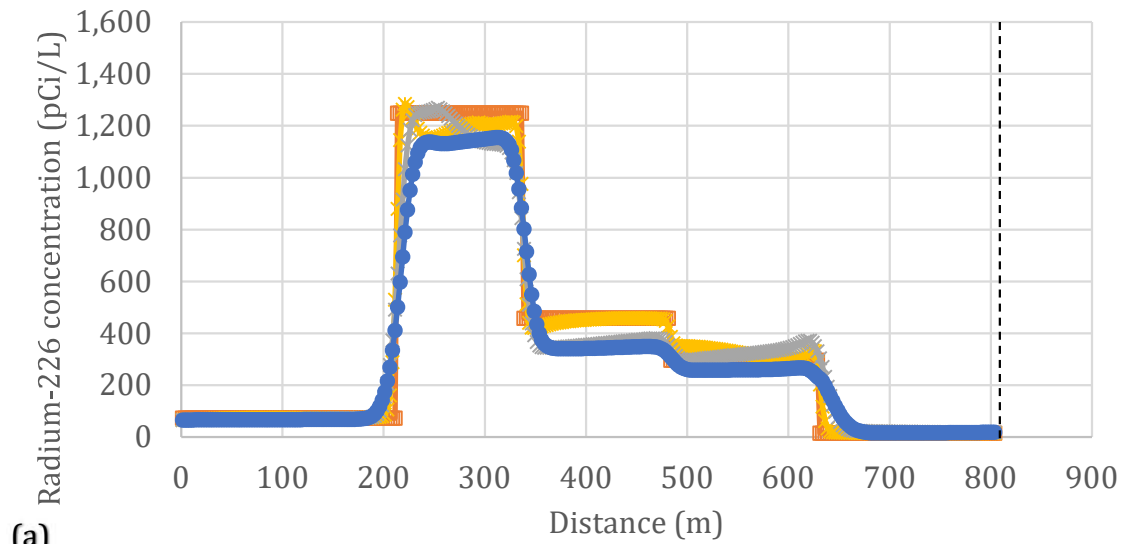
Table C.5-11. Production zone uranium and downgradient pyrite mass balance calculation results for Flow Paths A through F

Flow Path	Production Zone Distance (m)	Median Production Zone Uranium (moles)	Downgradient Distance to POE (m)	Median Downgradient Pyrite (moles)	Pyrite Needed to Reduce Uranium (moles)	Excess Pyrite Factor ^a
A	396	2.14	198	80.8	0.306	264
B	383	2.07	303	124	0.295	419
C	67	0.362	346	141	0.052	2,726
D	212	1.14	130	53.2	0.163	326
E	361	1.95	129	52.5	0.279	188
F	172	0.930	230	93.9	0.133	707

a – median downgradient pyrite (moles) divided by the moles of pyrite needed to reduce median production zone uranium

5.4 Radium-226

Radium-226 concentrations in the production zone groundwater are initially elevated compared to upgradient and downgradient groundwater, and decline slowly as a function of time (Figure C.5-14). Within the production zone and downgradient sediments, radium-226 is attenuated by exchange and precipitation as a barite-RaSO₄(s) solid solution, with a smaller amount of attenuation from Fe(OH)₃(a) adsorption.



—□— 0 years —*— 100 years —x— 500 years —●— 1,000 years

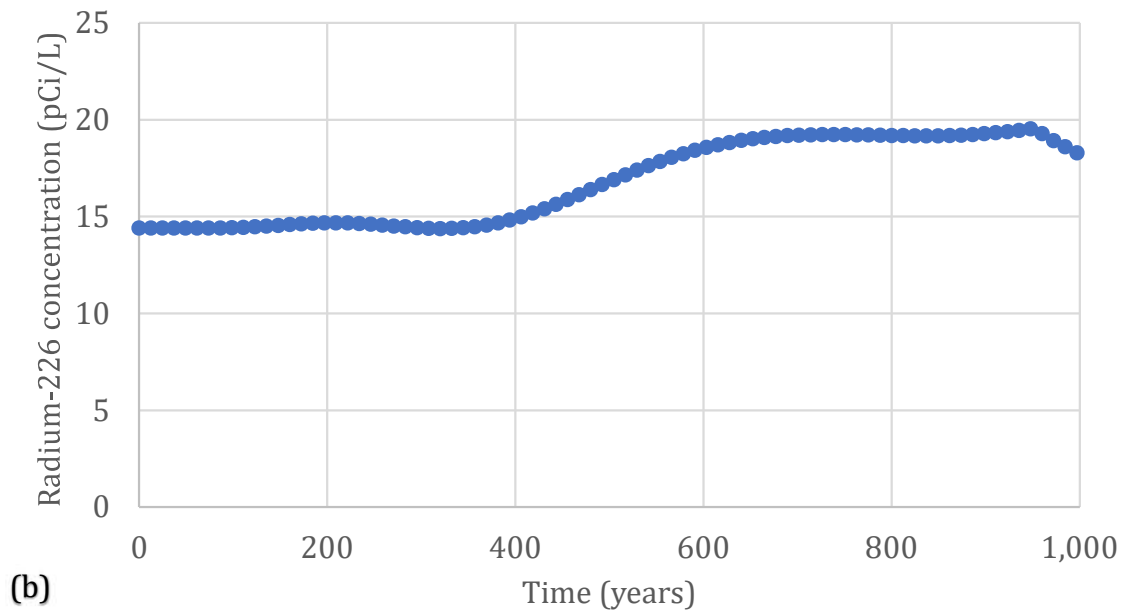


Figure C.5-14 Flow Path A groundwater radium-226 concentrations: (a) as a function of time and distance; (b) as a function of time at POE location A. Well locations on Flow Path A are: upgradient monitoring ring Well M-21 at 0 m, Well B-3 at 279 m, Well B-2 at 396 m, Well B-1 at 570 m and POE location A (dashed vertical line) at 808 m

The modeled POE groundwater concentrations of radium-226 are minimally affected by downgradient transport of radium-226 from the production zone (Table C.5-12). The modeled concentrations are likely to be slight overestimates because the effects of radium-226 decay are not included in the transport calculations. Increasing the initial production zone groundwater radium-226 concentration to 2,000 pCi/L had little effect on radium-226 concentrations at the POE locations (Table C.5-12). Eliminating the formation of the solid solution of barite-RaSO₄(s) from the model and assuming lower exchange site concentrations in the transport model each had only small effects on the radium-226 concentration range at POE location A (Table C.5-2). The assumption of lower downgradient sediment goethite concentrations, which would reduce the amount of radium-226 adsorption, and an increased groundwater flow rate also had little effect on the ranges of radium-226 concentrations predicted at POE location A.

Table C.5-12. Measured and modeled groundwater radium-226 concentrations at POE locations

POE	Downgradient Well	Measured Downgradient Concentrations (pCi/L)	Baseline Modeled POE concentrations (pCi/L)	Modeled POE Radium-226 Concentration with Initial 2,000 pCi/L POC Concentrations
A	M-2	12.7 - 15.7	14.4 - 19.5	14.2 - 17.7
B	M-2/M-3	12.7 - 30.7	20.7 - 23.7	20.8 - 22.3
C	M-5	14.2 - 19.8	15.0 - 16.6	15.0 - 16.6
D	M-7/M-8	12.9 - 13.0	13.4 - 16.7	13.2 - 16.6
E	M-8	13.0 - 18.1	14.1 - 22.4	14.7 - 21.0
F	M-9	5.4 - 12.7	4.8 - 6.4	5.1 - 6.2

5.5 Arsenic

Arsenic concentrations in the production zone groundwater are elevated relative to upgradient and downgradient groundwater concentrations (Figure C.5-15). Predicted arsenic concentrations decrease slightly over time in the upgradient portion of the production zone and increase slightly over time in the downgradient portion of the production zone. In the downgradient reducing sediments, arsenic is attenuated to below typical analytical detection limits (Table C.5-13) by adsorption on goethite as arsenite

[H₂AsO₃]. Increasing the initial arsenic concentration throughout the production zone groundwater to 0.1 mg/L had insignificant effects on modeled concentrations at POE A (Table C.5-13). Other parameter variations also had insignificant effects on modeled arsenic concentrations at POE A (Table C.5-2).

Using the March 2016 arsenic concentrations as the initial groundwater concentrations in the production zone, the maximum modeled arsenic concentrations were predicted at Wells B-1 and Well B-4 (Figure 5-16). For the sensitivity calculations with initial production zone groundwater arsenic concentrations assumed equal to 0.1 mg/L, the maximum modeled arsenic concentration at the POC wells was 0.18 mg/L at Well B-1 and at Well B-18 (Figure 5-16).

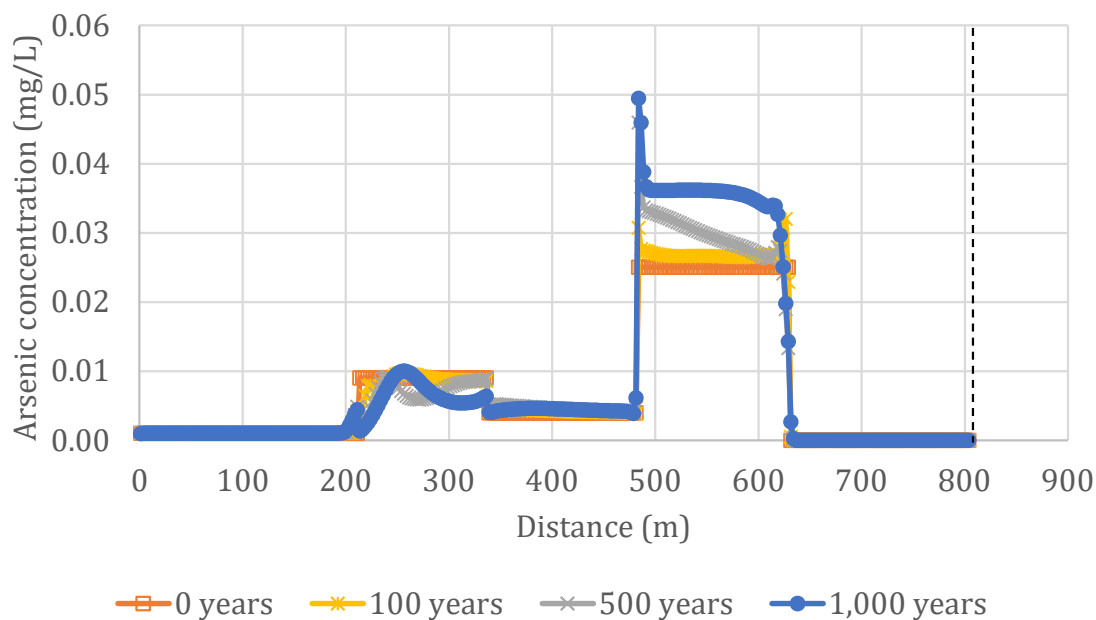


Figure C.5-15. Flow Path A groundwater arsenic concentrations as a function of time and distance. Well locations on Flow Path A are: upgradient monitoring ring Well M-21 at 0 m, Well B-3 at 279 m, Well B-2 at 396 m, Well B-1 at 570 m and POE location A (dashed vertical line) at 808 m

Table C.5-13. Measured and modeled groundwater arsenic concentrations at POE locations

POE	Downgradient Well	Measured Downgradient Concentrations (mg/L)	Modeled POE concentrations (mg/L)	Modeled POE Concentration with 0.1 mg/L Production Zone Groundwater Concentration
A	M-2	< 0.001	< 0.001	< 0.001
B	M-2/M-3	< 0.001	< 0.001	< 0.001
C	M-5	< 0.001	< 0.001	< 0.001
D	M-7/M-8	< 0.001	< 0.001	< 0.001
E	M-8	< 0.001	< 0.001	< 0.001
F	M-9	< 0.001 - 0.005	< 0.001	< 0.001

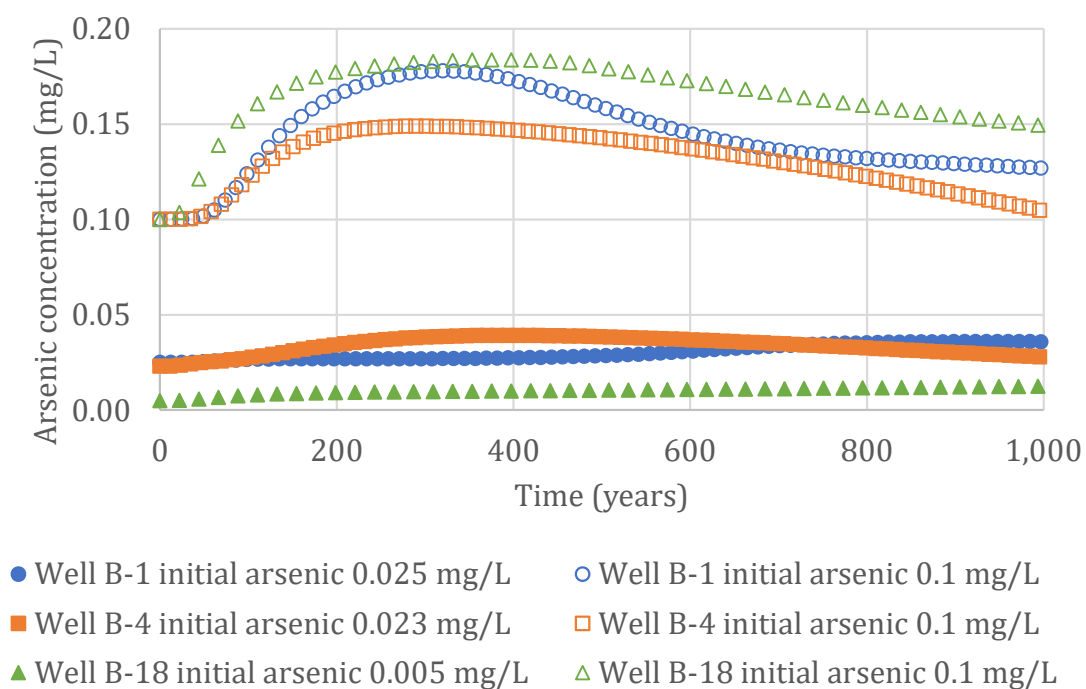


Figure C.5-16. Predicted arsenic concentrations at Wells B-1, B-4 and B-18 as a function of time and initial arsenic concentrations

The potential effects of initial groundwater pH on Well B-4 arsenic concentrations were examined in the sensitivity calculations also used to evaluate the effects of initial Well B-4 pH on uranium concentrations (Section 5.3, Figure C.5-13). Variation of the initial groundwater pH at Well B-4 from 6.3 and 7.0 had relatively small effects on predicted arsenic concentrations at Well B-4 (Figure C.5-17).

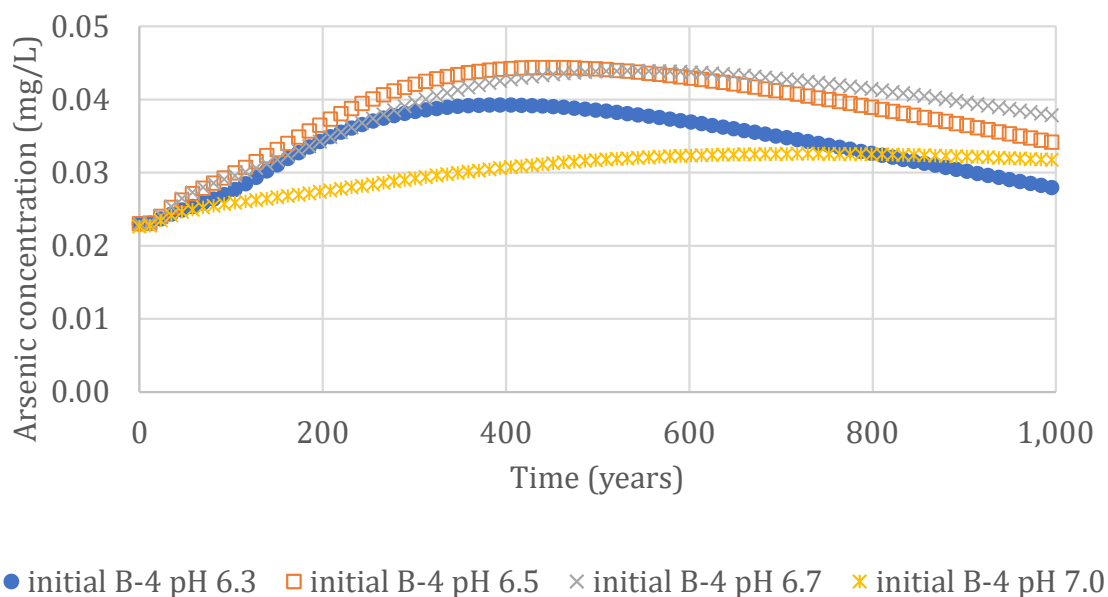
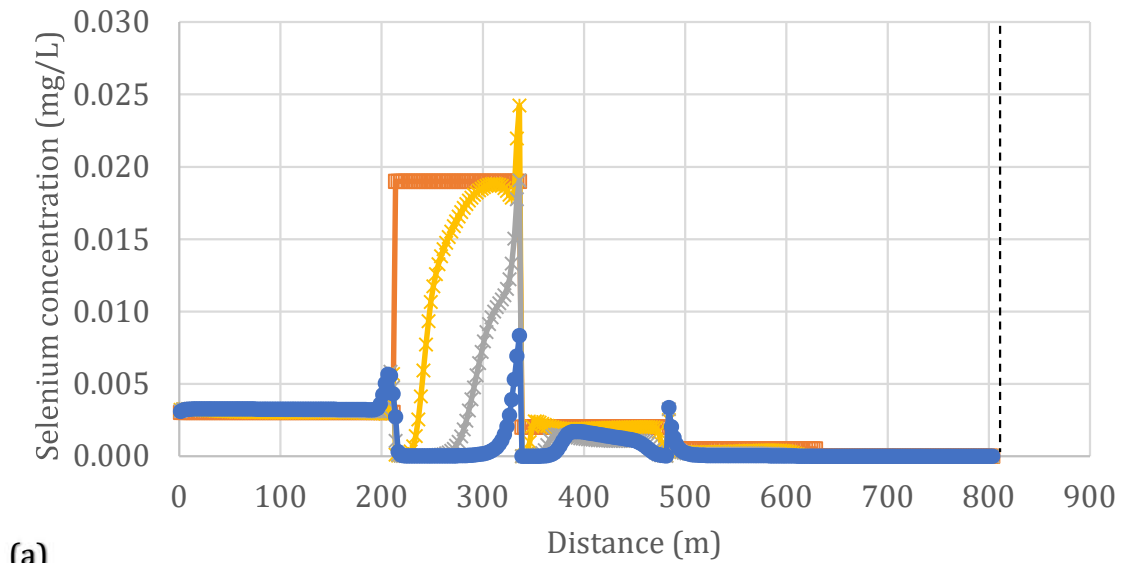


Figure C.5-17. Effect of initial Well B-4 pH values on predicted Well B-4 groundwater arsenic concentrations

5.6 Selenium

Selenium concentrations are below the drinking water standard of 0.05 mg/L in the initial production zone groundwater samples because of native Se precipitation. Selenium concentrations are predicted to decrease over time in the production zone as pH increases and additional native Se is precipitated (Figure C.5-18). Selenium reduction by reaction with reducing downgradient sediments results in the precipitation of ferroselite and predicted selenium concentrations below typical analytical detection limits (Table C.5-14). Increased initial production zone selenium concentrations of 0.2 mg/L had no effect on predicted POE location A concentrations of selenium (Table C.5-14). Variation of other modeling parameters also did not affect predicted selenium concentrations at POE location A (Table C.5-2).



— 0 years * 100 years x 500 years • 1,000 years

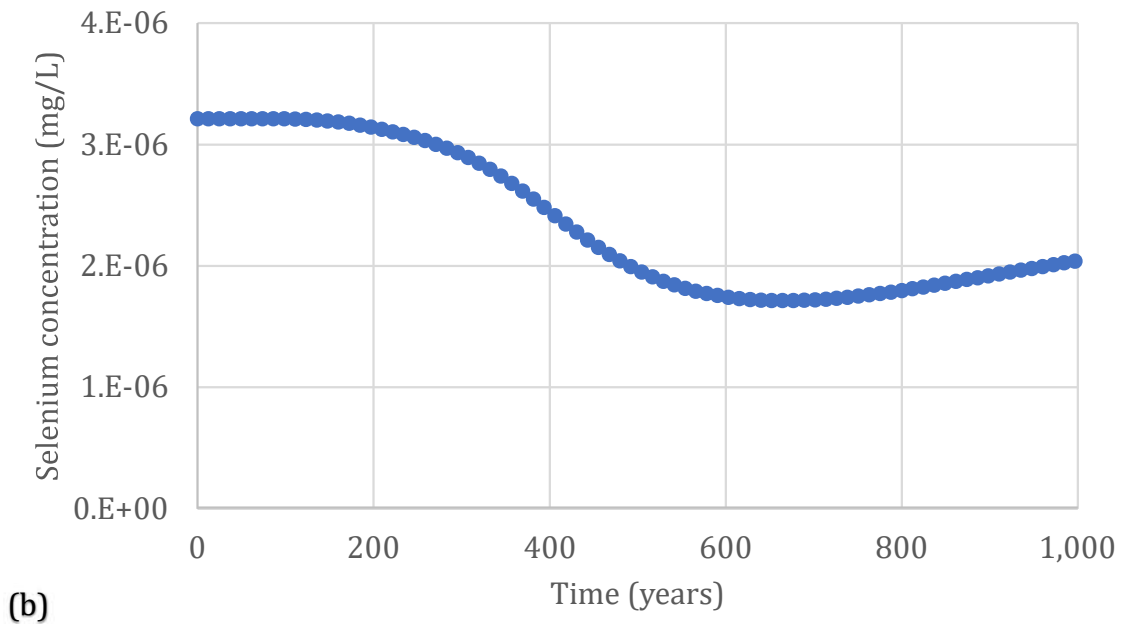


Figure C.5-18. Flow Path A groundwater selenium concentrations: (a) as a function of time and distance; (b) as a function of time at POE location A. Well locations on Flow Path A are: upgradient monitoring ring Well M-21 at 0 m, Well B-3 at 279 m, Well B-2 at 396 m, Well B-1 at 570 m and POE location A (dashed vertical line) at 808 m

Table C.5-14. Measured and modeled groundwater selenium concentrations at POE locations

POE	Downgradient Well	Measured Downgradient Concentrations (mg/L)	Modeled POE concentrations (mg/L)	Modeled POE Selenium Concentration with Initial 0.2 mg/L POC Concentrations
A	M-2	< 0.001 – 0.001	< 0.001	< 0.001
B	M-2/M-3	< 0.001 – 0.002	< 0.001	< 0.001
C	M-5	< 0.001	< 0.001	< 0.001
D	M-7/M-8	< 0.001 – 0.004	< 0.001	< 0.001
E	M-8	< 0.001 – 0.002	< 0.001	< 0.001
F	M-9	< 0.001 – 0.004	< 0.001	< 0.001

The highest March 2016 groundwater selenium concentrations were measured in samples from Well B-3 (Flow Path A), Well B-5 (Flow Path B) and Well B-13 (Flow Path E). Groundwater selenium concentrations predicted at these locations using the measured March 2016 groundwater concentrations remained below the drinking water standard of 0.05 mg/L throughout the modeled 1,000-year time period (Figure C.5-19). In calculations carried out with a higher assumed initial groundwater selenium concentration of 0.20 mg/L, selenium concentrations decreased over time (Well B-3) or exhibited reasonably small increasing trends (Wells B-5 and B-13). Regardless of the assumed initial selenium concentrations at the production-zone monitoring well locations, ferroselite precipitation prevented the downgradient transport of selenium to the POE locations (Table C.5-14).

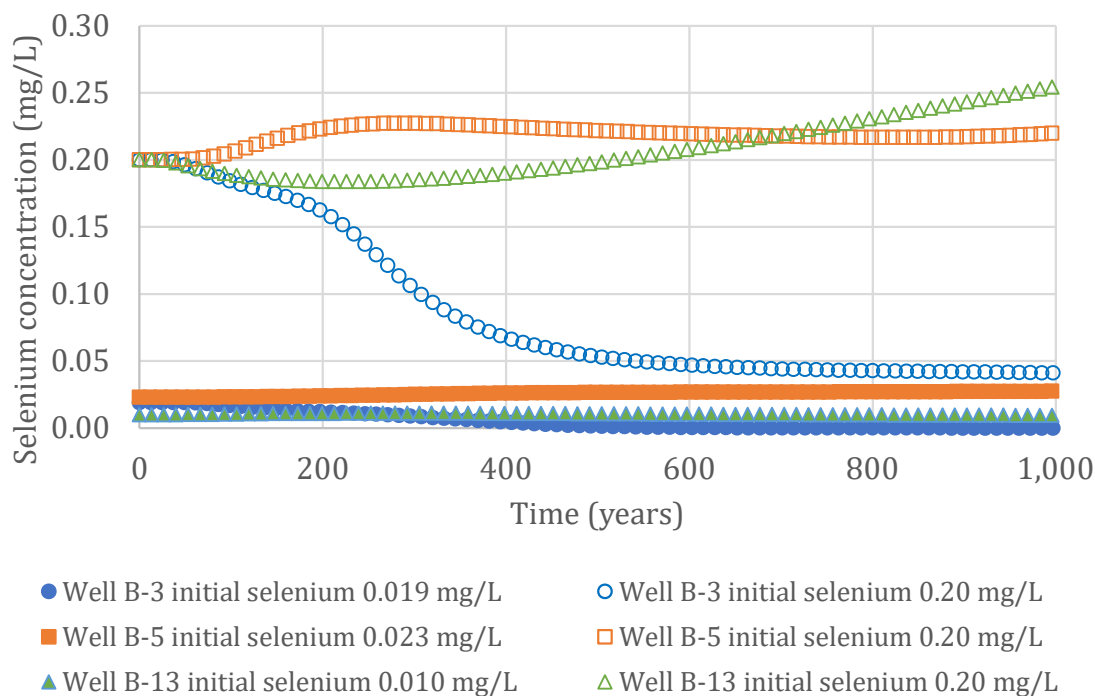


Figure C.5-19. Predicted selenium concentrations at Wells B-3, B-5 and B-13 as a function of time and initial selenium concentrations

5.7 Effects of Groundwater Stability on Transport Modeling Results

Cameco (2017) evaluated the intra-well stability of groundwater constituent concentrations in samples from production-zone monitoring Wells B-1 through B-19 during the Mine Unit 1 stability monitoring period (September 2014 through March 2017). The results for arsenic, radium-226, selenium and uranium are summarized in Table C.5-15.

Arsenic and selenium groundwater concentrations at the production-zone monitoring well locations have either no statistical trends or trend downward over time (Table C.5-15). Consequently, the arsenic and selenium concentrations predicted using the transport model at the Mine Unit 1 POE locations will not increase due to groundwater concentration instability.

Upward statistical trends were detected for radium-226 concentrations in samples from Wells B-1, B-5 and B-11 (Table C.5-15). Well B-1 groundwater was included in the transport model for Flow Path A and Well B-5 groundwater was included in the Flow Path B transport model (Table C.4-1). The radium-226 concentrations used for Wells B-1 and

B-5 groundwater in the transport model are the highest measured in the stability monitoring samples (Table C.5-16). The radium-226 concentrations measured in groundwater samples from Wells B-1, B-5 and B-11 (Table C.5-16) are significantly below the Mine Unit 1 RTV of 726 pCi/L. Consequently, the upward statistical trends observed in samples from these wells are unlikely to result in radium-226 concentrations that exceed this RTV. The potential effects of elevated production zone groundwater radium-226 concentrations on predicted groundwater concentrations at the POE locations were evaluated using calculations that included initial production zone groundwater radium-226 concentrations of 2,000 pCi/L (Section 4.4). This radium-226 concentration, which is significantly higher than both the RTV and production zone groundwater radium-226 concentrations measured during stability monitoring, had minimal effects on modeled radium-226 concentrations at the POE locations (Table C.5-12) because of the strong attenuation of radium-226 by exchange and precipitation as a barite-RaSO₄(s) solid solution (Section 5.4).

Upward statistical trends in production-zone groundwater uranium concentrations were observed in samples from Wells B-1, B-3, B-5 and B-19. These wells are in the western portion of Mine Unit 1 (Figure C.3-1); Wells B-1 and B-3 groundwater were included in the Flow Path A transport model and Well B-5 groundwater was included in the Flow Path B transport model (Table C.4-1). The locations with statistically increasing uranium concentrations (Table C.5-17) do not have the highest uranium concentrations in the Mine Unit 1 production zone, which were observed in samples from Wells B-2 (0.794 – 2.31 mg/L), B-4 (3.05 – 5.48 mg/L) and B-10 (1.23 – 3.09 mg/L).

The increasing trends in uranium concentrations in groundwater samples from Wells B-1, B-3, B-5 and B-19 are likely caused by desorption of uranium from iron oxide and hydroxide surfaces. This uranium desorption may be caused by increasing trends (Cameco 2017) in pH (Wells B-1, B-5 and B-19), calcium concentrations (Wells B-3, B-5 and B-19) and alkalinity (Wells B-3, B-5 and B-19), which would increase the stability of the Ca₂UO₂(CO₃)₃⁰ and CaUO₂(CO₃)₃²⁻ aqueous species.

Mass balance calculations demonstrate that the amounts of pyrite in sediments downgradient of Mine Unit 1 far exceed the amounts necessary to reduce and precipitate all production zone uranium (Section 5.3, Table C.5-11), so increased initial groundwater concentrations in the production zone will not affect modeled uranium concentrations at the Mine Unit 1 POE locations. This conclusion is supported by the results of transport modeling calculations carried out with initial production-zone uranium concentrations of 10 mg/L (Section 4.4). The results of transport calculations with increased groundwater uranium concentrations throughout the production zone showed no discernable effect on predicted groundwater uranium concentrations at the POE locations (Table C.5-7).

Table C.5-15. Results of statistical evaluation for stability of arsenic, radium-226, selenium and uranium in Mine Unit 1 POC wells (Cameco 2017)

Well Number	Arsenic (mg/L)	Radium-226 (pCi/L)	Selenium (mg/L)	Uranium (mg/L)
B-1	none	upward	none	upward
B-2	none	none	none	downward
B-3	none	none	none	upward
B-4	none	none	none	none
B-5	none	upward	none	upward
B-6	none	none	downward	downward
B-7	none	none	none	none
B-8	downward	none	none	none
B-9	none	none	downward	downward
B-10	downward	none	downward	none
B-11	none	upward	none	none
B-12	none	none	downward	none
B-13	none	none	none	none
B-14	none	none	none	none
B-15	none	downward	none	none
B-16	none	none	none	downward
B-17	none	none	none	none
B-18	none	none	none	downward
B-19	none	none	none	upward

Table C.5-16. Radium-226 concentrations in Well B-1, B-5 and B-11 groundwater samples

Radium-226 (pCi/L)			
Sample Date	Well B-1	Well B-5	Well B-11
September 2014	129	221	187
December 2014	120	241	215
March 2015	236	246	249
June 2015	213	259	292
September 2015	223	250	184
December 2015	244	224	269
March 2016	296	377	280
June 2016	n.m.	n.m.	n.m.
September 2016	264	n.m.	n.m.
December 2016	223	n.m.	n.m.
March 2017	232	309	314

n.m. = not measured

Table C.5-17. Uranium concentrations in Well B-1, B-3, B-5 and B-19 samples

Uranium (mg/L)				
Sample Date	Well B-1	Well B-3	Well B-5	Well B-19
September 2014	0.0375	0.381	0.233	0.179
December 2014	0.0206	0.228	0.242	0.144
March 2015	0.0286	0.250	0.221	0.229
June 2015	0.0305	0.272	0.214	0.257
September 2015	0.0461	0.415	0.257	0.250
December 2015	0.0749	1.02	0.346	0.772
March 2016	0.0438	0.511	0.264	0.688
June 2016	n.m.	n.m.	n.m.	n.m.
September 2016	n.m.	1.04	n.m.	0.676
December 2016	n.m.	0.97	n.m.	0.788
March 2017	0.0829	0.901	0.399	0.997

n.m. = not measured

6.0 Summary and Conclusions

Groundwater uranium, arsenic and selenium concentrations in some Mine Unit 1 production zone samples obtained during stability monitoring exceeded both the RTV and primary drinking water standards. However, uranium concentrations greater than the drinking water standard were observed in some Mine Unit 1 production-zone monitoring wells before ISR (Cameco 2014). Current Mine Unit 1 groundwater pH values are slightly less than the RTV range and some Mine Unit 1 groundwater pH measurements are slightly below the secondary drinking water standard. Dissolved iron, manganese and TDS concentrations in some stability monitoring groundwater samples exceeded both the RTV and secondary drinking water standards. Radium-226 concentrations, which were above the drinking water standard before ISR, have been restored to concentrations that are generally less than pre-ISR concentrations. Other constituent concentrations that exceeded their respective RTVs during stability monitoring do not have drinking water standards, such as calcium, or were less than the secondary drinking water standard, such as sulfate.

One-dimensional PHREEQC reactive transport calculations for six flow paths across Mine Unit 1 demonstrate that the concentrations of uranium, radium-226, arsenic and selenium will be attenuated by the reducing sediments located downgradient of the production zone and will not affect concentrations at the aquifer exemption boundary. Attenuation of uranium, radium-226, arsenic and selenium by these sediments is predicted to occur via the same processes that formed the uranium roll front deposits in Mine Unit 1. Mass balance calculations based on median total uranium concentrations in the production zone sediments and median pyrite concentrations in downgradient sediments demonstrate that a large excess of pyrite (188 to 2,726 times the amount required) is available in downgradient sediments to reduce and attenuate production-zone uranium before groundwater reaches the POE locations.

Slight increases are predicted in TDS at the POE locations for some flow paths, although TDS concentrations are predicted to remain slightly below the secondary drinking water standard at most POE locations. Dissolved iron and manganese concentrations are predicted to increase slightly in groundwater at the POE locations as a result of transport from the Mine Unit 1 production zone, and may slightly exceed secondary drinking water standards.

7.0 References

- Ames, L.L., J.E. McGarrah and B.A. Walker. 1983. Sorption of Trace Constituents from aqueous solutions onto secondary minerals. II. Radium. *Clays and Clay Minerals* 31:335-342.
- AquiferTek. 2017. *Draft Mine Unit 1 Hydrologic Assessment and Groundwater Modeling*. Prepared for Cameco Resources Smith Ranch – Highland Facility, Converse County, Wyoming, April 15, 2017.
- Balistreri, L.S., and T.T. Chao. 1990. Adsorption of selenium by amorphous iron oxyhydroxide and manganese dioxide. *Geochimica et Cosmochimica Acta* 54:739-751.
- Cameco. 2012. *Nuclear Regulatory Commission Source Material License No. SUA-1548 License Renewal Application Technical Report*. Prepared by Cameco Resources and Lidstone and Associates, February 2012.
- Cameco. 2014. *Groundwater Restoration Report, Request for Concurrence to Enter Stability Phase, Mine Unit 1, Smith Ranch/Highland Uranium Project*. September 2, 2014.
- Cameco. 2017. *Stability Report for Mine Unit 1*. July 24, 2017.
- Curti, E., K. Fujiwara, K. Iijima, J. Tits, C. Cuesta, A. Kitamura, M.A. Glaus and W. Müller. 2010. Radium uptake during barite recrystallization at $23 \pm 2^\circ\text{C}$ as a function of solution composition: An experimental ^{133}Ba and ^{226}Ra tracer study. *Geochimica et Cosmochimica Acta* 74:3553-3570.
- Davis, J.A. and G.P. Curtis. 2007. *Consideration of Geochemical Issues in Groundwater Restoration at Uranium In-Situ Leach Mining Facilities*. NUREG/CR-6870, prepared by the U.S. Geological Survey for the U.S. Nuclear Regulatory Commission.
- Dong, W., and S.C. Brooks. 2006. Determination of the formation constants of ternary complexes of uranyl and carbonate with alkaline earth metals (Mg^{2+} , Ca^{2+} , Sr^{2+} , and Ba^{2+}) using anion exchange method. *Environmental Science and Technology* 40:4689-4695.
- Dong, W., and S.C. Brooks. 2008. Formation of aqueous $\text{MgUO}_2(\text{CO}_3)_3^{2-}$ complex and uranium anion exchange mechanism onto an exchange resin. *Environmental Science and Technology* 42:1979-1983.
- Gallegos, T.J., K.M. Campbell, R.A. Zielinski, P.W. Reimus, J.T. Clay, N. Janot, J.R. Bargar and W.M. Benzel. 2015. Persistent U(IV) and U(VI) following in-situ recovery (ISR) mining of a sandstone uranium deposit, Wyoming, USA. *Applied Geochemistry* 63:222-234.

Gallegos, T.J., C.C. Fuller, S.M. Webb and W. Betterton. 2013. Uranium(VI) interactions with mackinawite in the presence and absence of bicarbonate and oxygen. *Environmental Science and Technology* 47:7357-7364.

Granger, H.C. and C.G. Warren. 1969. Unstable sulfur compounds and the origin of roll-type uranium deposits. *Economic Geology* 64:160-171.

Greeman, D. J., A.W. Rose, J.W. Washington, R.R. Dobos, and E.J. Ciolkosz. 1999. Geochemistry of radium in soils of the Eastern United States. *Applied Geochemistry* 14:365-385.

Hua, B. and B. Deng. 2008. Reductive immobilization of uranium(VI) by amorphous iron sulfide. *Environmental Science and Technology* 42:8703-8708.

Intera. 2013. *Cameco Geochemical Modeling Report*. Prepared for Cameco Resources, May 13, 2013.

Land, M., J. Thunberg and B. Öhlander. 2002. Trace metal occurrence in a mineralized and a non-mineralized spodosol in northern Sweden. *Journal of Geochemical Exploration* 75:71-91.

Ludwig, K.R. and R.I. Grauch. 1980. Coexisting coffinite and uraninite in some sandstone-host uranium ores of Wyoming. *Economic Geology* 75:296-302.

Macalady, D.L., D. Langmuir, T. Grundl and A. Elzerman. 1990. Use of model-generated Fe^{3+} iron activities to compute Eh and ferric oxyhydroxide solubilities in anaerobic systems. Chapter 28 in *Chemical Modeling of Aqueous Systems II*, D.C. Melchior and R.L. Bassett, eds., American Chemical Society, ACS Symposium Series 416.

Missana, T., U. Alonso and M. García-Gutiérrez. 2009. Experimental study and modelling of selenite sorption onto illite and smectite clays. *Journal of Colloid and Interface Science* 334:132-138.

Parkhurst, D.L., and C.A.J. Appelo. 2013. *Description of Input and Examples for PHREEQC Version 3—A Computer Program for Speciation, Batch-Reaction, One-Dimensional Transport, and Inverse Geochemical Calculations*. U.S. Geological Survey Techniques and Methods, Book 6, Chapter A43. Available at <http://pubs.usgs.gov/tm/06/a43/>

Reimus, P., M. Rearick, G. Perkins, O. Marina, J. Punsal, N. Wasserman, K. Chamberlain and J.T. Clay. 2015. *Field Evaluation of the Restorative Capacity of the Aquifer Downgradient of a Uranium In-Situ Recovery Mining Site*. Los Alamos National Laboratory, LA-UR-15-22858, Los Alamos, New Mexico.

Rio Algom Mining Corporation. 1997. *Smith Ranch Facility Q-Sand Wellfield 1 Multi-Well Pump Tests*. Prepared by Rio Algom Mining Corporation and Hydro-Engineering LLC, March 1997.

Sajih, M., N.D. Bryan, F.R. Livens, D.J. Vaughan, M. Descostes, V. Phrommavanh, J. Nos and K. Morris. 2014. Adsorption of radium and barium on goethite and ferrihydrite: A kinetic and surface complexation modelling study. *Geochimica et Cosmochimica Acta* 146:150-163.

Smedley, P.L., and D.G. Kinniburgh. 2002. A review of the source, behavior and distribution of arsenic in natural waters. *Applied Geochemistry* 17:517-568.

Stewart, C.L. 2002. *The Mineralogy of Uranium Rollfront Deposits and its Significance to In-Situ Carbonate Leach Mining*. Master's thesis, University of Wyoming.

Swapp, S.M. 2016. *MU1 Core Description and Analysis Including MU1-DG, MU1-ST, & MU1-DG*. Prepared for Cameco Resources, Department of Geology and Geophysics, University of Wyoming, Laramie, Wyoming, April 10, 2016.

WoldeGabriel, G., H. Boukhalfa, S.D. Ware, M. Cheshire, P. Reimus, J. Heikoop, S.D. Conradson, O. Batuk, G. Havrilla, B. House, A. Simmons, J. Clay, A. Basu, J.N. Christensen, S.T. Bowen, and D.J. DePaolo. 2014. Characterization of cores from an in-situ recovery mined uranium deposit in Wyoming: implications for post-mining restoration. *Chemical Geology* 390:32-45.